Department of Precision and Microsystems Engineering

RESONANT HAIR CLIPPER

Saurabh Shailendra Sontakke

Report no : 2018.042
Coach : Ir. Bernardo Mulder
Professor : Ir. Jo Spronck
Specialisation : Mechatronic System Design
Type of report : Thesis
Date : December 12, 2018

Resonant hair clipper

An exploratory research project at Philips

by

Saurabh Shailendra Sontakke

in partial fulfillment of the requirements for the degree of

Master of Science

in Mechanical Engineering

at the Delft University of Technology,

to be defended publicly on Tuesday December 19, 2018 at 01:00 PM.

Thesis committee:	Ir. B. Mulder,	Philips	Daily supervisor
	Ir. J. Spronck,	TU Delft	Academic supervisor
	Dr. F. Alijani,	TU Delft	
	Dr. A. Hunt,	TU Delft	

This thesis is confidential and cannot be made public until December 19, 2023.

TU Delft Delft University of Technology

Contents

Preface v

Summary viii

List of Figures ix

List of Tables xiii

1 Introduction 1
- 1.1 Resonance from the energy perspective. . . . 1
- 1.2 State-of-the-art Philips hair clippers 2
- 1.3 Problem statement of the thesis 4
- 1.4 Method of approach to the problem 4

2 Literature survey 7

3 A quick look at the practical possibility 11
- 3.1 Preliminary analysis. . . . 11
- 3.2 Practical possibility 14
  - 3.2.1 Creation of pressure without influencing stiffness 16
  - 3.2.2 Creation of stiffness for resonance 17
  - 3.2.3 Reduction of friction 19

4 Mathematical model of the system 23
- 4.1 Unidimensional dynamic analysis of the system 23
  - 4.1.1 Analysis without friction in the system 23
  - 4.1.2 Mathematical model 26
  - 4.1.3 Simulation results and observations 27
  - 4.1.4 Inferences from the simulation 28
  - 4.1.5 Analysis with friction in the system 29
  - 4.1.6 Motivation for further analysis 29
- 4.2 2D dynamic analysis of the system with friction 30
  - 4.2.1 Kinematic analysis of the system 30
  - 4.2.2 Mathematical model 32

5 Analysis with simulations 37
- 5.1 Parameter selection for the model 37
- 5.2 Power comparison 38
- 5.3 Sensitivity analysis of the reduction in power consumed 40
  - 5.3.1 Sensitivity with respect to the running frequency of the motor 40
  - 5.3.2 Sensitivity with respect to the resonance frequency of the system 42
  - 5.3.3 Sensitivity with respect to the co-efficient of friction in x-direction 43
  - 5.3.4 Sensitivity with respect to the co-efficient of friction in y-direction 44
  - 5.3.5 Sensitivity with respect to the friction loss torque in the motor 46

6 Validation of the mathematical model 49
- 6.1 Experiments. . . . 49
  - 6.1.1 First design of the experimental setup 49
  - 6.1.2 Experiments on the first experimental setup 53
  - 6.1.3 Second design of the experimental setup 55
  - 6.1.4 Experiments on the second experimental setup 56
- 6.2 Investigation of parameters in the experimental setup 59
  - 6.2.1 Spring constant 59

6.2.2 Friction in the motor 60
6.2.3 Friction between the cutter and the guard 63
6.2.4 Friction between the eccentric head and the drive bridge 69
6.3 Simulations using the obtained parameters 71

7 Results and discussion **73**
7.1 Comparison between simulations and experiments 73
7.2 Analysis of the comparison between simulations and experiments 74
7.2.1 Modification of parameters in the model 74
7.3 Power saved in a Philips hair clipper 76

8 Conclusion and recommendations **79**
8.1 Conclusion 79
8.2 Recommendations 80

A Electrical - mechanical analogies **83**

B SIMULINK models **87**
B.1 Ideal model in 1D 87
B.2 Real model in 2D 88

C CAD drawings and pictures **93**

Bibliography **101**

Preface

All the work presented in this report was conducted at Philips Consumer Lifestyle B.V. in Drachten in the period between 15th January and 31st December 2017.

First of all, I would like to thank Bernardo Mulder, who was my daily supervisor at Philips, for giving me the opportunity to work on this project. This project would have been extremely difficult without his guidance.

I would like to express my sincere gratitude towards Jo Spronck, who was my supervisor at TU Delft. He played a crucial role in my quest to graduate in 2018.

I would like to thank my dearest friends Pranav, Vinayak, Aniket, Tanvi, Elmira and Aleksandra for lending a helping hand when needed.

My parents have always been my pillar of strength. They have supported me throughout my life and there are no words to capture the gratefulness I feel towards them. I am lucky to be born as their child and I dedicate my work to them.

Last, but not the least, I thank Dr. Farbod Alijani and Dr. Andres Hunt for agreeing to be in my thesis defence committee.

Saurabh Shailendra Sontakke
Delft, December 2018

Summary

Philips is one of the most reputable companies in the Netherlands and also one of the top 50 global innovators. Philips is a giant in the consumer lifestyle goods and prides itself over the quality of equipment produced. Hair clippers are one of the more popular products manufactured by Philips and the hair clipper division of Philips focuses on innovation to maintain the popularity. This time, the idea was to make a resonant hair clipper which can increase the battery life and put Philips one step ahead of its competitors in the grooming market.

The aim of this project was to answer the question of whether the concept of resonance can be used in Philips hair clippers to reduce the overall power consumption without modifying the currently available driving mechanism for the reciprocating cutter, which is a combination of a permanent magnet direct current (PMDC) rotary motor and a Scotch-yoke type mechanism. An additional goal of this project is to mathematically model the hair clipper which can be used for predicting the power consumption in a Philips hair clipper.

The nature of this thesis project differs from previous research in the application of resonance in vibrating elements in consumer products. The previous inventions used an electromagnetic motor means without a rotating component to generate the reciprocating movement of an oscillating mass, while in this project, a PMDC rotary motor is used with a scotch-yoke type mechanism to oscillate the mass.

The approach to the problem was to start simple and gradually build the complexity in the problem. First, quick back-of-the-envelope calculations were done to analyze the feasibility of the project. As it was clear that there could be a possible benefit of using the concept of resonance in hair clippers, a kinematic analysis of the Scotch-yoke type motion conversion mechanism used in the hair clippers was done. A mathematical model of the system consisting of the input voltage, the DC motor, the motion conversion mechanism, and the dynamics of the cutter motion was formulated and built in SIMULINK using Simscape toolboxes. To validate the model, an experimental setup was made in the Rapid Prototyping department at Philips Drachten.

Experiments were conducted on the experimental setup and relevant data were recorded. For the first set of experiments, the springs were removed from the system. The cutter was oscillated at different frequencies ranging from $10\,\text{Hz}$ to $65\,\text{Hz}$ and the power consumed at each frequency was observed. For the second set of experiments, the cutter was oscillated at frequencies in the same range, with the springs attached to the cutter. This resulted in less power being consumed at the resonance frequency of the system, which is $26\,\text{Hz}$. This confirmed the possibility of benefiting from resonance without changing the driving mechanism in the currently produced Philips hair clippers; yes, resonance can be used to conserve energy and increase battery life.

In the quest to achieve the second goal, the parameters affecting the power consumed in the experimental setup, i.e. the friction in the motor, the friction between the cutter & the guard, the friction between the eccentric head & the drive bridge, and the stiffness of the springs used, were evaluated through separate experiments. Using these parameters, the SIMULINK model was simulated. The power consumed in the model was noted at different frequencies in both the scenarios with the springs present in and absent from the system. To check the accuracy of the model, the plots of the power consumed in the simulations at different frequencies for both scenarios were compared with the corresponding plots obtained from experiments. The plots match pretty well in the scenario where the springs are absent from the system. When the springs are present in the system, the plots match well at frequencies above $30\,\text{Hz}$; below this frequency, the simulation predicts the power consumed to be

lower than that observed in the experiments. This results in the model predicting a power saving of about 22% when the system is run at its resonance frequency while the experiments show a power saving of about 12%.

In conclusion, the use of resonance in a hair clipper is an idea worth pondering over. It can result in increasing the battery life and make Philips' hold over the consumer grooming market even stronger. In addition, a model of the hair clipper has been made, which can be used to predict the amount of power consumed by Philips hair clipper running at different speeds. This can be a useful technique to prevent over-designing of electrical elements in hair clippers, if it happens, and subsequently save a lot of money for the company.

List of Figures

1.1 Cutter and guard assembly in a common Philips hair clipper . . . 3
1.2 Eccentric head attached to the motor that drives the cutter in a common Philips hair clipper 3
1.3 Steps taken to explore whether the concept of resonance can be used to reduce the power drawn by Philips hair clippers . . . 5

2.1 Schematic representation of a mass-spring-damper system . . . 7
2.2 Composition of forces in the system at resonance . . . 8
2.3 Schematic representation of a crankshaft with a mass-spring-damper system . . . 8
2.4 Crankshaft with a mass-spring-damper system built by Fiebig and Wrobel . . . 8
2.5 Results obtained from the experiment . . . 9
2.6 Invention of Pagani . . . 10

3.1 Schematic representation of a mass-spring-damper system . . . 11
3.2 Type of torsion spring used in Philips hair clippers . . . 15
3.3 Pressure from top using compression springs and a pressure plate . . . 16
3.4 Pressure from bottom using tension springs . . . 16
3.5 Pressure from top using magnetic repulsion . . . 17
3.6 Pressure from bottom using magnetic attraction . . . 17
3.7 Resonance created with springs . . . 17
3.8 Resonance created using magnetic repulsion . . . 18
3.9 Resonance created using a leaf spring . . . 19
3.10 Friction reduced using linear bearings at the back end . . . 19
3.11 Friction reduced using embedded Teflon on the guard blade . . . 20
3.12 Friction reduced using ball & groove at the back end and a hinged knife . . . 20
3.13 Friction reduced to zero using 2 balls and maintaining a gap of 30 microns at the front end 21

4.1 Schematic of the eccentric head moving the cutter blade in x-direction . . . 24
4.2 Free body diagram of the cutter mass . . . 24
4.3 Simplified free body diagram of the cutter blade . . . 24
4.4 Electrical and mechanical sides of the motor . . . 26
4.5 Courtesy: [1] . . . 26
4.6 Electrical model of the motor . . . 27
4.7 Power input observed when no springs are used . . . 27
4.8 Power input observed when springs are used . . . 27
4.9 Angular speed of the motor when cutter mass is present . . . 28
4.10 Angular speed of the motor when cutter mass is absent . . . 29
4.11 Representation of the system with a simple pendulum . . . 31
4.12 Forces acting on the eccentric head . . . 31
4.13 Forces contributing to the load torque . . . 31
4.14 Electrical model of the motor . . . 33
4.15 Forces exerted by the motor in the x- and y-directions . . . 33
4.16 Electrical representation of the conversion of the motor's rotary motion to translation of the cutter mass . . . 34
4.17 Mathematical model of the whole system . . . 35

5.1 Power consumed when a 3 gm system without springs is run at 6000 RPM . . . 38
5.2 Power consumed when a 3 gm system with springs is run at 6000 RPM . . . 39
5.3 Power consumed when a 3 gm system without springs is run at 6000 RPM with very low x-direction friction . . . 39

5.4 Power consumed when a 3 gm system with springs is run at 6000 RPM with very low x-direction friction . . . 40
5.5 Comparison of power consumed with and without a resonant system when the motor frequency is varied . . . 41
5.6 Zoomed in image of the comparison of power consumed with and without a resonant system when the motor frequency is varied . . . 41
5.7 Reduction of power in percentage when the motor frequency is varied . . . 42
5.8 Percentage reduction in power when the resonance frequency of the system is varied . 43
5.9 Comparison of power consumed with and without resonance when the co-efficient of friction in x-dir. is varied . . . 44
5.10 Reduction of power in percentage when the co-efficient of friction in x-dir. is varied . . 44
5.11 Comparison of power consumed with and without resonance when the co-efficient of friction in y-dir. is varied . . . 45
5.12 Reduction of power in percentage when the co-efficient of friction in y-dir. is varied . . 45
5.13 Percentage reduction of power when the friction loss torque in the motor is varied . . . 46

6.1 Friction reduced using linear bearings at the back end . . . 49
6.2 Resonance created with springs . . . 50
6.3 Pressure from bottom using tension springs . . . 50
6.4 Experimental setup in NX . . . 51
6.5 Experimental setup in NX (magnified) . . . 51
6.6 Comparison of power consumed with and without springs in the first experimental setup 54
6.7 Comparison of torque required to run the motor with and without springs in the first experimental setup . . . 54
6.8 New experimental setup in NX . . . 56
6.9 New experimental setup in NX . . . 56
6.10 Comparison of power consumed with and without springs in the second experimental setup . . . 57
6.11 Comparison of torque required to run the motor with and without springs in the second experimental setup . . . 58
6.12 Comparison of average power consumed with and without springs in the second experimental setup . . . 59
6.13 Mecmesin load tester used in the experiment . . . 59
6.14 Characterization of resonance springs . . . 60
6.15 Generic representation of friction torque characteristics in a motor . . . 61
6.16 Plot of back emf generated in the test motor against its running speeds. the slope of this graph is the motor constant . . . 61
6.17 Plot showing the difference between motor friction torque when both motors are coupled and are run by the reference motor and when only reference motor is running. . . . 63
6.18 Polytec laser vibrometer OFV-552 . . . 64
6.19 Measurement of free vibration taken with a laser vibrometer . . . 65
6.20 The extreme displacement points fitted with a straight curve . . . 66
6.21 The extreme displacement points fitted with an exponential curve . . . 66
6.22 The extreme displacement points fitted with a combination of a straight curve and an exponential curve . . . 66
6.23 Linear decay of amplitude in presence of pure Coulomb friction . . . 67
6.24 Exponential decay of amplitude in presence of pure viscous friction[2] . . . 68
6.25 Friction characteristics in y-direction . . . 70
6.26 Comparison of power consumed with and without springs in simulations . . . 72

7.1 Comparison of power consumed in the experiments with that predicted by simulations 73
7.2 Comparison of power consumed in the experiments with that predicted by simulations without viscous friction in x-direction . . . 75
7.3 Comparison of power consumed in the experiments with that predicted by simulations with zero viscous friction and elevated Coulomb friction in x-direction . . . 76
7.4 Comparison of power consumed in a Philips hair clipper with and without springs . . . 78

8.1 Comparison of power consumed in the experiments with that predicted by simulations 80

A.1 A simple spring-mass-damper system 83
A.2 Electrical analogy of the mass-spring-damper system 85
A.3 Electrical analogy of a rotational-inertia-torsion-spring-torsion-damper system 85

B.1 SIMULINK model of the system with angular speed of the motor as input 87
B.2 SIMULINK model of the motor 87
B.3 SIMULINK model of the whole system with voltage as input to the motor 88
B.4 SIMULINK model of the whole system 90
B.5 SIMULINK model of the DC motor 91
B.6 SIMULINK model of the motion conversion from rotary to translation 92

C.1 A picture of the experimental setup 99
C.2 A picture of the motor and the eccentric head 99
C.3 A picture of the springs used in the setup 100
C.4 A picture of the linear bearings used in the setup - SKF LBBR3 100
C.5 A picture of the extension of the motor shaft used to find out the friction between the eccentric head and the drive bridge 100

List of Tables

3.1 A list of different concepts for different purposes 21

4.1 Spring force at different points in the path of the cutter 25

5.1 Values of motor parameters selected for simulation 37
5.2 Values of driven system parameters selected for simulation 38

6.1 A list of parts used in the experimental setup 52
6.2 Values of motor parameters obtained from motor characterization experiment 63
6.3 Values of system parameters obtained from the y-direction friction characterization experiment 70
6.4 Values of parameters of the experimental setup which are obtained from experiments . 71

7.1 Comparison between simulations and experiments 73
7.2 Comparison between simulations and experiments after modification of parameters . . 75

8.1 Comparison between simulations and experiments after modification of parameters . . 79

1. Introduction

Philips is a successful brand in the consumer electronics market, especially in the grooming market. For the eleventh consecutive year, Philips was named the most reputable company in the Netherlands in the annual RepTrak® rankings carried out by the Reputation Institute Benelux [3]. The Boston Consulting Group's worldwide survey published in January 2018 named Philips among the top 50 global innovators of the year [4]. For the survey, the Boston Consulting Group interviewed senior global innovation executives and studied Philips' performance in the marketplace [5]. To maintain such a status in the public eye and in the corporate world, Philips strives to be better than its competitors in every way possible. The hair clipper division always works hard to deliver the best it can for its customers and tries to bring in exciting innovations to the market. This time, the idea is to explore the possibility of introducing a resonant hair clipper in the grooming market. Philips hair clippers would obviously become more appealing to consumers if they can provide for more battery life; the resonant groomer is expected to be able to do the same. Before getting to mathematics and analysis involved it is important to understand the concept of resonance and look at it from an energy point of view.

1.1. Resonance from the energy perspective

It is better to look at resonance in an intuitive way rather than in a mathematical way. The concept of resonance is best applied, although unknowingly, in everyday life in playgrounds meant for children. When a child sits on a swing and a parent stands behind the swing to give a push, the parent applies the concept of resonance inadvertently.

Imagine that a swing is in motion with a child on it; the motion of the swing is a simple harmonic motion. The child's velocity is the highest when it is at the centre of the oscillation and it is zero at both the extreme points on both sides of the centre of oscillation. Picture the parent to be standing just a foot away from one of the extreme points of oscillation. As the swing travels from the centre of oscillation towards the parent, its velocity goes on decreasing and it becomes zero as it reaches the parent. The parent gives a small push to the swing. The swing goes back to the centre of oscillation, then to the other extreme point, then come back to the centre of oscillation and then back to the parent. This time the swing comes even further towards the parent, which means that there is an increase in the amplitude of oscillation of the swing, so the parent takes a step back and pushes the swing again. This goes on until the swing oscillation reaches the maximum safe amplitude as considered by the parent and then the parent stops pushing the swing. The swing slows down gradually and eventually comes to a halt.

Little known to the parent is the concept of resonance, but he uses it so well to spend the least possible amount of energy to get to the desired amplitude of oscillation of the swing. The parent pushes the swing every time it comes to the extreme point near him; this means that the frequency of the force input matches the frequency of the swing oscillations. Considering that there is some friction in the swing bearings, if the parent provides a certain amount of energy to the swing that is just enough to overcome the energy dissipated due to friction in every cycle of oscillation, the amplitude of the swing oscillation will remain constant. When the parent wants to increase the amplitude of the swing oscillation, he provides more energy than that. When the parent thinks that the maximum safe amplitude of

swing oscillation has been reached and the amplitude should decrease, he simply allows the energy in the oscillating swing to get dissipated through friction and doesn't provide any energy to the system.

The important point to note in this every day scenario is that the parent pushes the swing only at the extreme points, that is when the swing is at a temporary halt. As a result of this, the parent does not waste any energy in stopping the swing. Now imagine that the frequency of application of force by the parent is different than the frequency of oscillation of the swing, the direction of force application being the same as before. There will come a time when the parent will apply a force that is in the direction opposite to that of the velocity of the swing. In this case, the force applied by the parent will be opposed by the momentum of the swing. In other words, the energy expended by the parent will be used in breaking the swing in contrast to the intention which was to accelerate it. This will result in the braking of the swing and instead of the amplitude increasing, it will decrease. This is the result of not matching the forcing frequency with the oscillation frequency of the swing, which is its natural frequency. It can be concluded from this thought experiment that to achieve the same amplitude of the swing, the least amount of energy is used when the forcing frequency matches with the natural frequency of the swing.

For a moment imagine that the swing has no friction in its bearings. All the potential energy that the swing has when it is at the extreme point of oscillation starts getting converted into kinetic energy as it moves towards the centre of oscillation. At the centre of oscillation, there is no potential energy in the swing but the kinetic energy is at the maximum value that it can be. As it goes to the other extreme point, the kinetic energy is again converted into potential energy completely and this whole process repeats as the swing comes back to the parent. This conversion of energy will go on until eternity if there is no friction in the system. As in reality there is friction, some energy is lost in every cycle of oscillation. This means that the total energy in the swing at the same point goes on decreasing in consecutive cycles; this corresponds to a decrease in amplitude of the swing. If the energy provided by the parent is just enough to overcome the energy lost due to friction, this kind of system can work with constant amplitude. Hence, it can be concluded that when the forcing frequency, which is also called the excitation frequency, matches the natural frequency of the swing, the only input energy required to be given to the system is the energy required to overcome the energy lost in friction.

These concepts hold true in all resonating systems and not only in pendulums. The important ingredients to create resonance are an element that can possess kinetic energy, which can be just a mass, an element that can store and release energy, which can be a spring element, and a forcing element that can apply the force at the same frequency as the natural frequency of the system, which can be a linear motor or a rotary motor with a mechanism to convert the rotational motion to translation motion.

1.2. State-of-the-art Philips hair clippers

In the Philips hair clippers that are currently available in the market, a rotary motor is fitted with an eccentric pin, also called the eccentric head, on its shaft as shown in Fig. 1.2. As the motor shaft rotates, the eccentric head revolves around the centre of the shaft. This eccentric head is inserted in a long slot made in a plastic drive bridge which is attached firmly to the metal cutter as shown in Fig. 1.1. The cutter and the drive bridge are allowed to move only in one direction, which is the direction of cutting hair. This is achieved by using a torsion spring to keep the cutter and the guard always in contact with each other. The eccentric head is free to slide in the drive bridge slot. This converts the rotational motion of the motor into the translation motion of the drive bridge and the cutter, just like the famous scotch-yoke mechanism. The cutter rests on a stationary guard as the relative motion between the oscillating cutter and the guard is used to cut hair.

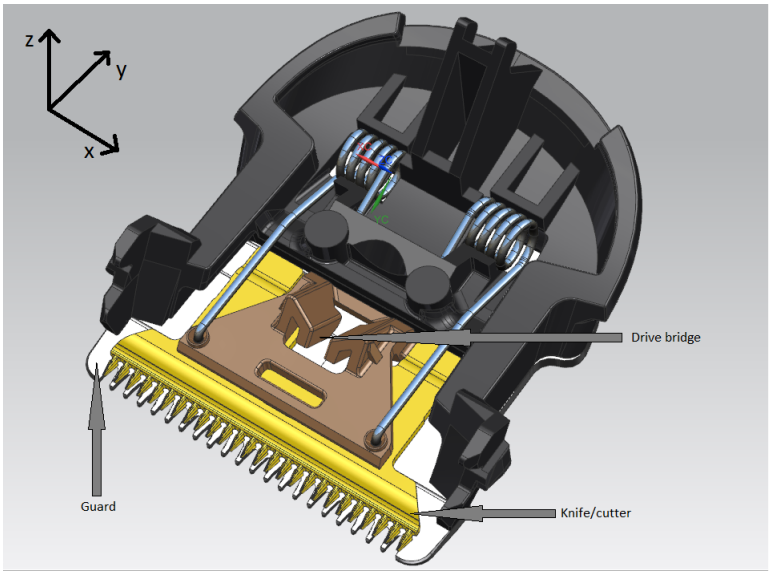

Figure 1.1: Cutter and guard assembly in a common Philips hair clipper

Courtesy: Philips Consumer Lifestyle B.V.

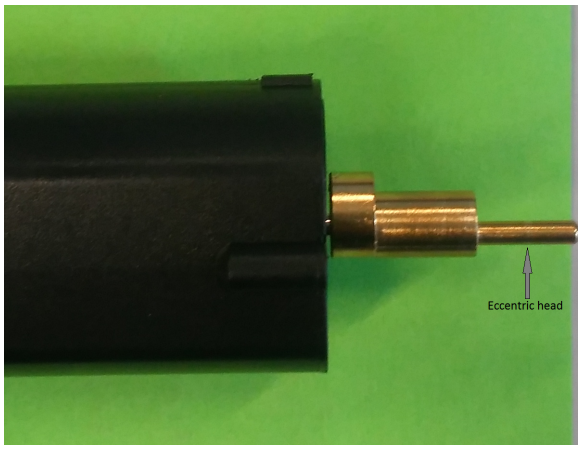

Figure 1.2: Eccentric head attached to the motor that drives the cutter in a common Philips hair clipper

Courtesy: Philips Consumer Lifestyle B.V.

During every oscillation of the cutter, the motor has to provide the energy required to accelerate the cutter to the centre of the oscillation and then provide the energy to decelerate the cutter while it moves to its extreme point of oscillation. In one complete cycle there are two acceleration periods and two deceleration periods that come alternatively. This is a kind of brute force approach to the operation and entails a lot of waste of energy.

If a spring element is introduced in the driven system, it becomes a mass-spring system instead of the current mass system and the equation of energy consumed changes drastically. The mass can possess kinetic energy and the spring can store and release potential energy, as discussed earlier. The complete system becomes very similar to the swing and parent system, the driven mass-spring system being the swing and the motor being the parent. If the system is excited at its natural frequency, the energy required to accelerate and decelerate the cutter will be provided by the spring. There will be no time instant when the motor tries to decelerate the cutter mass, thus, it will not use energy in that sense. The motor will have to provide for nothing more than the energy lost due to friction in each

cycle. Hence, this kind of system can save a lot of energy. In other words, the current drawn form the battery will reduce to a very low value, which in turn means that either Philips can use a smaller battery in their hair clippers or the same battery will last for a longer period of time. Both the possibilities are beneficial to the consumers and will give Philips an advantage over its competitors. An important point to note here is that the torsion spring used to maintain contact between the cutter and the guard does provide some stiffness to the system in the x-direction as shown in Fig. 1.1, but this stiffness is not known and it is not known to the designers at Philips whether these springs are manufactured for the purpose of resonance. It is a common consensus that these springs are primarily for the purpose of maintaining enough pressure over the cutter so that it does not bounce during the cutting of hair.

Of course, when the clipper is cutting hair, the dynamics of the system will get altered as the hair will act as external forces acting on the system in addition to the force provided by the motor, and the resonance won't be as effective as it is when the clipper runs idle. It has been observed by the Customer Research department at Philips that on an average for more than 50% of the time of operation of a normal hair clipper by a randomly selected customer, the hair clipper runs idle. This makes it worthwhile to investigate the effects of introducing resonance in the system.

1.3. Problem statement of the thesis

1. The aim of this project is to answer the question of whether the concept of resonance can be used in Philips hair clippers to reduce the overall power consumption without having to modify the currently available driving mechanism for the reciprocating cutter, which is a combination of a permanent magnet direct current (PMDC) rotary motor and a Scotch-yoke type mechanism.
2. It is also a goal of this project to mathematically model the hair clipper so that the model can be used for predicting the power consumption in a Philips hair clipper.

The hypothesis, based on first thought, is that resonance will be helpful in saving power, but how helpful it will be and whether it will be worth investing in this project cannot be answered without analyzing the problem in a detailed manner. The objective of the thesis is to know whether the hypothesis is correct.

1.4. Method of approach to the problem

To explore the possibility of introducing the concept of resonance in hair clippers while maintaining the design of the drive train, the steps shown in Fig. 1.3 are taken. Until now, the idea has been generated and the thesis problem has been already formulated. The next steps are as follows:

1. Quick **back-of-the-envelope calculations** are done to analyze the feasibility of the project.
2. **Kinematic analysis** of the motion conversion mechanism and the reciprocating system is carried out.
3. A **mathematical model** of the whole system, meaning, the input voltage, the DC motor, the motion conversion mechanism, and the dynamics of the cutter motion, is formulated using an analytic approach. The model is built in **Simulink** using Simscape toolboxes.
4. **Simulations** are carried out in different conditions by changing the values of different parameters like motor speed, motor friction, friction between the cutter and the blade, friction between the eccentric head and the drive bridge, value of the spring constant, etc.
5. The **model is validated** by building an **experimental setup** with all the important degrees of freedom as there are in the actual hair clipper. Experiments are carried out on the setup to check whether there is any energy advantage when resonance is introduced in the system. Plots obtained from the experiments are superimposed over the plots obtained from the simulations and the accuracy of the model is checked.

6. If the model is found to be accurate enough, **predictions** are made regarding feasibility of introducing resonance in actual hair clippers which might run under different conditions than that chosen for the experimental setup.

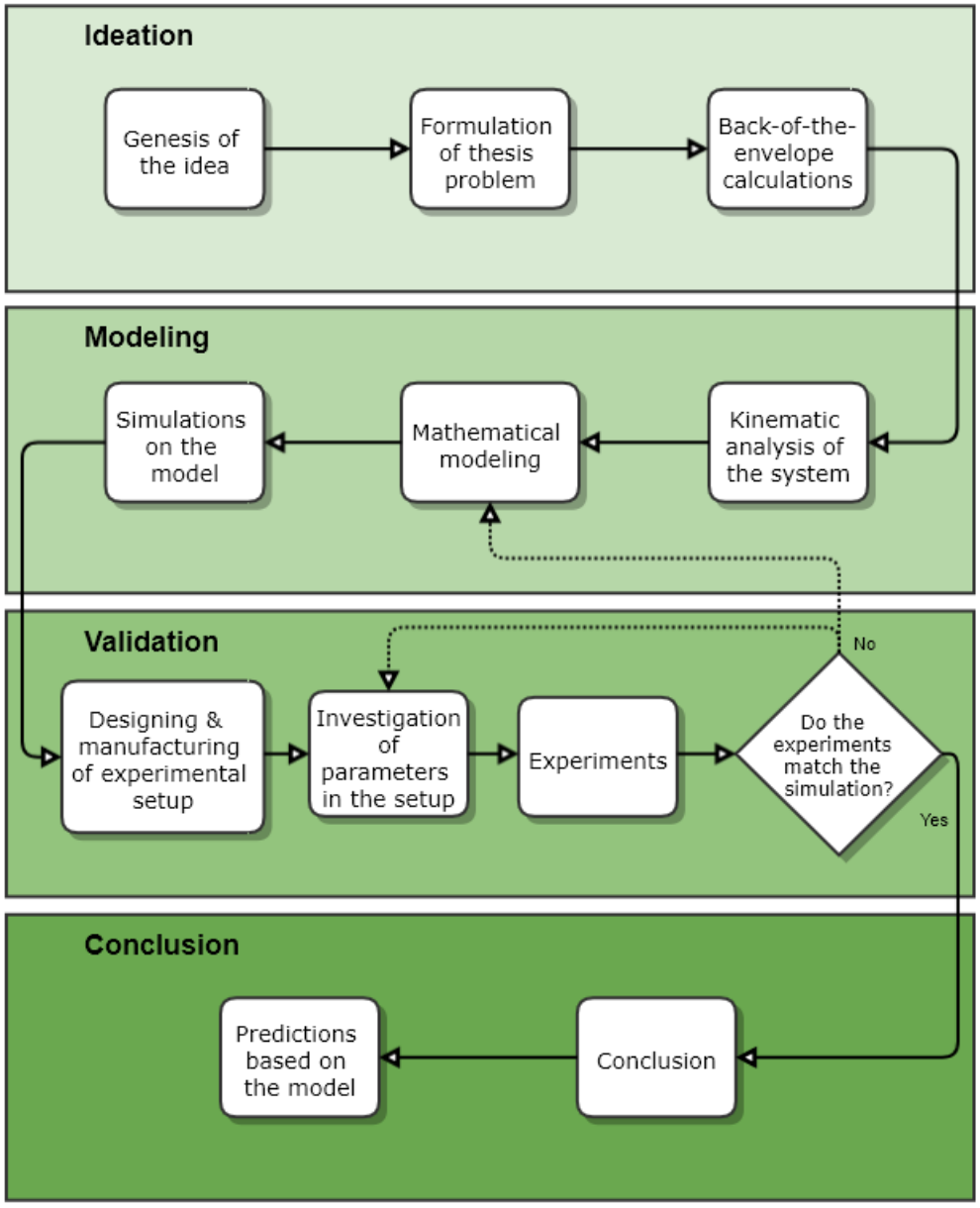

Figure 1.3: Steps taken to explore whether the concept of resonance can be used to reduce the power drawn by Philips hair clippers

2. Literature survey

In most of the mechanical engineering applications, resonance is looked at as a bane and not a blessing. As resonance causes increased vibrations, it can produce fatigue in the vibration components. It can also be looked at as a disturbance causing phenomenon in high precision applications. The most famous example of resonance acting as a menace is the failure of the Tacoma Narrows Bridge in Washington, USA. On the contrary, some good qualities of the resonance phenomenon can also be capitalized on. Fiebig and Wrobel in [6] explain some of the ways in which mechanical resonance can be useful in saving energy.

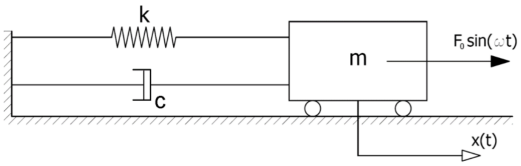

Figure 2.1: Schematic representation of a mass-spring-damper system

Courtesy: [6]

A schematic representation of a harmonically excited mass-spring-damper (m-s-d) system is shown in Fig. 2.1. The forces acting in the driven system are the spring force, the inertia force of the mass and the damping force. The external force acting on the system is harmonic with the frequency ω which is equal to the natural frequency of the m-s-d system so that the system is in the state of resonance. The amplitude of the excitation force is kept such that the amplitude of oscillation of the mass does not change over time. Figure 2.2 presents the time variation of the forces acting in the system when it is in such a state. It can be seen that the inertia force and the spring force at resonance have the same amplitude but are shifted in phase by 180^0 Hence, their sum is equal to zero at all times. This means that the acceleration and deceleration of the mass is taken care of by the spring. The excitation force is used to overcome the damping force only. This is analogous to the parent-swing example.

Fiebig and Wrobel further verified the simulated results with an experiment, a simple representation of which is shown in Fig. 2.3. They constructed a system that consists of an oscillating mass driven by a crankshaft system which was driven by an AC motor as shown in Fig. 2.4a and 2.4b. The mass was connected to 4 springs, two on each side, and was mounted on a low friction slide. The rpm of the AC asynchronous motor was increased over time, starting from zero. They measured the force in the crankshaft with a force sensor and the displacement of the mass with a laser vibrometer.

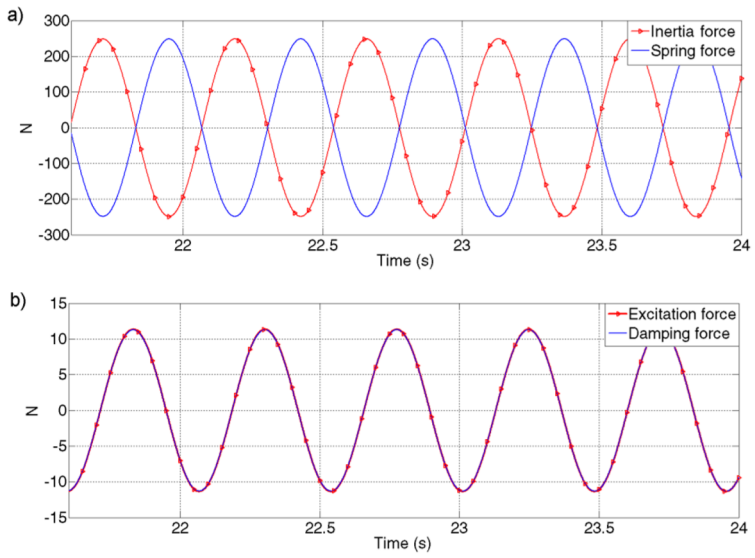

Figure 2.2: Composition of forces in the system at resonance

Courtesy: [6]

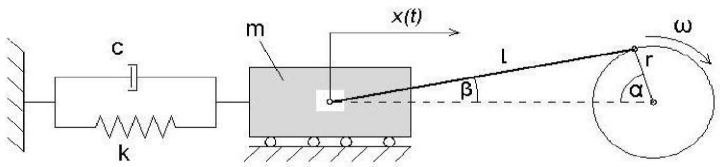

Figure 2.3: Schematic representation of a crankshaft with a mass-spring-damper system

Courtesy: [6]

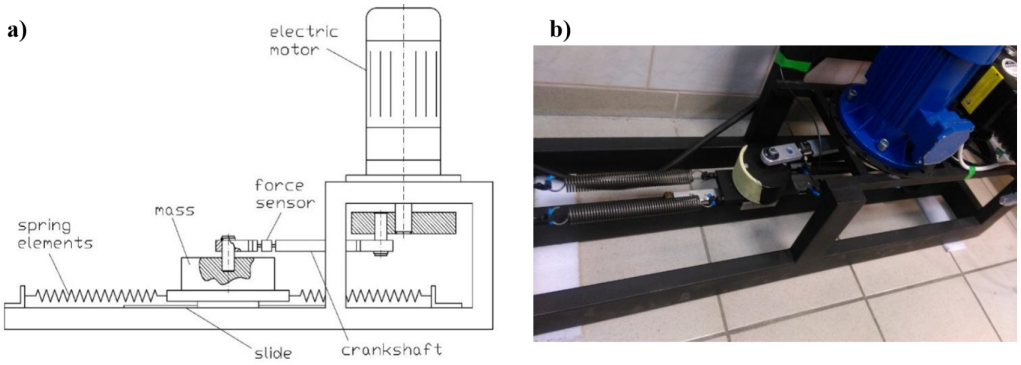

Figure 2.4: Crankshaft with a mass-spring-damper system built by Fiebig and Wrobel

Courtesy: [6]

Figure 2.5 shows the displacement of the oscillating mass and the force in the crankshaft plotted against time. Figure 2.5b shows the force acting on the crankshaft when the springs were removed from the system and figure 2.5c shows the force acting on the crankshaft when the springs were added to the system. In the first case, the amplitude of the force went on increasing as the frequency of oscillation increased. This is attributable to the increase in inertia forces of the mass at as the frequency increases. In the second case, the amplitude of the force decreased as the frequency of oscillation approached the natural frequency of the m-s-d system. It was minimum at the point of resonance after which

it increased again. The amplitude of the force was not zero at resonance because the motor had to overcome the friction in the system. Had the friction been zero, the amplitude would have been zero at resonance. Figure 2.5a shows the variation in displacement of the mass with time which is the same in both the conditions. The reduction in amplitude of the force acting on the crankshaft at the point of resonance meant a reduction in amplitude of the load torque experienced by the motor. This led to a reduction in the current drawn and as a result in the power required to oscillate the mass.

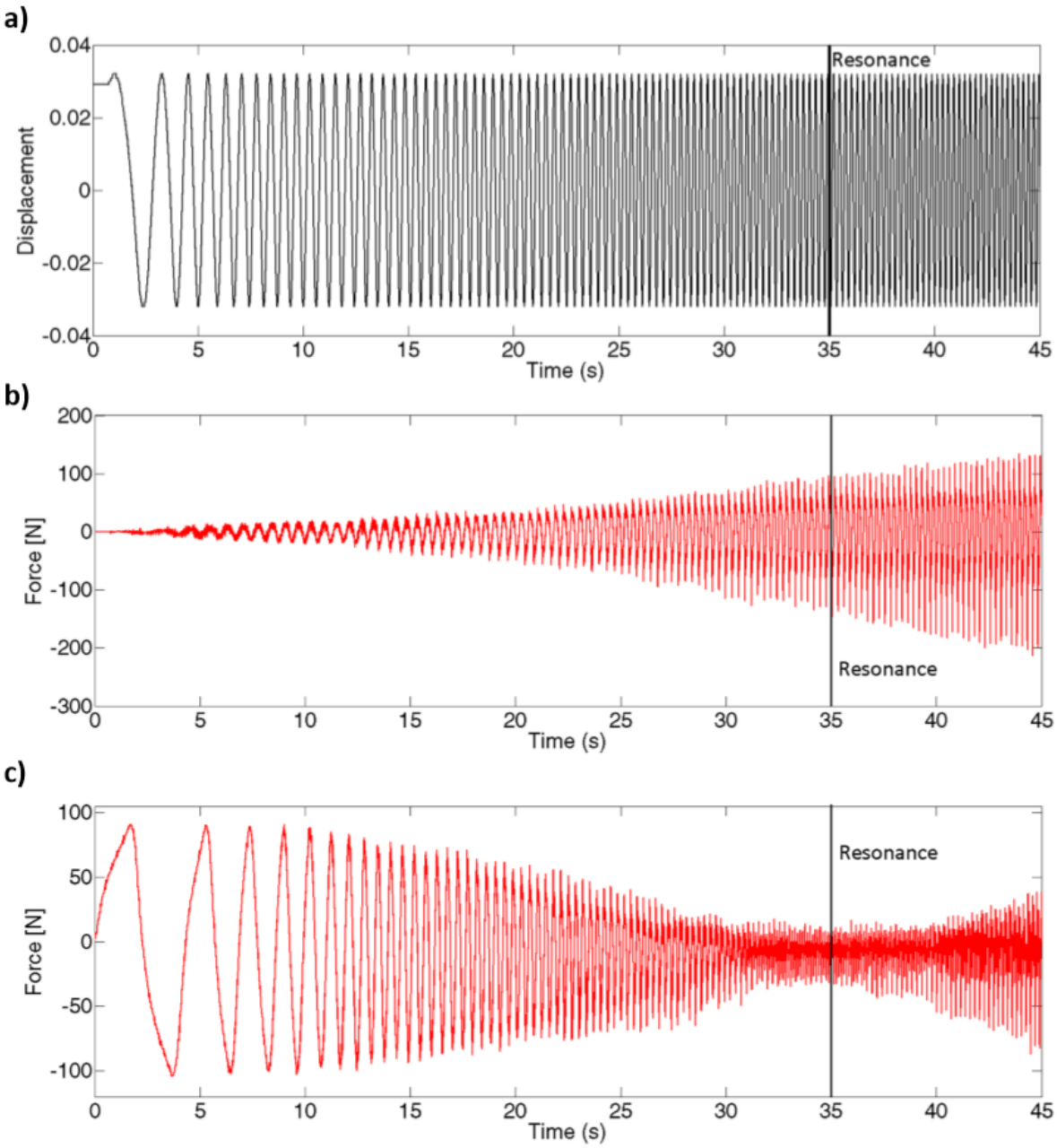

Figure 2.5: Results obtained from the experiment

Courtesy: [6]

Inventors have thought about using the phenomenon of resonance to their advantage in grooming equipment prior to this project. Pagani, in 1975, patented a reciprocating razor in which the guard is reciprocated and the cutter is kept steady [7]. The guard is oscillated by using a coil which is capable of providing an alternating flux on two sides of the guard, which is made of a magnetic material.

Another preferred embodiment of the patented invention was the inclusion of a ”resiliently deflectable” material or segment of magnetic material attached on one end to the guard and on the other end to the stationary body of the razor. In this case, the coil is used to deflect this ”resiliently deflectable element” to either sides, which in turn reciprocates the guard. The deflectable element is made in the form of a tuned reed which can be tuned to resonate at the reciprocation frequency of the guard. Figure 2.6 shows one of the representations of the invention as presented by the inventor in his patent application [7]. The tuned reed is shown as the object number 61. It is essentially used as a spring element and the guard mass is reciprocated with the help of an alternating flux producing coil arrangement.

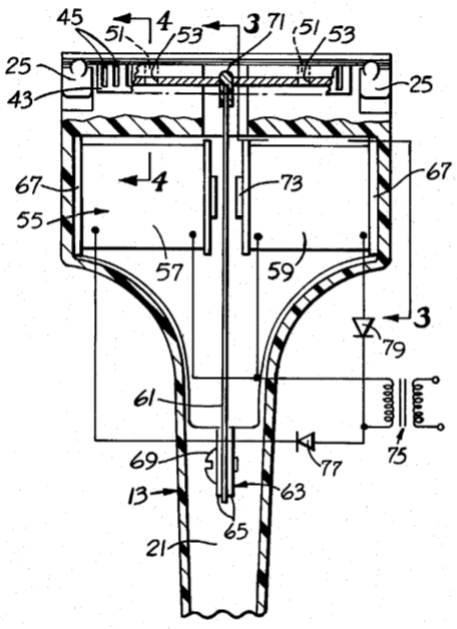

Figure 2.6: Invention of Pagani

Courtesy: [7]

Furthermore, inventors have also come up with different motors of similar type wherein there is a reciprocating mass element, a spring element and an electromagnetic motor means to make the mass reciprocate. In some of these inventions, instead of using a tuned reed made of a magnetic material to cause the oscillations, like it was used by Pagani, a permanent magnet is used. Different inventors have named it differently; Green called it an ”Alternating current oscillating motor” [8], Heyek called it a ”Vibratory motor” [9] while Marinescu called it an ”Electric motor with alternating linear motion” [10]. Every invention had a change in the type of construction of the whole system or one of the elements of the system. Ibuki et. al used a similar system in an epilator and further controlled the motion of the reciprocating mass using a controller [11].

The nature of this thesis project is different than the previous research in the sense that all the previous inventions used an electromagnetic motor means without a rotating component to generate the reciprocating movement of the oscillating mass, while in this project, a PMDC rotary motor is used with a scotch-yoke type mechanism to oscillate the mass.

3. A quick look at the practical possibility

It is always a good practice to do some back of the envelope calculations to assess the feasibility of a project before diving deep into analytic or numerical solutions. A preliminary analysis of whether it is possible to save some power by introducing resonance in hair clippers is done below.

3.1. Preliminary analysis

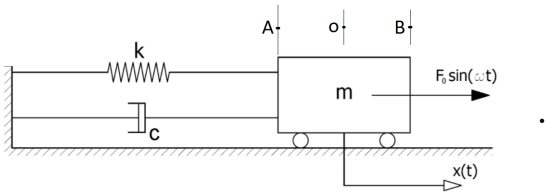

Figure 3.1: Schematic representation of a mass-spring-damper system

Courtesy: [6]

Consider an m-s-d system as shown in Fig. 3.1. As mentioned in the previous chapter, there is continuous conversion of kinetic energy into potential energy and vice-versa in a vibrating system like this.

When the springs are not attached to the system, the system becomes a mass-damper system and the energy required to run the system can be calculated as explained in the coming sections.

Energy to overcome inertia forces

The motor has to accelerate the mass while moving the centre of the mass from point A to point O. The mass has zero Kinetic energy at point A and has the maximum kinetic energy at point O. The motor has to provide this energy to the mass.

$$E_{max} = \frac{1}{2} m {v_{max}}^2 = \frac{1}{2} m r^2 \omega^2 \tag{3.1}$$

where E_{max} is the maximum kinetic energy of the mass, m is the mass, v_{max} is the maximum velocity of the mass, which occurs at point O, r is the amplitude of oscillation and ω is the frequency of the oscillation.

The motor has to then decelerate the mass as its centre moves from point O to point B. In this movement, the kinetic energy of the mass reduces from its maximum value as mentioned in Eq. 3.1 to its minimum value which is zero. The motor bears the work of achieving this ans so, it again expends energy equivalent to the kinetic energy lost by the mass in this quarter cycle.

This process of acceleration and deceleration happens twice in one cycle of oscillation. Thus energy expended by the motor to accelerate and decelerate the motor is given by the following formula:

$$E_1 = 2mr^2\omega^2 \tag{3.2}$$

Energy to overcome Coulomb friction

As shown in Fig. 2.1 there is friction between the mass and the surface that it is resting on. The motor has to give energy to overcome this friction. The work that the friction does in quarter of a cycle is given by the product of force and displacement.

$$W = \mu N r \tag{3.3}$$

where μ is the co-efficient of friction between the two surfaces and N is the normal force acting on the mass.

Hence the total work done by the friction force in one complete cycle, which is also the total energy expended by the motor to overcome Coulomb friction in one cycle of oscillation is given by the following formula:

$$E_2 = 4\mu N r \tag{3.4}$$

Energy to overcome viscous friction

The motor has to also provide energy to overcome the dissipation due to viscous damping. Energy dissipated in one cycle due to viscous damping is given by the following formula [12]:

$$E_3 = \pi c \omega r^2 \tag{3.5}$$

Total energy spent when there are no springs in the system

The total energy spent by the motor in one cycle is the summation of the three energies mentioned above.

$$E_n = E_1 + E_2 + E_3 \tag{3.6}$$

If there is only Coulomb friction in the system, $E_3 = 0$ and the total energy spent by the motor in one complete cycle is given by the following formula:

$$E_n = E_1 + E_2 \tag{3.7}$$

The "n" in E_n represents the fact that the springs aren't present in the system ("NO").

Total energy spent when there is resonance

When the forcing frequency matches the natural frequency of the m-s-d system resonance occurs. During this phenomenon, the inertia forces of the mass are completely nullified by the spring forces as shown in Fig. 2.2. Hence the total energy expended by the motor is given by the following formula:

$$E_y = E_2 + E_3 \tag{3.8}$$

The "y" in E_n represents the fact that the springs are present in the system and the system is running at resonance ("YES").

If there is only Coulomb friction in the system, $E_3 = 0$ and the total energy spent by the motor in one complete cycle is given by the following formula:

$$E_y = E_2 \tag{3.9}$$

Energy saved by using the concept of resonance

The energy saved due to resonance is given by the difference between the energy expended in the absence of springs and the energy expended when the system is in resonance.

In the case that viscous friction is absent, $E_3 = 0$ and the energy saving quotient is given by the following formula:

$$S = \frac{E_n - E_y}{E_n} = \frac{E_1}{E_1 + E_2} = \frac{2mr^2\omega^2}{2mr^2\omega^2 + 4\mu Nr} \tag{3.10}$$

$$\therefore \quad S = \frac{1}{1+\phi} \tag{3.11}$$

where,

$$\phi = \frac{4\mu Nr}{2mr^2\omega^2} \tag{3.12}$$

ϕ is the ratio of the energy needed per cycle to overcome Coulomb friction to the energy needed per cycle to overcome inertia forces. It can be called the Coulomb friction influence factor.

In the case that Coulomb friction is absent but viscous friction is present, $E_2 = 0$ and the energy saving quotient is given by the following formula:

$$S = \frac{E_n - E_y}{E_n} = \frac{E_1}{E_1 + E_3} = \frac{2mr^2\omega^2}{2mr^2\omega^2 + \pi c\omega r^2} \tag{3.13}$$

$$\therefore \quad S = \frac{1}{1+\psi} \tag{3.14}$$

where,

$$\psi = \frac{\pi c\omega r^2}{2mr^2\omega^2} \tag{3.15}$$

ψ is the ratio of the energy needed per cycle to overcome viscous friction to the energy needed per cycle to overcome inertia forces. It can be called the viscous friction influence factor.

In the case where there are both Coulomb and viscous types of friction present in the system, the energy saving quotient is given by the following formula:

$$S = \frac{E_n - E_y}{E_n} = \frac{E_1}{E_1 + E_2 + E_3} = \frac{2mr^2\omega^2}{2mr^2\omega^2 + 4\mu Nr + \pi c\omega r^2} \tag{3.16}$$

$$\therefore \quad S = \frac{1}{1+\phi+\psi} \tag{3.17}$$

$$\therefore \quad S = \frac{1}{1+\chi} \tag{3.18}$$

where,

$$\chi = \phi + \psi \tag{3.19}$$

$$\therefore \quad \chi = \frac{4\mu Nr + \pi c\omega r^2}{2mr^2\omega^2} \tag{3.20}$$

χ is the ratio of the energy needed per cycle to overcome the total friction to the energy needed per cycle to overcome inertia forces. It can be called the total friction influence factor.

Energy saved in hair clippers using the concept of resonance

Using the data provided by the design team, for a generic Philips hair clipper, the mass of the cutter may range anywhere between 3 g and 3 g. For the sake of this calculation, mass is taken as $m = 10\,\mathrm{g}$, amplitude of oscillation is $r = 2\,\mathrm{mm}$, co-efficient of friction $\mu = 0.4$, normal force $N = 3.5\,\mathrm{N}$ and the motor speed $\omega = 628\,/\mathrm{s}$ which is 6000 rpm. It has been observed by the design team that Coulomb friction dominates over viscous friction in these hair clippers and so, viscous friction can be neglected. Using the equations 3.2, 3.4, 3.7, 3.9 and 3.10, the following calculation can be done.

$$\begin{aligned} E_1 &= 2mr^2\omega^2 \\ &= 2 \times 0.003 \times (0.002)^2 \times (628)^2 \\ &= 0.0095 \end{aligned}$$

$$\begin{aligned} E_2 &= 4\mu N r \\ &= 4 \times 0.4 \times 3.5 \times 0.002 \\ &= 0.0112 \end{aligned}$$

$$E_n = E_1 + E_2$$
$$E_y = E_2$$

$$\begin{aligned} S &= \frac{E_n - E_y}{E_n} = \frac{E_1}{E_1 + E_2} \\ &= \frac{0.0095}{0.0095 + 0.0112} \end{aligned}$$

$$\therefore \quad S = 0.46 \tag{3.21}$$

This shows that energy consumption per cycle can be reduced by 46% if the concept of resonance is used in Philips hair clippers. Hence, it is indeed worthwhile to investigate further with a more detailed analysis of the system. Of course, this estimate does not take into account the losses in the motor and the friction losses in the contact between the eccentric head and the drive bridge. How much energy can actually be saved in reality needs to be calculated with a deep dive into the matter.

3.2. Practical possibility

It is necessary to have a quick look at how such a concept of resonance can be realized in the future before it is investigated for the amount of power saved. This will provide further motivation to go ahead with the thesis project.

To get good resonance characteristics, it is necessary to have as low friction in the system as possible. That is why in some of the current trimmer systems, a ball is used between the cutter blade and the guard at the back end, which is the non-cutting end, although the front end, that is the cutting end, has friction between the two steel components. Although it is not a standard ball bearing that is used, henceforth, this method of creating a bearing between the 2 components using a ball will be called the ball bearing method and the bearing will be called a ball bearing.

For the smooth operation of a ball bearing, it is necessary to have high level precision and if friction is present in the system, high level precision is difficult to obtain. If, because of the friction at the front end, there is some bouncing of the cutter, then that would compromise the precision guiding that the

ball needs to function smoothly as a bearing. That may result in slipping of the ball instead of pure rolling. It may also result in sideways movement of the ball, which is not desired. Analysis of systems where such a ball bearing was installed shows that wear marks (grooves) appear on the guard surface at the back end where the ball is supposed to roll smoothly. The reason could also be that there is not enough pressure on the cutter to avoid such bouncing.

Figure 3.2: Type of torsion spring used in Philips hair clippers

Other than that, the torsion spring that is currently used in the system to create pressure as shown in Fig. 3.2 and figure 1.1 gives some stiffness to the movement of the cutter in the direction of allowed movement of the cutter. This direction is called the x-direction from this point onward. The main purpose of this spring in the assembly is to stop the cutter from moving in the direction away from the guard, that is moving in a way that it will lose contact with the guard. This direction is called the z-direction henceforth. Although possible to approximate, it is difficult to accurately estimate the stiffness of this spring in the x-direction because of the way it bends at the middle when the 2 extreme points are dragged by the cutter in the x-direction. If a resonant system is to be created, the stiffness in the system needs to be known accurately.

Hence, in order to make a resonant system, the following aspects become important to explore:

1. Creation of pressure without influencing the stiffness
2. Reduction of friction
3. Creation of spring element for resonance

It becomes important to design something that would reduce the friction but at the same time avoid the above mentioned phenomenon of bouncing of the cutter at the back end. Linear bearings can be an option to explore. If at the back end, instead of a ball, a linear bearing is installed, there would be no effect of the friction at the cutting end on its performance. The smallest bearings that could be found on the internet were with an inner diameter of $3\,\mathrm{mm}$. Initial thought is that it would be difficult to implement such big bearings in the actual trimmer because of the size. This option can be explored in detail at a later stage of the project but won't be a part of this thesis project. The aforementioned aspects of design of a resonant hair clipper are discussed as an overview in the text below.

Terminology used for directions

The cutter reciprocates relative to the guard in order to achieve the hair clipping action. This direction of motion is called the x-direction. The direction perpendicular to the x-direction but in the same plane as the surface of contact between the cutter and the guard is called the y-direction. The direction perpendicular to the this plane is called the z-direction. These directions are shown in Fig. 1.1.

3.2.1. Creation of pressure without influencing stiffness

1. *Use of pressure plate and ball bearings*

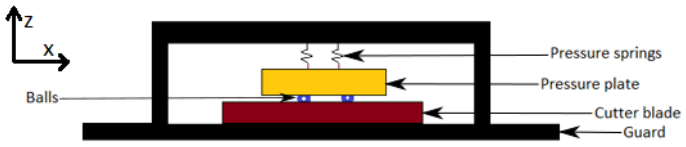

Figure 3.3: Pressure from top using compression springs and a pressure plate

Advantages:

- It does not give any stiffness to the motion of the knife like the current pressure spring.

Disadvantages:

- It is bulkier than the current pressure method. Hence, it is a little bit difficult to fit it in the trimmer.
- More moving parts means more care will be needed when the user washes the system.

2. *Use of tension springs on the bottom side of the knife*

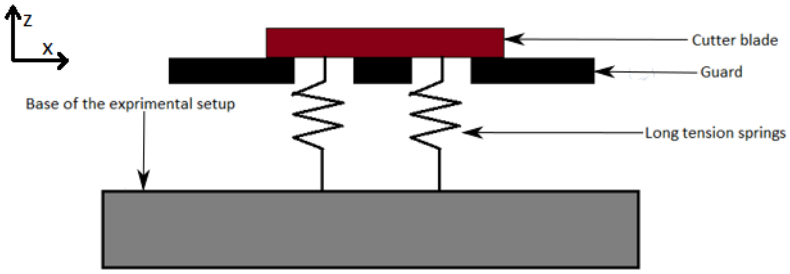

Figure 3.4: Pressure from bottom using tension springs

Advantages:

- It is easy to make such a system for the experimental setup.
- If the tension springs are very long as compares to the amplitude of the simple harmonic motion of the knife, there will be virtually no change in length of those springs and thus they won't give the system any stiffness in the x-direction. They will give the system some stiffness only in the z-direction (perpendicular to the plane of motion of the knife), which is needed to create the required pressure.
- No moving parts will be added to the system and hence the friction in the system won't increase.

Disadvantages:

- It is impossible to fit such a system in the trimmer.

3. *Use of repelling magnets*

Figure 3.5: Pressure from top using magnetic repulsion

Advantages:

- Construction of such a system is very easy.
- There is no extra contact created and hence no friction will be added to the system.

Disadvantages:

- This is a costlier solution as compared to springs because of the cost of magnets.

4. *Use of attracting magnets*

Figure 3.6: Pressure from bottom using magnetic attraction

Advantages:

- Construction of such a system is very easy.
- There is no extra contact created and hence no friction will be added to the system.

Disadvantages:

- This is a costlier solution as compared to springs because of the cost of magnets.

3.2.2. Creation of stiffness for resonance

1. *Use of tension or compression springs*

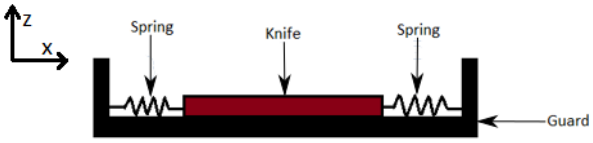

Figure 3.7: Resonance created with springs

Advantages:

- The standard deviation in the stiffness of springs is generally very low in a big sample. Hence there are no repeatability issues.
- This is a very cheap solution.
- If compression springs are used and the alignment is not proper, there can be a problem of buckling of springs. It can be avoided if tension springs are used.
- This can be easily incorporated in the experiment as well as in the trimmer.

2. *Use of repelling magnets*

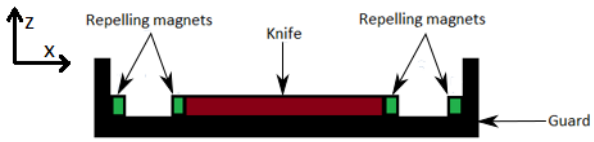

Figure 3.8: Resonance created using magnetic repulsion

Advantages:

- Construction of such a system is very easy.
- There is no extra contact created and hence no friction will be added to the system.
- No moving parts will be added to the system and hence the friction in the system won't increase.

Disadvantages:

- This is a costlier solution as compared to springs because of the cost of magnets.
- The standard deviation in the magnetic strength of cheap permanent magnets could be large in a big sample. This creates repeatability issues.
- The force between the magnets is not directly proportional to the distance between them. The force decreases with the inverse cube law.

3. *Use of a leaf spring*
A leaf spring can be used in the manner shown in the figure below. It is attached firmly to the guard on one side and is free on the other side. When the knife is moved by the motor in the x-direction which is perpendicular to the plane of the figure, the spring will give the required stiffness to the motion. As the leaf spring has very stiff in rotation about the x-direction, it will not allow any bouncing of the back end of the knife. The leaf spring cannot be attached to the knife on the other end because that would lead to parasitic motion of the knife in the y-direction, which is the direction perpendicular to the x-direction and in the plane of the figure. To avoid this, the other end is kept free but it is bounded by rotating pins which are attached at the bottom to the knife. A schematic representation of this idea is shown in Fig. 3.9

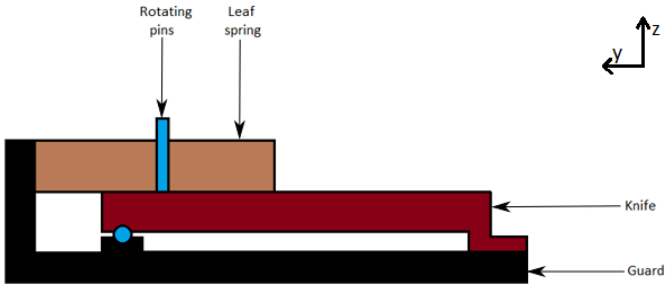

Figure 3.9: Resonance created using a leaf spring

Advantages:

- With this design, there will be no bouncing at the back end.
- The motion will be exactly linear in the x-direction and there will no parasitic motion in other directions.
- This design can be made in small sizes and can be incorporated in the actual trimmer.

Disadvantages:

- Rotating pins require bearings inside them which will increase the cost.
- If bearings are not used, friction will increase.
- This also requires to have high manufacturing accuracy.

3.2.3. Reduction of friction

1. *Use of linear bearings*
   A linear bearing could be used and the knife can then be forced to move in a straight line. A schematic representation of this idea is shown in Fig. 6.1

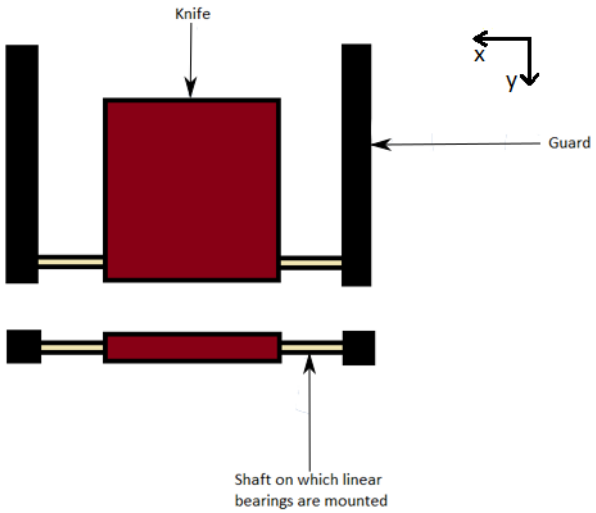

Figure 3.10: Friction reduced using linear bearings at the back end

Advantages:

- With this design, there will be no bouncing at the back end.

- The motion will be exactly linear in the x-direction and there will no parasitic motion in other directions.
- The co-efficient of friction is just like that of balls.

Disadvantages:

- This design cannot be made very small. The smallest linear bearings available online are with an inner diameter of 3 mm and an outer diameter of 7 mm. The size makes it difficult for this design to be incorporated in the actual trimmer.
- This design is also costlier as compared to the one using just balls and grooves.

This design looks perfect to be used in the experimental setup.

2. *Use of Teflon on the guard surface*
   The spacing between the teeth of the cutter blade is different than the spacing between the teeth of the guard. Hence, at a particular point in time, some cutter teeth are fully over their counterpart guard teeth, some teeth are over the gap between two teeth of the guard while some are touching half of the teeth of the counterpart. Teflon can be embedded in the steel guard in a way shown in the above figure. This will reduce the co-efficient of friction at the cutting end from 0.7 to the average of 0.7 and 0.04. This means that friction will be reduced to almost half of the present friction.

Figure 3.11: Friction reduced using embedded Teflon on the guard blade

3. *Use of balls with proper grooves on the guard and a hinged knife*
   This design can eliminate the bouncing at the back end with one addition to the current design of the knife. The force that causes the bouncing originates at the front end. To avoid the transfer of this force to the back, the knife can be divided into 2 parts by a cut along the x-direction (cutting movement direction). The figure above is a rough sketch of this design. The 2 parts can be joined by a hinge. The hinge can be a compliant material which is stiff in the x-direction but compliant in the rotation about the axis passing through the center of the hinge and parallel to the x-direction.

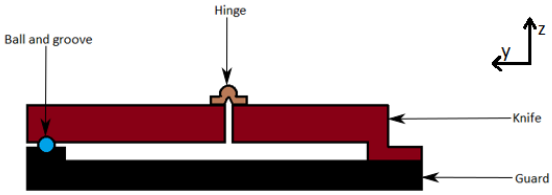

Figure 3.12: Friction reduced using ball & groove at the back end and a hinged knife

4. *Use of two balls between the guard and the knife with a gap of less than 30 microns at the cutting end*
   At Philips, it has been observed that a maximum gap of 30 microns is allowable between the cutter blade and the guard blade at the cutting end, in order to achieve a cutting performance equivalent to that achieved by the Philips oneBlade hair trimmer. This design eliminates the friction at the cutting end because there is no contact between the knife and the guard.

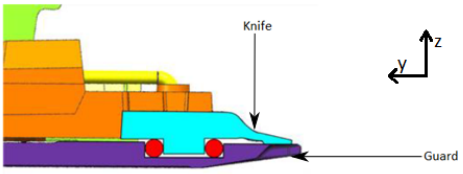

Figure 3.13: Friction reduced to zero using 2 balls and maintaining a gap of 30 microns at the front end

Use of ultrasonic vibrations
There has been extensive research on the topic of reduction of friction with the use of high frequency vibrations. These vibrations are generally ultrasonic, can be produced piezoelectrically [13] [14]. Such vibrations can be provided to the cutter or the guard and can be oriented in the x-direction or the y-direction.[12]

Advantages:

- The ultrasonic vibrations will also help in cutting the hair faster.
- This method can reduce the friction between sliding metals by a drastic amounts, sometimes even by 80% [13].

Disadvantages:

- The effect of such vibrations on the users needs to be assessed. Whether it has detrimental effects on human skin or not needs to be investigated.
- This kind of design can be costlier than other options.

These concepts can be ranked according to the ease and feasibility of implementing them and can be combined to form a resonant system. All this goes to show that such a system is practically realizable in the actual trimmer and it is worth exploring the dynamics involved in creating such a system. All the concepts are listed in Tab. 3.1 with their purposes written in the first column.

Purpose	**Option 1**	**Option 2**	**Option 3**	**Option 4**
Pressure	Pressure plate and ball bearings	Tension springs on the bottom	Repelling magnets	Attracting magnets
Stiffness creation	Compression springs on the sides	Tension springs on the sides	Repelling magnets	Leaf spring on top
Friction reduction	Linear bearings	Teflon embedding	Ball bearings, no friction at cutting end	Ultrasonic vibrations

Table 3.1: A list of different concepts for different purposes

Some of these ideas were also combined to make an experimental test setup as shown in chapter named ”Validation of the mathematical model”.

4. Mathematical model of the system

After having done the back-of-the-envelope calculations and having given the practical possibilities of including the concept of resonance in hair clippers a thought, it is time to dive deeper into the dynamic behaviour of the system and eventually predict the power saving that can be done by taking advantage of the resonance phenomenon. To study the dynamic behaviour, it is smart to take the help of simulation software. In this project, the software packages chosen are MATLAB & SIMULINK. A mathematical model of the system must be made and built in these software packages to be able to analyze the dynamic behaviour of the system.

This chapter explains how the whole model was established, starting with the simplest model and adding complexities gradually. The equations that govern the dynamic behaviour of the elements involved in the system are derived and based on them a mathematical model is built.

4.1. Unidimensional dynamic analysis of the system

4.1.1. Analysis without friction in the system

It is always a good practice to start simple and add complexities as the project moves ahead. It allows to first understand the basic model in detail and then look at the complex phenomena. So, the first step is to consider the dynamics occurring only in one direction, that is the direction of cutting, which is called the x-direction. This means that the friction forces between the eccentric head and the drive bridge, which are oriented along the y-direction, are ignored. For all practical purposes, through out this project, it is assumed that the cutter can move only in one direction, that is the x-direction. Even though in the real world, there will always be friction between the cutter blade and the guard blade, it is neglected at this stage of the model. It shall be considered at a later stage.

A schematic representation of the system is shown in the figure 4.1. Torque is applied by the motor at the center and it is converted into a force applied on the cutter mass with the help of the eccentric head and drive bridge combination. As shown in the figure, the distance between the center of the motor and the eccentric head is r_1. Two tension springs are connected to the mass as shown in the figure. These springs are also referred to as resonance springs in this report. An important point to note here is that both the springs have to be connected with a preset tension corresponding to a deflection of x_p, where x_p is greater then r_1. The initial position where there is only preset displacement in the springs is at $\theta = \omega t = 0$. In the figure 4.1, the cutter mass can be seen to have moved to the right of the centre and hence, the tension in the left spring is more than the tension in the right spring. The free body diagram of the cutter mass is shown in Fig. 4.2.

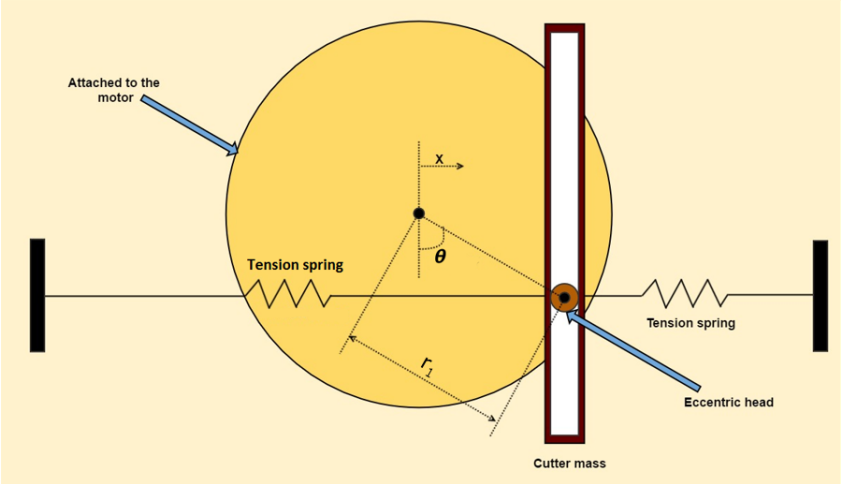

Figure 4.1: Schematic of the eccentric head moving the cutter blade in x-direction

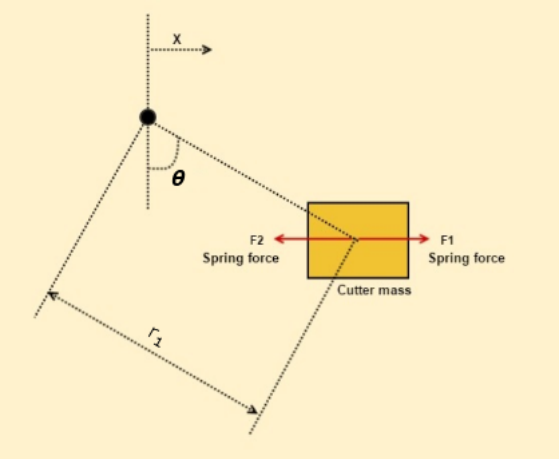

Figure 4.2: Free body diagram of the cutter mass

It can be simplified as shown in the figure 4.3. Here, F_s is the total spring force acting on the mass.

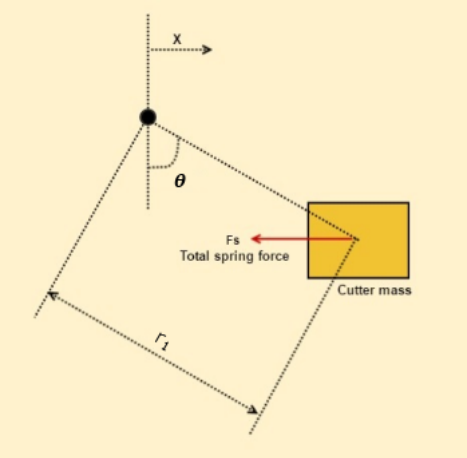

Figure 4.3: Simplified free body diagram of the cutter blade

Let x_1 be the displacement of spring 1 which is on the right side and x_2 be the displacement of spring

$\boldsymbol{\theta(deg)}$	$\boldsymbol{x_1}$	$\boldsymbol{F_1}$	$\boldsymbol{x_2}$	$\boldsymbol{F_2}$	$\boldsymbol{F_s = F_2 - F_1}$
0	x_p	kx_p	x_p	kx_p	0
90	$x_p - r_1$	$k(x_p - r_1)$	$x_p + r_1$	$k(x_p + r_1)$	$2kr_1$
180	x_p	kx_p	x_p	kx_p	0
270	$x_p + r_1$	$k(x_p + r_1)$	$x_p - r_1$	$k(x_p - r_1)$	$-2kr_1$

Table 4.1: Spring force at different points in the path of the cutter

2 which is on the left. Let $k/2$ be the spring rate of each of these springs. F_1 is the force acting on the mass due to spring 1 and F_2 is the force acting on the mass due to spring 2. The the total spring force $F_s = F_2 - F_1$. The spring force changes as the motor rotates and the cutter moves. The expressions for spring force at different points in the cutter's path are given in below in Tab. 4.1

It can be seen from the above table that $Fs = 2kr_1 \sin(wt)$

The equations of motion of the the system could be written as follows:

$$\begin{aligned} F &= m\ddot{x} + F_s \\ &= m\ddot{x} + F_2 - F_1 \end{aligned} \tag{4.1}$$

where F is the total force acting on the cutter.

As the cutter is in a simple harmonic motion, the displacement x can be expressed as follows:

$$\begin{aligned} x &= r_1 \sin(\omega t) \\ \dot{x} &= \omega r_1 \cos(\omega t) \\ \ddot{x} &= -\omega^2 r_1 \sin(\omega t) \end{aligned}$$

Substituting the value of displacement in the equation of motion, the following can be obtained:

$$\begin{aligned} F &= -m\omega^2 r_1 \sin(\omega t) + 2kr_1 \sin(\omega t) \\ &= ((2k - m\omega^2) r_1 \sin(\omega t) \end{aligned} \tag{4.2}$$

The force F acting on the system is provided by the motor through the eccentric head. It follows from Newton's 3rd law of motion that the cutter will put an equal and opposite force on the eccentric head. This force can be decomposed into 2 components, one along the moment arm and one perpendicular to the moment arm. The components are named F_{par} and F_{per} respectively. F_{per} will produce a moment on the motor, which is called the load torque.

Thinking conceptually, when the motor is operated at a frequency which is not the resonance frequency of the system, the inertia forces and the spring forces will not cancel each other. This means that at some points in the simple harmonic motion, henceforth referred to as SHM, the system will oppose the motor and at some points it will assist the motor. When the motor is opposed by the system, the load torque will be positive and when it is assisted by the system, it will be negative. The value of load torque can be derived as follows:

$$\begin{aligned} T_{load} &= F_{per} r_1 \\ &= \frac{1}{2} r_1^2 (2k - m\omega^2) \sin(2\omega t) \end{aligned} \tag{4.3}$$

It can be seen from the equation for T_{load} that its value will be zero if $2k = m\omega^2$, that is if the system is run at it's resonant frequency. Because of the fluctuation of the value of $\sin(2\omega t)$ from 1 to -1, the value of the load torque switches between positive and negative, as expected. A SIMULINK model was made to observe this. It is shown in Fig. B.1

4.1.2. Mathematical model

The next step is to make a mathematical model of the unidimensional system without friction in the system. The model needs to have a voltage input, a DC motor and a load torque acting on it as a result of the SHM.

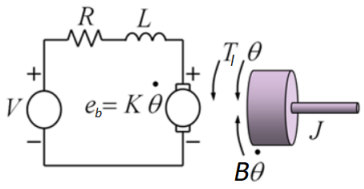

Figure 4.4: Electrical and mechanical sides of the motor

Figure 4.5: Courtesy: [1]

The motor converts electrical energy to mechanical energy; when a voltage is applied across its terminals, it produces rotation of the motor shaft. In other words, a voltage produces an angular frequency as shown in Fig. 4.4. On the electrical side of the motor the circuit has the voltage input V, self inductance L and resistance R of the electrical winding in the motor. The back emf generated by the rotor in the electrical winding is represented by e_b. On the mechanical side of the motor is a rotor with a rotational inertia J, viscous friction B opposing the motion of the rotor and the total load torque on the rotor T_l which is the summation of the Coulomb friction in the motor T_c and the external load torque T_{load} acting on the motor. The motor constant that interconnects the electrical and mechanical sides of the motor is represented by K.

Given below are the motor equations that govern the dynamics of the motor:

The torque produced and the current in the winding are related as follows:

$$T(t) = Ki(t) \tag{4.4}$$

The back EMF e_B and the rotational speed of the motor ω are related as follows:

$$e_b(t) = K\omega(t) \tag{4.5}$$

The electrical and mechanical equations of the DC motor can be written as follows:

$$v(t) = e_b(t) + i(t)R + Li(t)t \tag{4.6}$$

$$J\ddot{\theta}(t) = T(t) - B\dot{\theta}(t) - T_l(t) \tag{4.7}$$

Taking the Laplace transform of both the equations, they could be written as follows:

$$\begin{aligned} V(s) &= E_b(s) + I(s) + sLI(s) \\ &= E_b(s) + (R + sL)I(s) \end{aligned}$$

$$\therefore \quad I(s) = \frac{V(s) - E_b(s)}{R + sL} \tag{4.8}$$

$$\begin{aligned} s^2J\theta(s) &= T(s) - B\omega(s) - T_l(s) \\ sJ\omega(s) &= (T(s) - T_l(s)) - B\omega(s) \end{aligned}$$

$$\therefore \quad \omega(s) = \frac{T(s) - T_l(s)}{B + sJ} \tag{4.9}$$

A mathematical model that represents both the electrical and mechanical sides of the motor is shown in Fig. 4.6. The method of representing a DC motor, an electro-mechanical component, in the form of an electrical circuit diagram is explained in Appendix A.

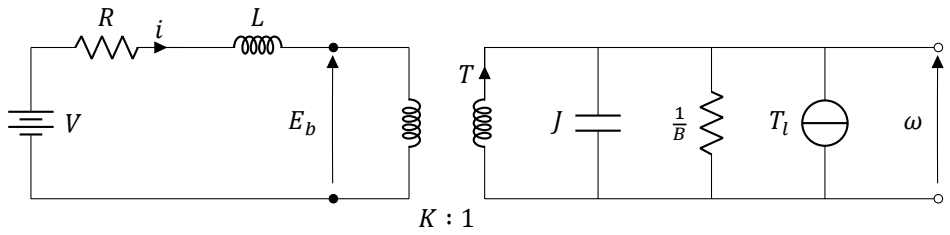

Figure 4.6: Electrical model of the motor

4.1.3. Simulation results and observations

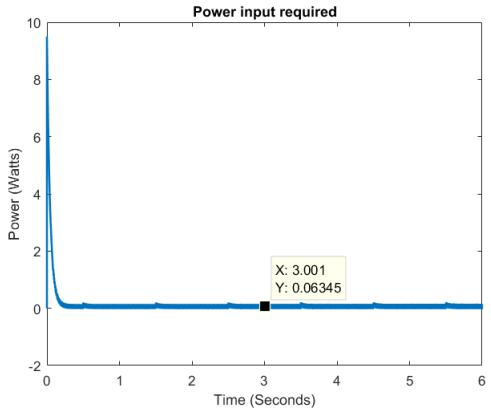

Figure 4.7: Power input observed when no springs are used

This model is established in SIMULINK and is simulated to observe the behaviour of the unidirectional system without friction. A SIMULINK model of the motor is made and it is shown in Fig. B.2. Values of the parameters needed in the model are taken from the data sheet of the motor used in one of the Philips hair clippers and the friction values are taken from the characterization experiment done with the motor by other engineers in Philips. The complete model of the system including the motor and voltage as input is shown in Fig. B.3 in the appendix.

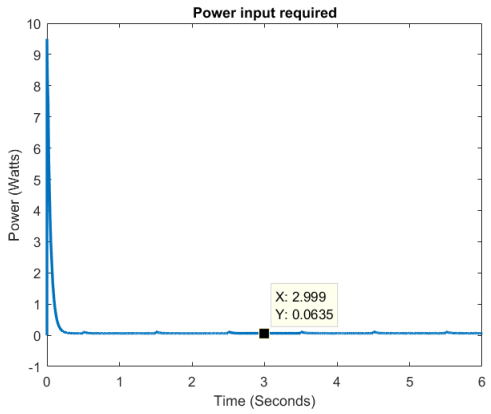

Figure 4.8: Power input observed when springs are used

In order to observe the advantage of resonance in the system, the system with springs in it is given an input voltage that varies from 4.3 V to 4.45 V in steps of 1 second interval. That corresponds to a variation in ω from about 610 rad/s to 635 rad/s. The resonance frequency (ω_n) is picked to be 100 Hz, that is, 628 rad/s because this is the frequency at which a high-end Philips hair clippers operate. The cutter mass(m) is taken to be 10 g, arbitrarily. The resonance frequency of an undamped system is given by the formula $\omega_n = \sqrt{k/m}$ [12]. Hence, for the resonance to happen at the target frequency ω_n, the stiffness in the system should be

equal to $m\omega_n^2$. Hence each of the tension springs has a stiffness value (k) equal to $\frac{1}{2}m\omega_n^2$ each. This would make the total stiffness equal to $m\omega_n^2$ and this would create resonance at the target resonance frequency. The power input required to move the cutter mass is observed around the resonance frequency of $628\,\mathrm{rad/s}$.

This simulation is done again with the same input voltages to the system but with no springs in the system. The power input required is observed this time as well. The plots of power input in Watts vs time in seconds observed in both the cases are shown in Fig. 4.7 and 4.8

The markers in the plots are plotted when the system is oscillating with a frequency of $628\,\mathrm{rad/s}$, which is the resonance frequency. The plots show that there is absolutely no change in the power input required; the graphs are almost identical, except the fact that the variation in power consumed is more in the case of no springs. It can be seen that the power required is almost identical in both the cases. This shows that when a unidimensional analysis of the system is done with no friction in it, there is absolutely no advantage of creating resonance in the system.

4.1.4. Inferences from the simulation

It was expected that because of the nullification of inertia forces by spring forces, the power drawn at the resonance frequency would drop significantly with the introduction of springs into the system, as shown in the back-of-the-envelope calculations. These calculations were done without considering the dynamics of the motor. As it was observed that there is no change in power drawn, it can be inferred that the load experienced by the motor due to the inertia of the mass when there are no springs in the system is not significant enough to cause a noticeable increase in the power drawn. The power required to accelerate and decelerate the mass is way less than the power required to run the motor, owing to its friction losses. Hence, even after springs are introduced in the system, the power drawn remains the same.

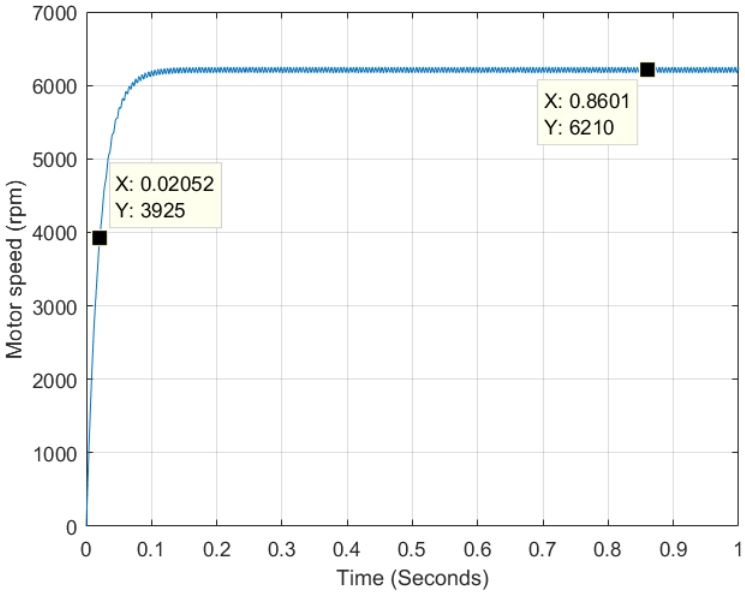

Figure 4.9: Angular speed of the motor when cutter mass is present

To prove that the inertia forces of the mass do not affect the power drawn and that the motor is dominant, the system was simulated at $628\,\mathrm{rad/s}$ firstly with and then without the cutter mass present in the system. In both the cases, no springs were included in the model. The results are shown in Fig.

4.9 and 4.10

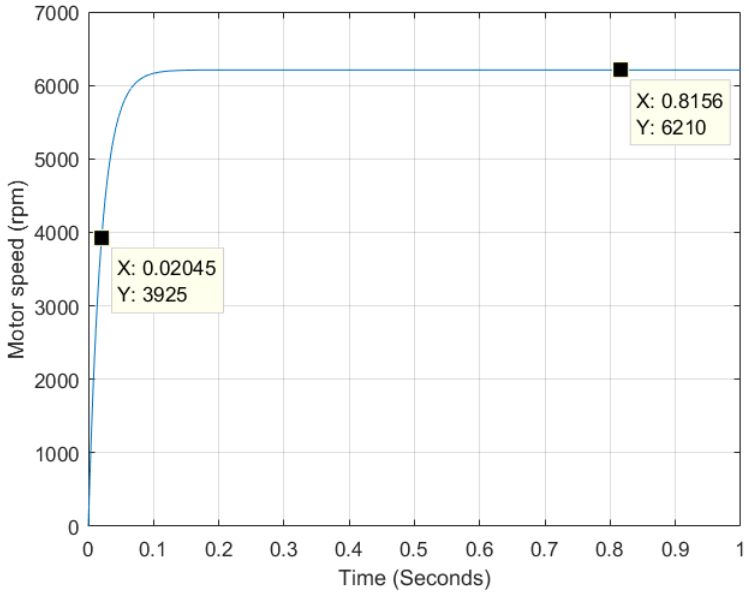

Figure 4.10: Angular speed of the motor when cutter mass is absent

In Fig. 4.9, it can be seen that the angular speed of the motor is not perfectly constant at any point. It never achieves steady state. This is because the acceleration and deceleration of the translation mass causes the motor to accelerate and decelerate. After some time, the speed keeps varying between 2 constant peak values and the mean is at 6210 rpm. The time constant, which is the time taken to reach 63.21% of this value, that is 3925 rpm, is 20.5 ms. Figure 4.10 shows that when there is no cutter mass, the rotational speed of the motor becomes constant after some time and reaches steady state and settles at 6210 rpm. In this case as well, the time constant is very close to 20.5 ms, but just a little lower, as expected. This means that the presence of the cutter mass does not provide enough load torque in the form of inertia to significantly increase the DC value of the current drawn by the motor. Hence, there is no change in the power drawn when the springs are attached and the system is excited at resonance frequency.

4.1.5. Analysis with friction in the system

When the system was analyzed unidimensioinally without considering any friction between the cutter and the guard, it was found out that the motor friction dominates over the inertia of the mass, in terms of power required to overcome them. It is then obvious that if the friction between the cutter and the guard is added to the system, the power saving with the addition of resonance will still be non-existent.

4.1.6. Motivation for further analysis

Until now, simulations showed that introduction of resonance in the system could not reduce the power consumed. There is still enough motivation to carry out the two-dimensional (2D) analysis. The absence of power saving until this point was mainly because the phenomenon of resonance could only obliterate the amount of power lost in accelerating and decelerating the mass which was insignificant as compared to the power lost in friction between the cutter and the guard and the friction in the motor. If a 2D analysis is done, the load torque experienced by the motor will also include the friction present between the drive bridge and the eccentric head of the motor in the y-direction, that is the direction perpendicular to the SHM motion. When a resonant system is made, the force arising at the contact of the eccentric head and the drive bridge will drop to zero, ideally, because both the eccentric head and the drive bridge will have the same velocity in the x-direction. Hence the friction between these

components, which is the product of this force and the co-efficient of friction, will be zero. This means that the value of load torque will be reduced when a resonant system is made and hence the power drawn will decrease.

4.2. 2D dynamic analysis of the system with friction

A two-dimensional analysis of the system entails modeling the behaviour of the system in both the x-direction, that is the direction of the movement of the cutter, and the y-direction, that is the direction perpendicular to the x-direction. A better understanding of these directions can be gained by reading the next section. In this analysis, the forces in the driven system that are considered are the inertia force of the mass in the x-direction, the friction force arising at the contact surface of the cutter and the guard, which is also in the x-direction, the spring forces in x-direction, and the friction forces arising at the contact between the eccentric head and the drive bridge, which are in the y-direction. All these forces are shown in Fig. 4.13 and 4.15 and are explained in detail in the next section. This means that the motor has to perform work in both x- and y-directions. When the system doesn't run at resonance, the work in x-direction is to overcome the mass inertia of the cutter mass, the spring force of the springs and x-direction friction. The work in y-direction is only the work needed to overcome the y-direction friction.

4.2.1. Kinematic analysis of the system

As seen in Fig. 4.11, the displacement of the eccentric head in the x-direction is given by x and that in the y-direction is given by y. It is important to note that this figure is a schematic representation of the actual system. The drive bridge attached to the cutter mass is represented by the slotted link. The eccentric head can move up and down in the slotted link. The eccentric head is revolved around the hinge at the centre by the motor. This is essentially a Scotch yoke mechanism. The motion of the eccentric head can be described by the following equations:

$$x = r_1 \sin(\theta)$$
$$\dot{x} = \omega r_1 \cos(\theta)$$
$$y = -r_1 \cos(\theta)$$
$$\dot{y} = \omega r_1 \sin(\theta)$$

$$\begin{bmatrix} \dot{x} \\ \dot{y} \end{bmatrix} = \begin{bmatrix} r_1 \cos\theta \\ r_1 \sin\theta \end{bmatrix} [\omega] \tag{4.10}$$

It should be noted that the displacement of the drive bridge, and thus the cutter mass, in the x-direction is the same as the displacement of the eccentric head in the x-direction.

Let the total load torque acting on the motor be T_{load}. Let the total force acting on the motor at the end of the eccentric head be F. Thus, from the construction of the system, $F = T_{load}/r_1$. This force F can be expressed as a vector sum of 2 perpendicular forces. Let F_x be the x-direction component of the force F and F_y be the y-direction component of force F as shown in Fig. 4.12. Thus, the force acting on the eccentric head in the x-direction is F_x and that in the y-direction is F_y.

As mentioned earlier, the components contributing to the rise of F_x are the friction between the cutter and the guard, the extension of the resonance springs and the mass inertia of the cutter. F_y is produced by the friction between the drive bridge and the eccentric head.

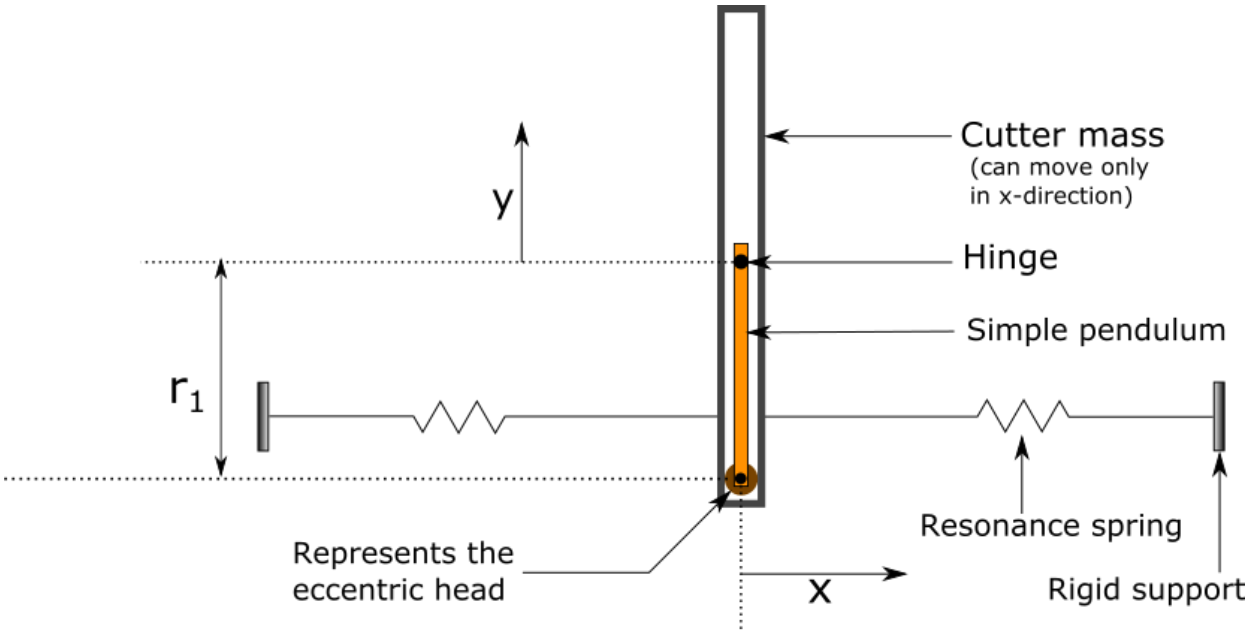

Figure 4.11: Representation of the system with a simple pendulum

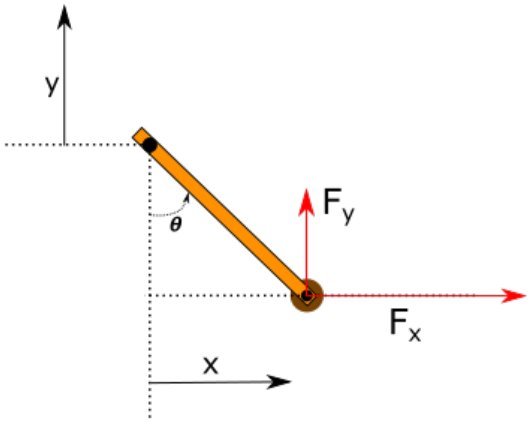

Figure 4.12: Forces acting on the eccentric head

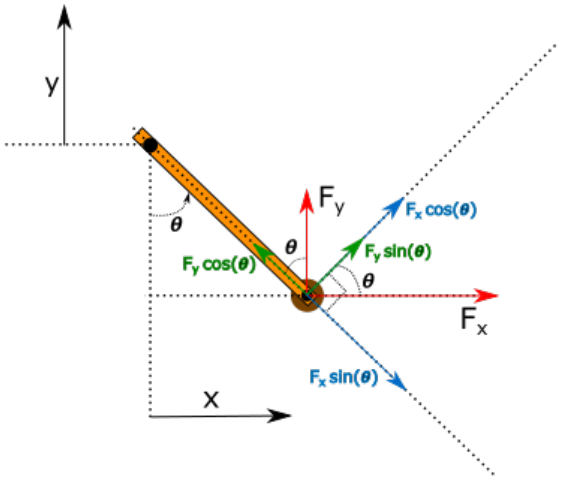

Figure 4.13: Forces contributing to the load torque

F_x can be resolved into 2 perpendicular directions, one along the moment arm and one perpendicular to the moment arm, as shown in Fig. 4.13. As it can be seen from the figure, the motor does not have to expend any torque to overcome the component of F_x along the moment arm. It has to expend some torque to overcome the component perpendicular to the moment arm. The value of this load torque is $r_1 F_x \cos\theta$

Similarly, F_y can be resolved into 2 perpendicular directions, one along the moment arm and one perpendicular to the moment arm. As it can be seen from the figure, the motor does not have to expend any torque to overcome the component of F_y along the moment arm. It has to expend some torque to overcome the component perpendicular to the moment arm. The value of this load torque will be $r_1 F_y \sin\theta$

Hence, the load torque T_{load} on the motor is given by

$$\begin{bmatrix} T_{load} \end{bmatrix} = \begin{bmatrix} r_1 \cos\theta & r_1 \sin\theta \end{bmatrix} \begin{bmatrix} F_x \\ F_y \end{bmatrix} \tag{4.11}$$

If the transformation factor is represented by the vector M, then

$$\begin{bmatrix} M \end{bmatrix} = \begin{bmatrix} r_1 \cos\theta \\ r_1 \sin\theta \end{bmatrix} \tag{4.12}$$

If the translation velocities of the eccentric head in x- and y-direction are represented by the vector v, then

$$\begin{bmatrix} v \end{bmatrix} = \begin{bmatrix} \dot{x} \\ \dot{y} \end{bmatrix} \tag{4.13}$$

If the forces F_x and F_y acting on the motor are written represented by the vector F, then

$$\begin{bmatrix} F \end{bmatrix} = \begin{bmatrix} \dot{F_x} \\ \dot{F_y} \end{bmatrix} \tag{4.14}$$

Equation 4.10 can be written as

$$\begin{bmatrix} v \end{bmatrix} = \begin{bmatrix} M \end{bmatrix} \begin{bmatrix} \omega \end{bmatrix} \tag{4.15}$$

and equation 4.11 can be written as

$$\begin{bmatrix} T_{load} \end{bmatrix} = \begin{bmatrix} M^T \end{bmatrix} \begin{bmatrix} F \end{bmatrix} \tag{4.16}$$

The transformation factor is the same in both the cases, that is, in transformation of load forces to load torque on the motor and in transformation of rotational velocity of the motor to the translation velocities of the eccentric head. This shows that the dynamics were correctly represented by the given equations.

4.2.2. Mathematical model

DC motor

The mathematical model of the motor remains the same as explained earlier. The model is shown again in Fig. 4.14

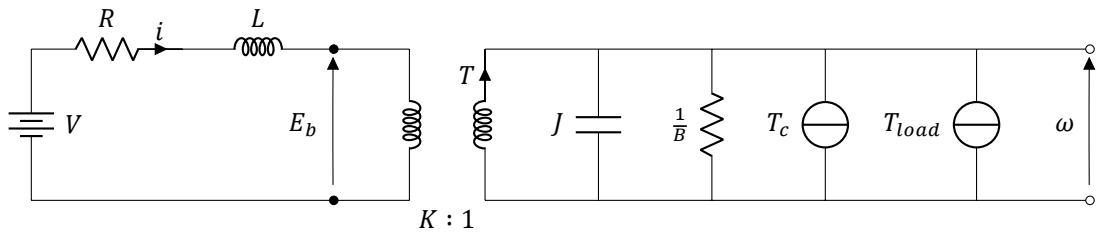

Figure 4.14: Electrical model of the motor

The motor rotates with an angular speed of ω and gives out a torque T. The Coulomb friction in the motor is represented by T_c. The rotary motion of the motor is converted to translation of the cutter mass by the eccentric head.

Conversion of rotary motion of the motor to translation motion of the cutter

The torque T is converted to a force F' by the Scotch yoke mechanism, as explained in the kinematic analysis, and is exerted on the cutter mass. This force can be divided into 2 components: one acting in the x-direction and the other acting in the y-direction. Let F_x' be the force that the motor exerts through the eccentric head on the cutter mass in the x-direction and F_y' be the force that the motor exerts through the eccentric head on the cutter mass in the y-direction. Then by the same reasoning as given while explaining the kinematics of the system, the following equations will be true:

$$\begin{bmatrix}\dot{x}\\ \dot{y}\end{bmatrix} = \begin{bmatrix}r_1\cos\theta\\ r_1\sin\theta\end{bmatrix}[\omega] \tag{4.17}$$

$$\begin{bmatrix}T_{load}'\end{bmatrix} = \begin{bmatrix}r_1\cos\theta & r_1\sin\theta\end{bmatrix}\begin{bmatrix}F_x'\\ F_y'\end{bmatrix} \tag{4.18}$$

It is noteworthy that equation 4.18 is what can be obtained by multiplying both sides of equation 4.11 by -1. Indeed, $F_x' = -F_x$, $F_y' = -F_y$ and $T_{load}' = -T_{load}$

For representational ease, the apostrophes are dropped and the forces exerted by the motor on the cutter mass are represented by F,F_x and F_y henceforth in the report. It should be noted that these are the forces exerted by the motor and not those acting on the motor.

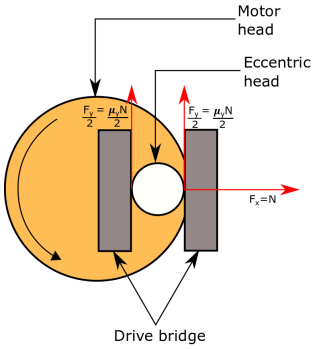

Figure 4.15: Forces exerted by the motor in the x- and y-directions

In simple terms, the eccentric head is a transformer that converts the combination of T and ω to a combination of $F_x, \dot{x}$ and $F_y, \dot{y}$. The mathematical model of this conversion is shown in Fig. 4.16. The left side of the transformer represents the output of the motor and the right side represents the dynamics in the x- and y-directions. The Coulomb friction force in x-direction is represented by F_{cx} and that in y-direction is represented by F_{cy}. B_x is the coefficient of viscous friction in x-direction and B_y is the coefficient of viscous friction in y-direction.

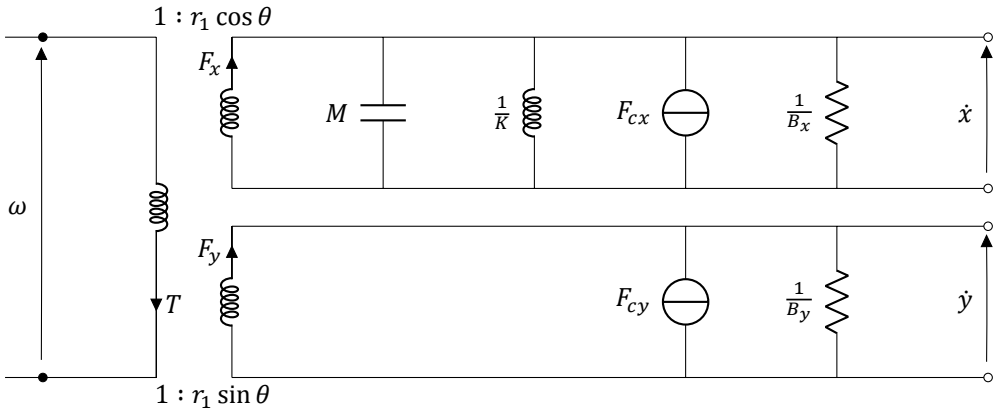

Figure 4.16: Electrical representation of the conversion of the motor's rotary motion to translation of the cutter mass

A short summary of the elements represented in the established mathematical model is given below.

Dynamics of motion of the cutter in the x-direction

The cutter mass is moved in a simple harmonic motion (SHM) in the x-direction by the eccentric head. There are 3 dynamic elements acting in the x-direction:

1. The inertia of the cutter mass.
2. The resonance springs
3. The Coulomb friction force acting between the cutter blade and the guard blade
4. The viscous friction force acting between the cutter blade and the guard blade

These elements are shown in the mathematical model shown in Fig. 4.16

Dynamics of motion of the cutter in the y-direction

The elements acting in the y-direction are as follows:

1. The Coulomb friction force acting between the eccentric head and the drive bridge
2. The viscous friction force acting between the eccentric head and the drive bridge

These elements are represented shown in the mathematical model shown in Fig. 4.16

Complete mathematical model of the system

The complete mathematical model of the system from the voltage input to the cutter movement is shown below in Fig. 4.17

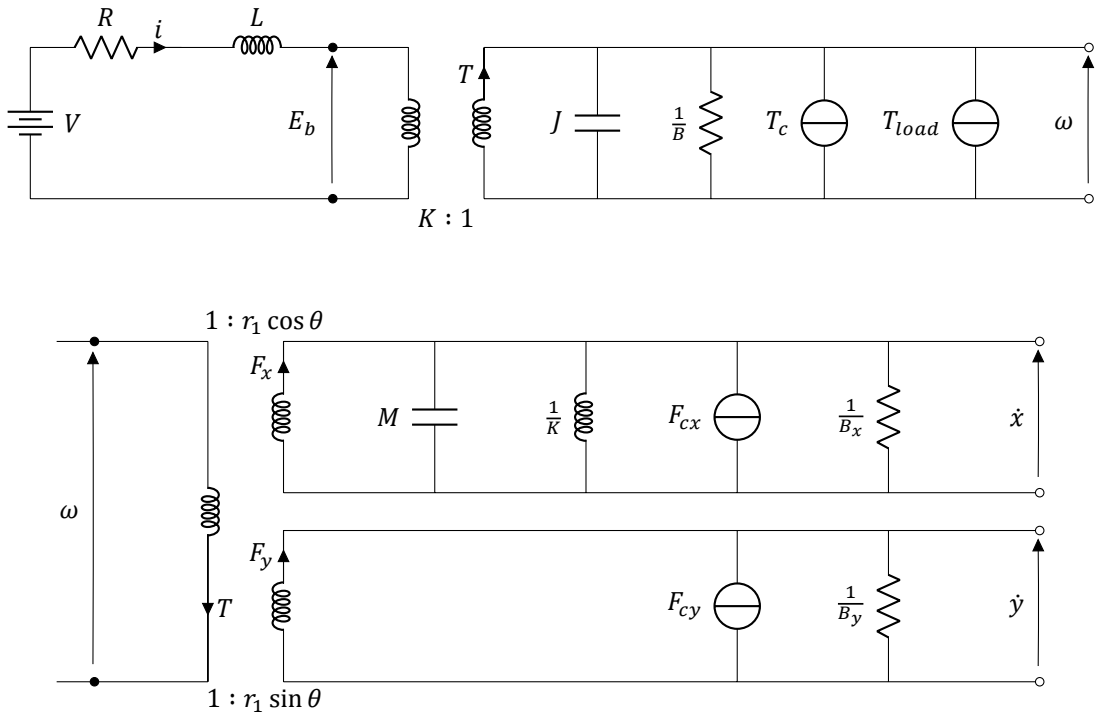

Figure 4.17: Mathematical model of the whole system

5. Analysis with simulations

In Chap. 4, it became clear that the power required to accelerate and decelerate the cutter mass is very low as compared to that required to run the motor at 6000 rpm. As a result, considering friction inside the motor and at the cutter-guard contact surface, in a unidimensional analysis the introduction of resonance cannot save any power. It is expected to have an effect in a two-dimensional analysis as it can result in the reduction of friction force between the eccentric head and the drive bridge.

Having made the mathematical model of the two-dimensional system in Chap 4, it is a good idea to check with simulations whether there can be any advantage of having a resonant system in place. A Simscape model of the system is created in SIMULINK, based on the mathematical model explained in the previous chapter, and it is simulated using the parameters mentioned in Tab. 5.1 and 5.2. The complete SIMULINK model is shown in Appendix B.

5.1. Parameter selection for the model

The motor selected for the simulation is Faulhaber 2224006SR DC motor. Sometimes, values of some motor parameters can be different in reality than the values given in the data sheet of the motor. Hence, it is necessary to confirm these values. This is done by running an experiment to characterize the motor. The values found through this experiment are used in the simulation and are mentioned in Tab 5.1. The mass of the cutter is selected by observing cutters in various Philips hair clippers. The target frequency is chosen to be 6000 rpm because that is the frequency at which most of the Philips hair clippers work. The pressure force between the cutter and the guard is chosen according to general Philips design requirements. It is known to Philips designers that all the friction present in Philips hair clipping systems is of Coulomb type and hardly any viscous friction exists. Values chosen for the parameters of the driven system to be used in the simulation are shown in Tab. 5.2 and the reasons for choosing them are also mentioned.

Parameter	Symbol	Value	Unit	Reason
Resistance	R	1.94	ohm	Motor characterization
Inductance	L	45×10^{-6}	H	Motor characterization
Motor constant	K	0.0072	$V \cdot s/rad$	Motor characterization
Motor inertia	J	2.7×10^{-7}	$kg \cdot m^2$	Data sheet
Motor Coulomb friction	T_c	0.2×10^{-3}	$N \cdot m$	Motor characterization
Motor viscous friction co-efficient	B	0	$N \cdot m/rad$	Motor characterization

Table 5.1: Values of motor parameters selected for simulation

Parameter	Symbol	Value	Unit	Reason
Amplitude	r	0.002	m	General Philips design
Cutter mass	m	0.003	kg	General Philips design
Spring constant	k	1184	N/m	Resonance requirement
Coulomb friction co-eff. in x-direction	μ_{cx}	0.4	N	General Philips design
Viscous friction co-eff. in x-direction	c_x	0	N · s/m	General Philips design
Coulomb friction co-eff in y-direction	μ_{cy}	0.25	N	General Philips design
Viscous friction co-eff. in y-direction	c_y	0	N · s/m	General Philips design
Target resonance frequency	ω_n	6000	rpm	General Philips design
Pressure force	N	3.5	N	General Philips design

Table 5.2: Values of driven system parameters selected for simulation

5.2. Power comparison

The behaviour of the mathematical model is observed under two circumstances. Firstly, the model is simulated with all the parameters mentioned above except for the motor friction losses and spring stiffness which are kept zero. A plot of the power consumed in Watts in this situation against time in seconds is shown in Fig. 5.1. In the next step it is simulated by keeping the spring stiffness value as mentioned in the above table. Figure 5.2 shows the power consumed in Watts against time in seconds when resonance occurs. The power consumed in both the scenarios is compared.

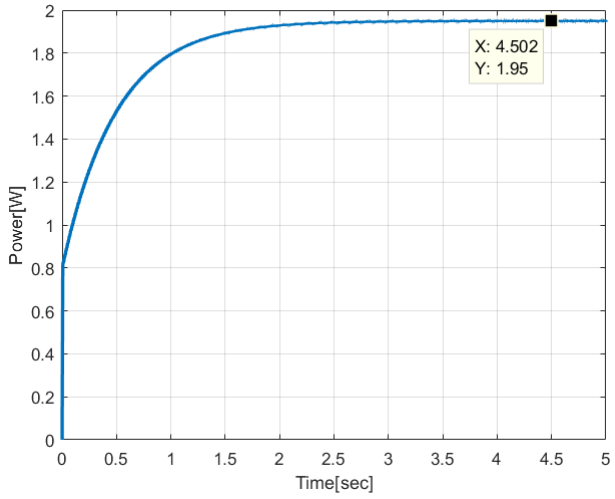

Figure 5.1: Power consumed when a 3 gm system without springs is run at 6000 RPM

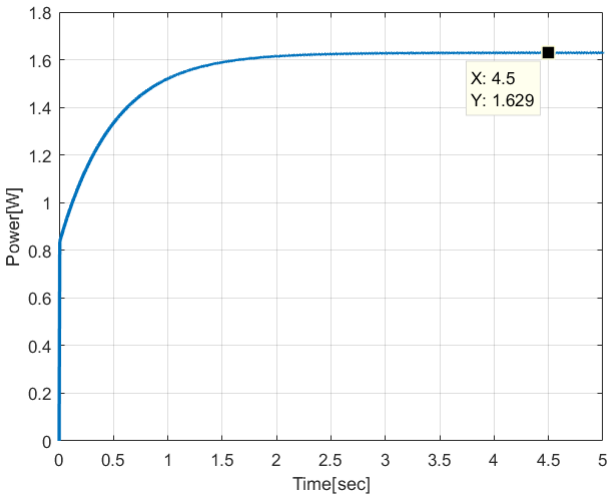

Figure 5.2: Power consumed when a 3 gm system with springs is run at 6000 RPM

As the plots above show, here, the power saving with the introduction of resonance is about 17%. This value holds only if the friction losses in the motor are zero. If these losses are increased to $0.2\,\mathrm{mN\,m}$, the value of power saving drops to about 15%. It is worth noting that if, somehow, the Coulomb friction in the x-direction is reduced to almost zero, the power saving will increase will increase to a very high percentage. To prove this, the Coulomb friction co-efficient in x-direction was reduced to 0.01 while keeping all the other parameters the same, and the model was simulated again in the same manner. Figures 5.3 and 5.4 show the power consumed in the system when springs are not used and when springs are used respectively.

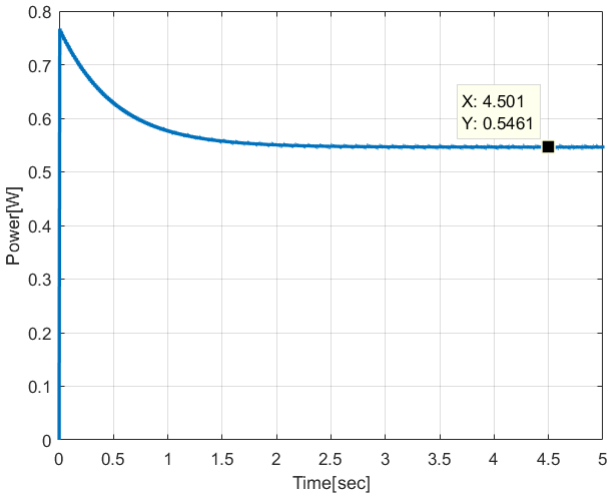

Figure 5.3: Power consumed when a 3 gm system without springs is run at 6000 RPM with very low x-direction friction

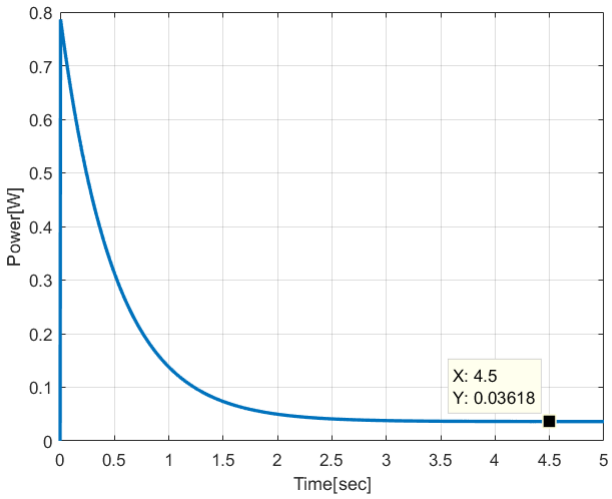

Figure 5.4: Power consumed when a 3 gm system with springs is run at 6000 RPM with very low x-direction friction

The power saving in this case is about 93%. It should be noted however that these values hold only when the mechanical losses in the motor are assumed to be zero. The percentage of power saved will decrease when those losses are included in the model. The system is simulated again with motor mechanical losses of $0.2\,\mathrm{mN\,m}$ and it shows that in the case of a $3\,\mathrm{g}$ cutter, run at 6000 rpm, the power saving is about 75%. The mechanical losses in the motor used in an actual Philips hair clipper can be more than those in a Faulhaber motor. The value depends on the motor used and hence, it is clear that the reduction in power will reduce subsequently with an increase in motor losses. Simulation with $0.6\,\mathrm{mN\,m}$ mechanical losses in the motor leads to a power saving of about 55%

5.3. Sensitivity analysis of the reduction in power consumed

As it was seen in the previous section, the percentage of power saved changes with a change in parameters. There are various parameters in this system that can change over a period of time. Other than that, some parameters might be difficult to control, right from the beginning. It would be wise to see the effect of variation in some of these parameters on the percentage power saved. When a particular parameter is varied, all other parameters have to be kept constant to get an accurate sensitivity analysis.

5.3.1. Sensitivity with respect to the running frequency of the motor

It might not be always possible to control the frequency of the motor exactly at the resonance frequency of the system. It is necessary to look at the sensitivity of the reduction in the consumption of power with respect to the running speed of the motor.

For this analysis, the motor frequency in the simulation is varied from $50\,\mathrm{Hz}$ to $150\,\mathrm{Hz}$ with a step size of $5\,\mathrm{Hz}$, the resonance frequency of the system being $100\,\mathrm{Hz}$. The same is repeated again but with no springs in the system. The power consumed in both the scenarios is observed and plotted against the motor frequency in Fig. 5.5. For greater accuracy, the simulation is done again for frequencies ranging from $75\,\mathrm{Hz}$ to $125\,\mathrm{Hz}$ with a step size of 1 Hz. This is shown in Fig. 5.6. The variation of percentage saving in power with variation in motor frequency can be seen in Fig. 5.7

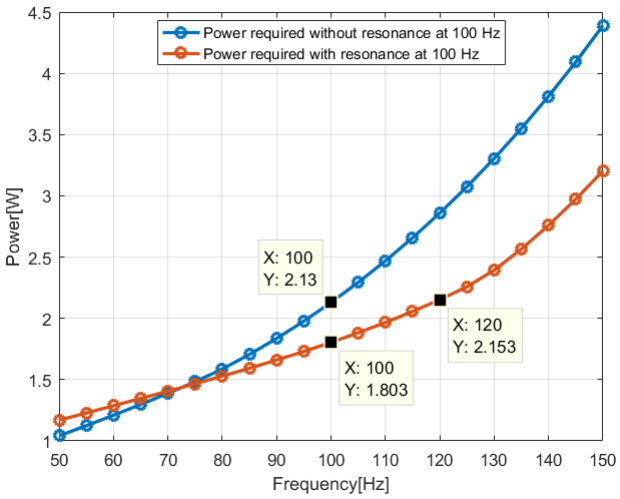

Figure 5.5: Comparison of power consumed with and without a resonant system when the motor frequency is varied

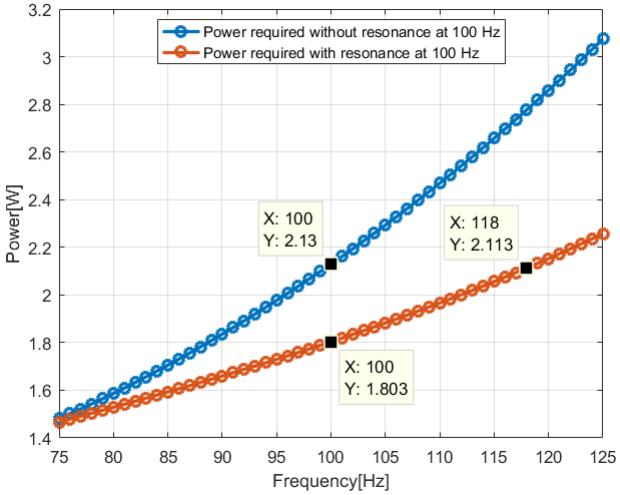

Figure 5.6: Zoomed in image of the comparison of power consumed with and without a resonant system when the motor frequency is varied

From Fig. 5.5 and 5.6, it can be seen that even if the system with a resonant frequency of 100 Hz is run at a speed of 100 Hz, the power consumed would be less than the power consumed at 100 Hz without resonance. A better way to put it is that with the introduction of resonance at 100 Hz, it would be possible to run the system at 118 Hz without any difference in the power consumption as compared to a non-resonant system running at 100 Hz. Hence, another advantage of a resonant hair clipper is that it can be run at a higher rpm, which can make the cutting process faster and more effective, without putting in any extra power.

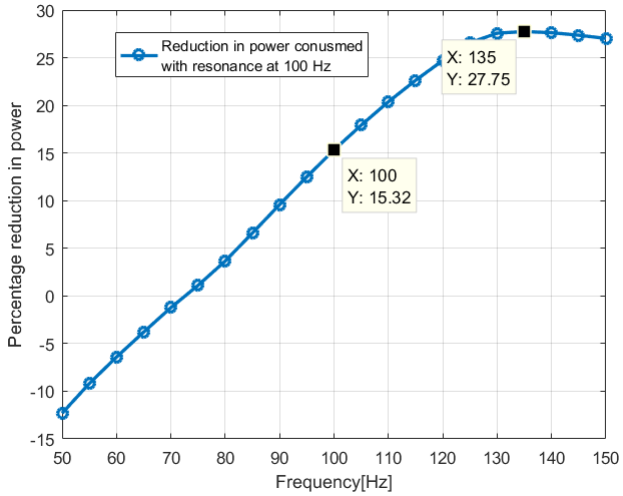

Figure 5.7: Reduction of power in percentage when the motor frequency is varied

From Fig. 5.7 it can be seen that the power saving, which is the percentage reduction in power consumed, reduces to zero percent approximately at about 73 Hz and has its maximum value of 27.75% at 135 Hz.

5.3.2. Sensitivity with respect to the resonance frequency of the system

It is possible that the stiffness of the spring might not be exactly as modeled. In the manufacturing process, stiffness of springs can vary by about $\pm 10\%$. This would create a variation in the resonance frequency of the system. Hence, it becomes necessary to analyze how much the reduction in power is affected by this variation.

The relation of variation in stiffness of the system to variation in its resonance frequency can be calculated as follows:

$$\omega_n = \sqrt{\frac{k}{m}}$$

$$\delta\omega_n = \sqrt{k}\left(-\frac{1}{2}\frac{1}{m\sqrt{m}}\right)\delta m + \frac{1}{\sqrt{m}}\left(\frac{1}{2}\frac{1}{\sqrt{k}}\right)\delta k$$

$$= \frac{1}{2}\sqrt{\frac{k}{m}}\left(\frac{\delta k}{k} - \frac{\delta m}{m}\right)$$

$$\therefore \quad \delta\omega_n = \frac{\omega_n}{2}\left(\frac{\delta k}{k} - \frac{\delta m}{m}\right) \tag{5.1}$$

The cutter of a Philips trimmer is manufacture in an extremely controlled manner. Hence the variation in mass can be assumed to be zero. Hence, $\delta m = 0$.

$$\therefore \quad \left(\frac{\delta\omega_n}{\omega_n}\right) = \frac{1}{2}\left(\frac{\delta k}{k}\right) \tag{5.2}$$

This means that if the variation in the stiffness is $\pm 10\%$, then the variation in the resonance frequency will be $\pm 5\%$.

To analyze the sensitivity of the percentage power reduction with respect to variation in spring stiffness, the resonance frequency of the system is varied from 80 Hz to 120 Hz, which is a $\pm 20\%$ variation from the desired resonance frequency of 100 Hz, with an interval of 5 Hz. From equation 5.2, this accounts to a variation of $\pm 40\%$ in the stiffness. The motor is run at a constant speed of 100 Hz. The power required in each case is observed and is compared with the power consumed for running a system without springs at 100 Hz. The plot of percentage reduction in power consumed in these cases can be seen in Fig. 5.8.

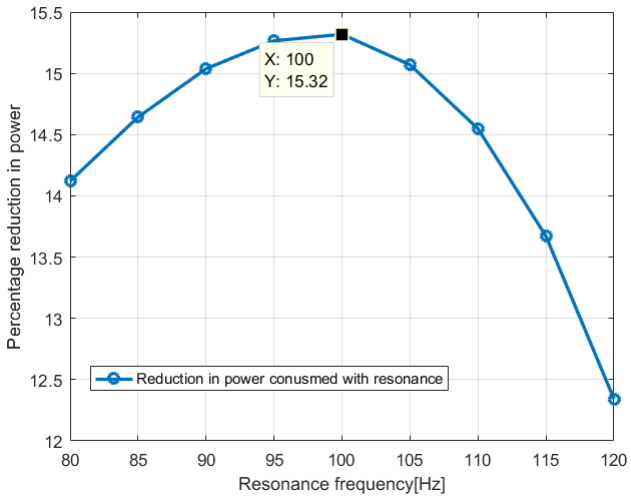

Figure 5.8: Percentage reduction in power when the resonance frequency of the system is varied

It can be seen that the maximum amount of power reduction is achieved when the resonance is exactly at the running frequency of the motor, which is 100 Hz. This is a pretty obvious result as the friction loss in the y-direction will be minimum when the two frequencies, namely the motor running frequency and the natural frequency of the system, match. It can also be concluded from the plot that the rate of decrease in percentage power reduction per unit variation in the resonance frequency of the system is higher when the resonance frequency is higher than the motor frequency as compared to when it is lower than the motor frequency. In other words, it is preferable to have springs with spring constants lower than the design value rather than higher. Of course, ideal would be to have springs with spring constants that match the design value exactly. This also means that, if it is difficult or cost intensive to control the motor speed exactly at the resonance frequency, a faster running motor is more acceptable as compared to a slower running motor.

5.3.3. Sensitivity with respect to the co-efficient of friction in x-direction

The co-efficient of friction between the guard and the cutter may vary with time and with varying working conditions. Thus, it would be wise to look at the sensitivity of the reduction in the consumption of power with the variation in the co-efficient of friction in x-direction.

For this analysis, the co-efficient of friction is varied from 0.1 to 0.7, the resonant frequency of the system being 100 Hz. The same is repeated again but this time, with no springs in the system. The power consumed in both the scenarios is observed and plotted against the co-efficient of friction in Fig. 5.9. The sensitivity of percentage reduction in power with respect to variation in x-direction friction can be seen in Fig. 5.10.

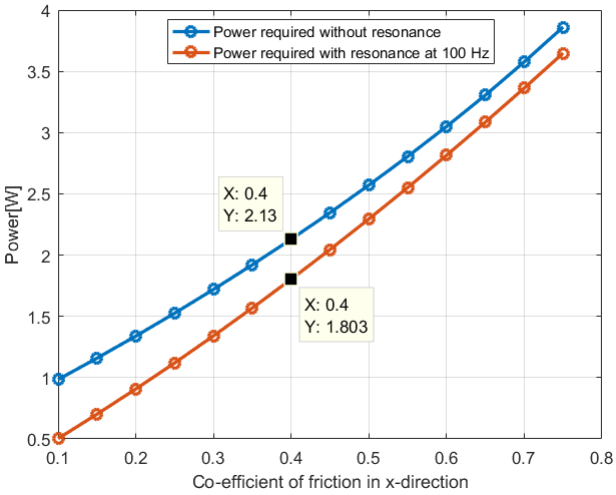

Figure 5.9: Comparison of power consumed with and without resonance when the co-efficient of friction in x-dir. is varied

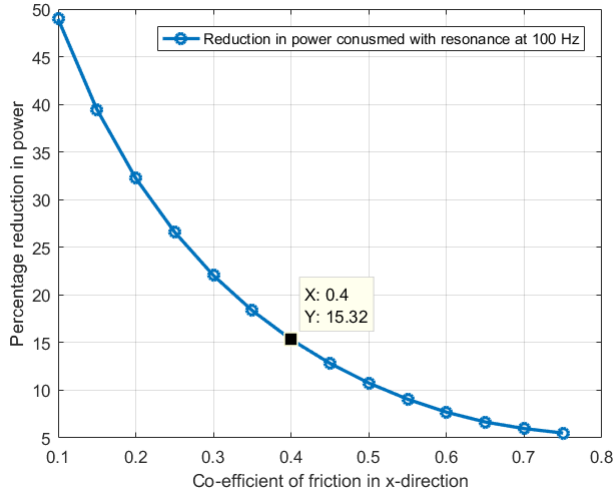

Figure 5.10: Reduction of power in percentage when the co-efficient of friction in x-dir. is varied

It can be seen from the figures above that as the friction in x-direction increases, the percentage reduction in power consumption decreases. This is just as one would expect after looking at the increase in power saving when the x-direction friction is reduced to almost nil, shown in section 5.2. It can be also concluded that the reduction in power consumed is pretty sensitive to the variation in friction between the cutter and the guard.

5.3.4. Sensitivity with respect to the co-efficient of friction in y-direction

The co-efficient of friction between the eccentric head of the motor and the drive bridge may vary with time and with varying working conditions. Thus, it would be advisable to look at the sensitivity of the reduction in consumption of power with variation in co-efficient of friction in y-direction.

The co-efficient of friction between the eccentric head and the drive bridge is known to Philips engineers and it lies between 0.12 and 0.25. For this analysis, the co-efficient of friction was varied from 0.1 to 0.5, the resonance frequency of the system being 100 Hz. The same is repeated again but

this time, with no springs in the system. The power consumed in both the scenarios is observed and plotted against the co-efficient of friction in Fig. 5.11. The sensitivity of percentage reduction in power with respect to variation in y-direction friction can be seen in Fig. 5.12.

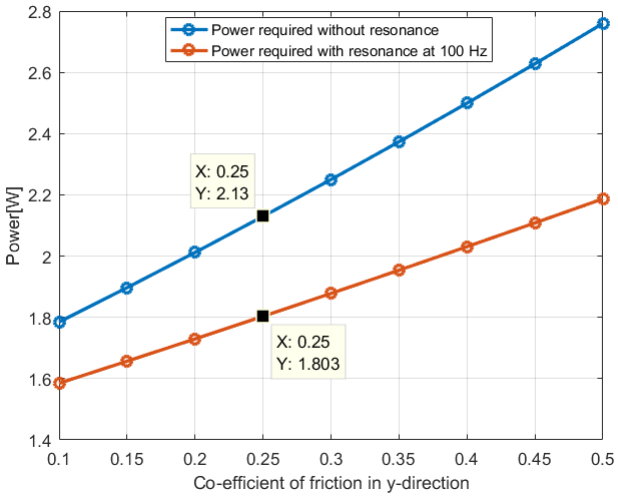

Figure 5.11: Comparison of power consumed with and without resonance when the co-efficient of friction in y-dir. is varied

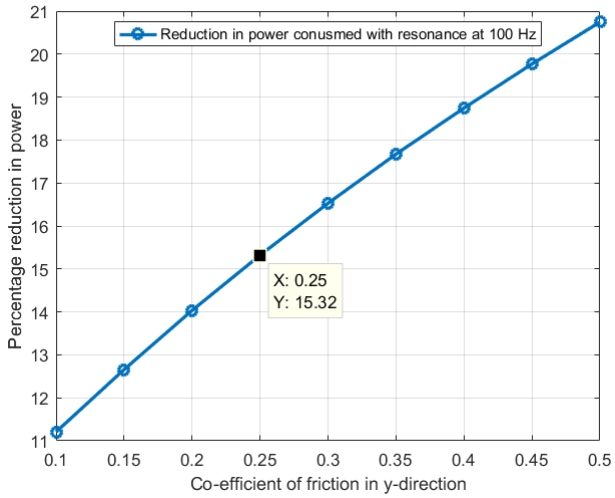

Figure 5.12: Reduction of power in percentage when the co-efficient of friction in y-dir. is varied

It can be seen from the figures 5.12 and 5.11 that as the friction in y-direction increases, the percentage reduction in power consumption increases. This can be explained in the following manner.

When the system is excited at the resonance frequency, the x-direction force (F_x) required to be delivered by the motor to move the cutter is only the Coulomb friction force between the cutter and the guard. When there are no springs in the system, the force required to accelerate and decelerate the mass also has to be provided by the motor. The friction force in y-direction is the product of the force delivered by the motor in x-direction through the eccentric head and the co-efficient of friction in y-direction, which is the co-efficient of friction between the eccentric head and the drive bridge $(F_y = \mu_y F_x)$.

Let the difference between the x-direction force required to run the non-resonant system at 100 Hz (F_{x_1}) and the force required to run the resonant system at 100 Hz (F_{x_2}) be ΔF_x. Thus, the difference between the y-direction forces (F_{y_1}) and (F_{y_2}) required to run the 2 systems becomes $\Delta F_y = \mu_y \Delta F_x$. This shows that if the co-efficient of friction in the y-direction increases, the value of ΔF_x remains the same but the value of ΔF_y increases. A large ΔF_y corresponds to a large difference in power consumption. Hence, a higher percentage of reduction in power consumed is observed at higher values of co-efficient of friction in the y-direction.

Of course, this does not mean that it is desired to have a high co-efficient of friction between the drive bridge and the eccentric head. This exercise was done just to see how the reduction in power consumed is affected by it. The actual reduction in power will depend on the actual co-efficient of friction present between the two components in real life.

5.3.5. Sensitivity with respect to the friction loss torque in the motor

It is possible that friction in the motor varies with time or from motor to motor. It would therefore be advantageous to vary it in the simulation and check the sensitivity of the reduction in power with respect to it.

To simulate this, the Coulomb friction in the motor is varied from $0.1\,\mathrm{mN\,m}$ to $0.6\,\mathrm{mN\,m}$. These values are chosen because the friction torque of a Faulhaber 2224 006 SR motor is $0.2\,\mathrm{mN\,m}$ and that of a Mabuchi 2290 SV motor is $0.6\,\mathrm{mN\,m}$ at 6000 rpm. The motors that are used in Philips hair clippers are of quality that lies between these 2 motors. In the first simulation, the resonance frequency of the system is set to be $100\,\mathrm{Hz}$. The simulation is repeated but this time, with no springs in the system. The power consumed in both the scenarios is observed and the percentage reduction in power is plotted against the motor friction loss in Fig. 5.13

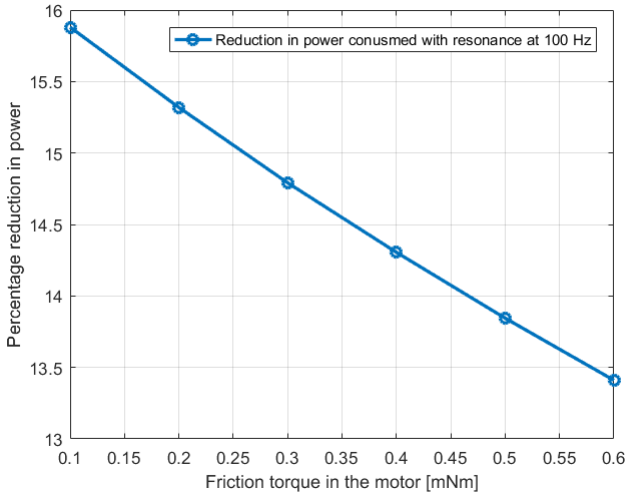

Figure 5.13: Percentage reduction of power when the friction loss torque in the motor is varied

The obvious result that the percentage reduction in power decreases as the friction in the motor increases can be seen in Fig. 5.13. Worthy of noting is the fact that even though the friction loss is varied by $0.5\,\mathrm{mN\,m}$, the decrease in the power reduction is only about 2.5%. So, this sensitivity is not something to worry about.

This sensitivity analysis provides an important insight into which parameters are more important to be controlled to achieve a certain amount of power saving in the hair clipper. As it can be observed, the

amount of power saving is very sensitive to the friction in x-direction. Hence, it is important to have as low friction in the x-direction as possible.

6. Validation of the mathematical model

To be able to do accurate predictions based on simulations, it is important for the model to be dependable. From the sensitivity analysis done, it can be concluded that even if the model is a bit inaccurate and the real values of the parameters deviate from the values put in the model, there will still be some power saving in the hair clipper with the use of a resonant system. Even so, to be able to predict exactly the amount of power that can be saved under different conditions, accuracy of the model is the key.

To validate the model, an experimental setup is designed that can replicate the behaviour of the hair clipper. It is not important in this project for the experimental setup to replicate the cutting behaviour of the hair clippers but only the dynamic behaviour of the motor, the eccentric head, the drive bridge, and the cutter.

6.1. Experiments

6.1.1. First design of the experimental setup

While designing the experimental setup, it is important to again consider the design aspects discussed in chapter 3 section 3.2, namely, introduction of stiffness in the cutter assembly, reduction of x-direction friction, and creation of pressure on the cutter without influencing the resonance characteristics. Various possible designs to handle these aspects were described in said section. Some of them are chosen to be included in the experimental setup owing to the advantages mentioned in said section. These designs are mentioned again below with relevant figures to represent them.

Design chosen to reduce friction: Use of linear bearings

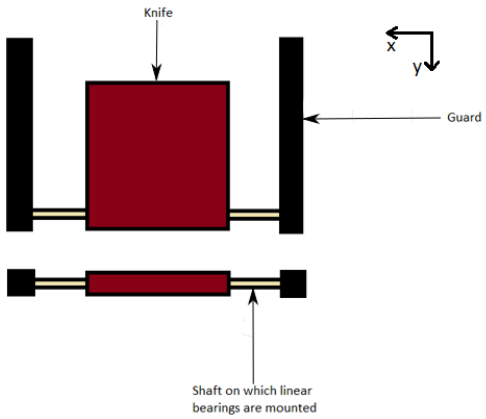

Figure 6.1: Friction reduced using linear bearings at the back end

Design chosen to create stiffness for resonance: Use of tension springs

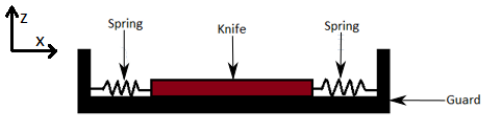

Figure 6.2: Resonance created with springs

Design chosen to create pressure: Use of tension springs on the bottom side of the knife

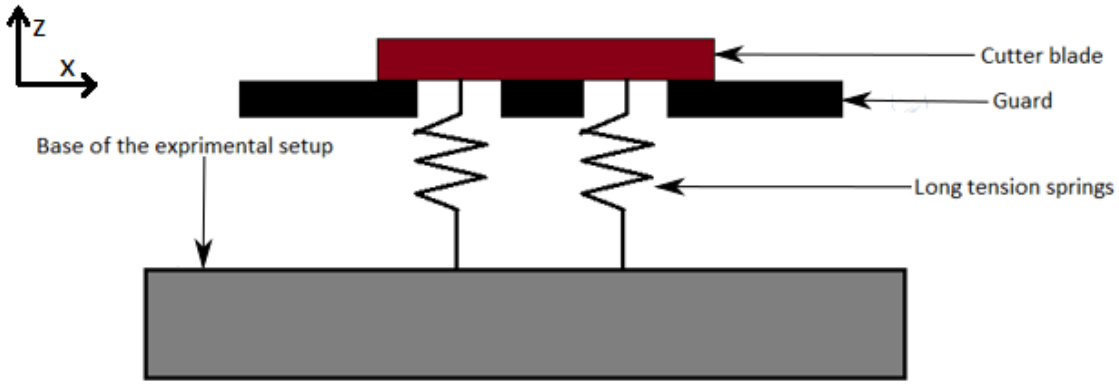

Figure 6.3: Pressure from bottom using tension springs

It is a good practice to note down all the requirements that the design should fulfill and then proceed to make the design.

Requirements

1. The resonance frequency of the system should be around 15 Hz. This is chosen arbitrarily. A low value is chosen to avoid high power requirements during the experiment.
2. There should be provision to change the resonance frequency of the setup by changing the cutter mass.
3. There should be provision to change the co-efficient of friction in the x-direction.
4. It should be possible to change the normal force between the cutter and the guard.
5. It should be possible to change the preset displacement of the resonance springs.
6. Any kind of bouncing between the cutter and the guard should be avoided.
7. It should be possible to measure the displacement of the cutter mass accurately with the laser vibrometer.
8. It should be easy to attach and remove the springs to the setup.

The experimental setup is an assembly of various components. The setup is modeled in the CAD modeling software NX and is manufactured in the prototyping department of Philips. The CAD model of the whole assembly is shown in Fig. 6.4. A magnified view of the same is shown in Fig. 6.5. The parts used in the setup are numbered in the figures shown and their names are mentioned in Tab. 6.1. Appendix C contains figures showing some of the individual parts.

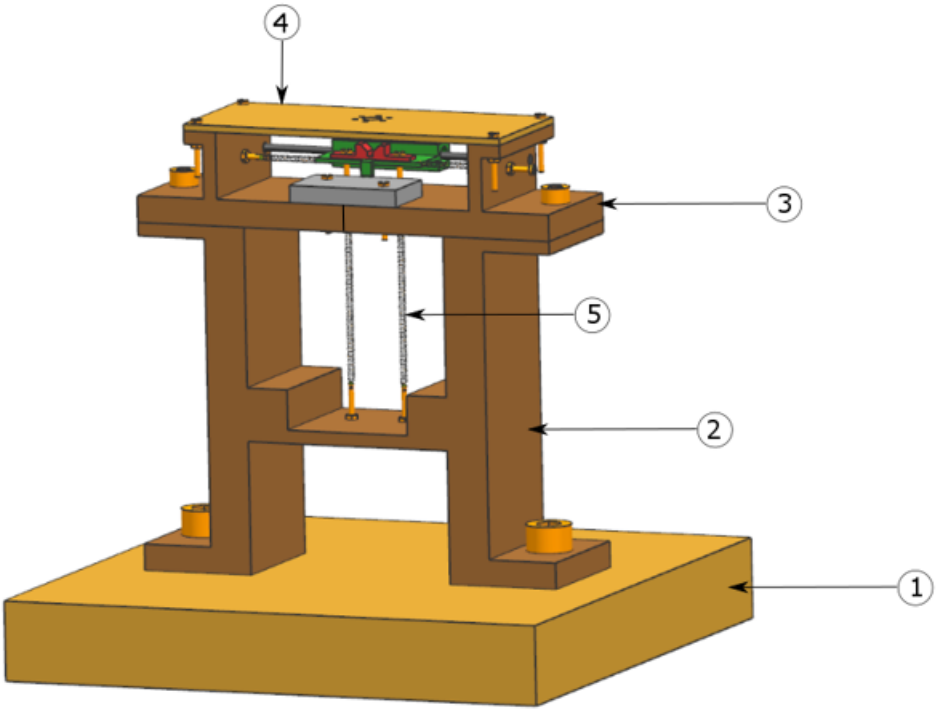

Figure 6.4: Experimental setup in NX

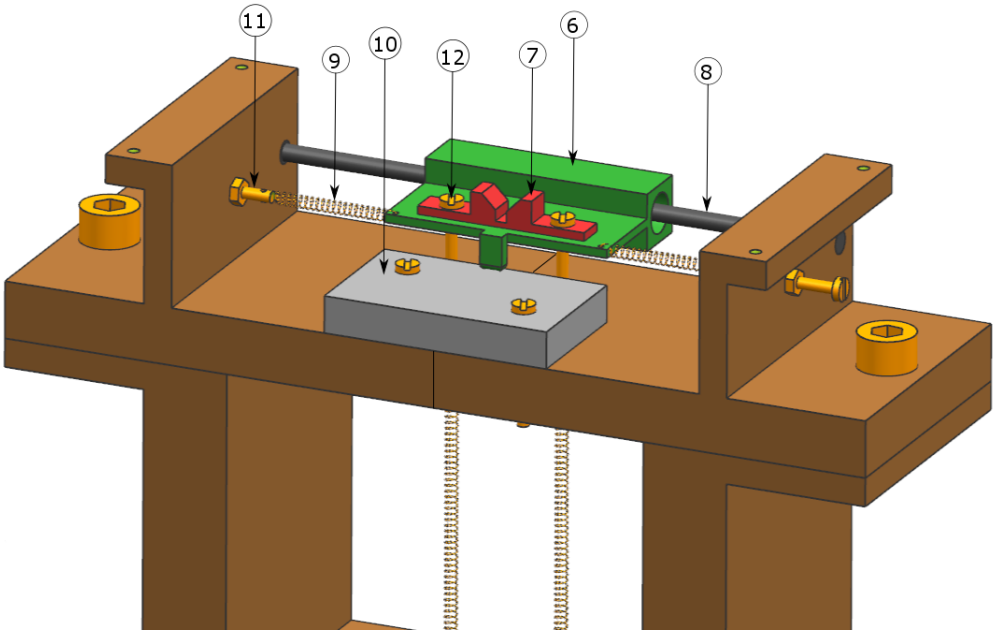

Figure 6.5: Experimental setup in NX (magnified)

Part nr.	Part name
1	Base plate
2	Ground level structure
3	Top level structure
4	Motor mounting plate
5	Pressure spring
6	Model of the cutter
7	Drive bridge
8	Shaft
9	Resonance spring
10	Model of the guard
11	Screw to adjust resonance spring force
12	Screw to adjust pressure spring force

Table 6.1: A list of parts used in the experimental setup

Description of the parts

1. **Base Plate:** It provides for a heavy and steady base for the setup. The material used is aluminium.
2. **Ground level structure:** It provides for the height required between the top level structure and the base plate. The material used is aluminium.
3. **Top level structure:** It acts as a support for the shaft and the screws for adjusting the resonance spring force. The material used is aluminium.
4. **Motor mounting plate:** It provides for the motor mounting. The material used is aluminium.
5. **Spring for creating pressure:** It provides for the continuous contact needed between the cutter and the guard in the vertical direction.
6. **Model of the cutter:** It acts as the mass in the resonant system. It represents the cutter used in an actual hair clipper. The material used is steel. Henceforth, in this report, it is referred to as the cutter.
7. **Drive bridge:** This is designed similar to the drive bridge used in the actual Philips hair clipper. It provides for a Scotch-yoke type mechanism. The eccentric head attached to the motor is inserted into the slot in the drive bridge. As the motor the rotational motion of the motor gets converted to the translation motion of the drive bridge and thus of the cutter. The material used is Polyoxymethylene(POM).
8. **Shaft:** It supports the cutter model which is free to run along the length of the shaft. There are linear bearings between the shaft and the cutter model. The material used is steel.
9. **Spring for creating resonance:**It provides for the stiffness in the resonant system.
10. **Model of the guard:** It provides for the friction surface on which the cutter model rubs against while vibrating. It represents the guard blade of an actual trimmer. The material used is steel.
11. **Screw to adjust resonance spring force:** It provides for the adjustment of resonance spring tension and thus of the spring force.
12. **Screw to adjust pressure spring force:** It provides for the adjustment of pressure spring tension and thus of the spring force.

The most important parameters to note in the setup is the natural frequency of the cutter-spring combination. The mass of the cutter is $28\,\mathrm{g}$ and the stiffness is $320\,\mathrm{N\,m^{-1}}$. As a result, the natural frequency of the system is approximately $17\,\mathrm{Hz}$.

6.1.2. Experiments on the first experimental setup

Having manufactured the setup, the first set of experiments are run on the experimental setup using the following steps:

1. A variable voltage source is connected across the motor terminals. The motor used is Faulhaber 2224 006SR, which has an encoder inside it. The encoder output is read by a digital frequency sensor. A digital ammeter is connected in series with the motor to measure the current through the motor at different speeds.
2. Python is used to write a computer program that controls the voltage supplied to the motor and reads the values sensed by the ammeter and the frequency sensor. It is to be noted that the motor speed is not controlled by any controller. It is determined by the voltage supplied, the friction losses in the motor and the load torque that it experiences as it reciprocates the cutter mass.
3. The setup is made ready to start the experiment. The springs are attached to the cutter so that the system becomes a mass-spring-damper system and all screws are tightened.
4. The program commands the motor to run at various voltages ranging from $0.3\,\mathrm{V}$ to $2\,\mathrm{V}$ in equidistant steps. This results in the motor running at frequencies approximately between $4\,\mathrm{Hz}$ and $42\,\mathrm{Hz}$.
5. The values of current drawn by the motor to reciprocate the system at different speeds are noted. Using the motor equations mentioned in section 4.1.2, corresponding values of torque required by the motor are calculated.
6. Using the values of current drawn and voltage supplied, values of power consumed by the motor at different speeds are calculated.
7. The springs are removed from the system. Now the reciprocating system is a mass-damper system which represents the current hair clippers.
8. Steps 4,5 and 6 are repeated.

The values of torque required by the motor to reciprocate the system at different speeds in both conditions, that is when the springs are attached to and detached from the system, are plotted on a chart for comparison. The same is done for the values of power drawn by the motor. The same experiment is repeated again and again to check repeatablility. Fig. 6.6 shows the comparison of the power consumed in the two cases while Fig. 6.7 shows the comparison of the torque required to run the system in the two cases.

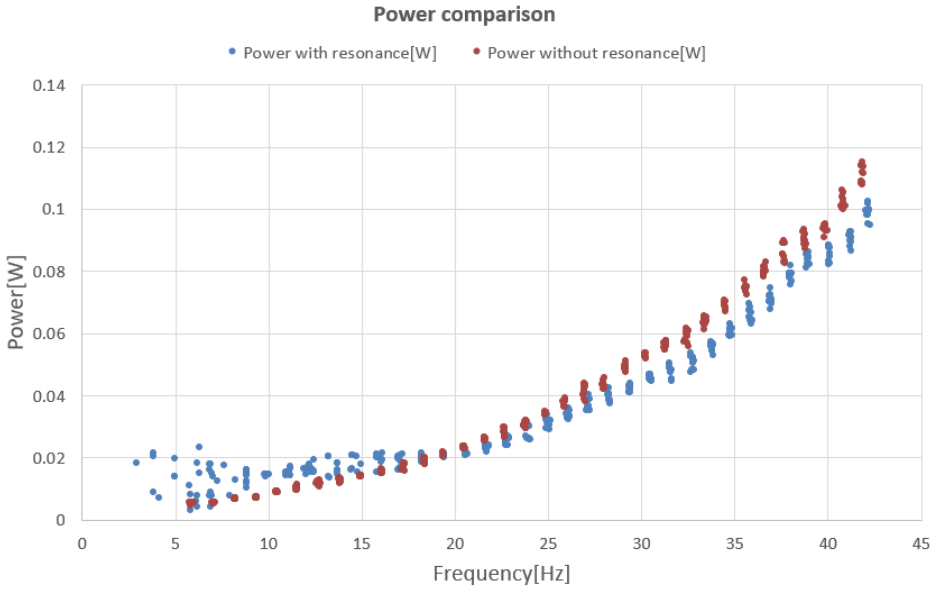

Figure 6.6: Comparison of power consumed with and without springs in the first experimental setup

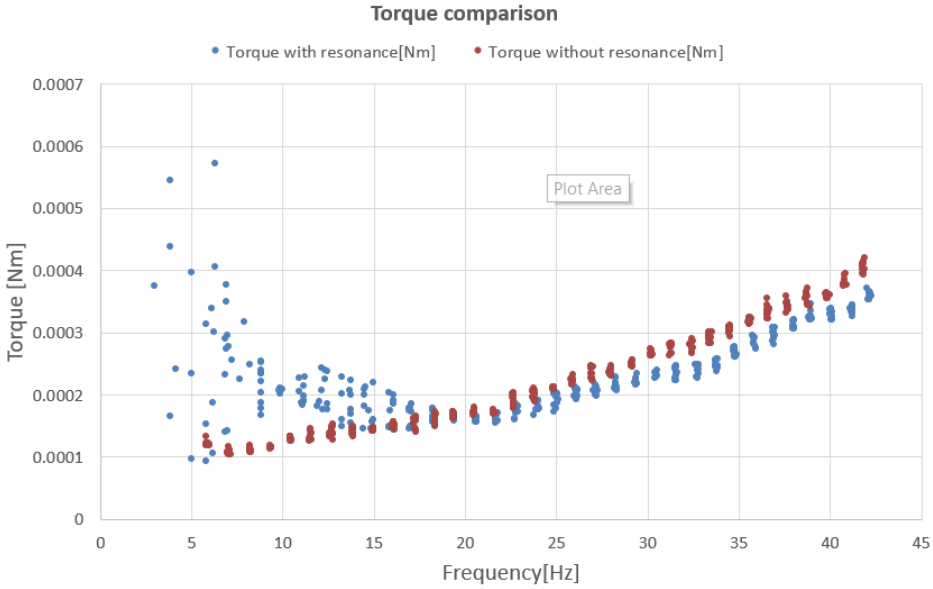

Figure 6.7: Comparison of torque required to run the motor with and without springs in the first experimental setup

From Fig. 6.7 it can be concluded that when the system is run with springs, the least amount of average torque needed to the run the system happens around the resonance frequency, which is 17 Hz.

When the system is run at extremely low speeds, that is around 5 Hz, the variation in the torque consumed is extremely large. This phenomenon can be explained by considering the forces acting on the cutter during oscillations at low frequencies. The spring force acting on the cutter at each point in the path of oscillation only depends on the extension of the two resonance springs. It is independent of the motor speed. The inertia force of the cutter mass however is directly proportional to the square of the angular velocity of the motor. The system is designed in such a way that these two forces become equal at the resonance frequency of 17 Hz. This implies that at low running speeds of the motor, the

spring force will be very high as compared to the inertia force. The inertia of the motor is also very low at low speeds. As a result, during certain parts of the oscillation, the spring force will impede the motor considerable while during other parts of the oscillation, it will assist the motor. This is reflected in the current drawn by the motor and thus in the torque required to drive the system.

It can be observed that this phenomenon of large variation in torque happens also very close to the resonance frequency. This renders the experimental data unreliable. It can be seen that the variation reduces as the motor speed increases. Hence, it is decided to move the natural frequency of the system to about $25\,\mathrm{Hz}$. To increase the natural frequency, either the stiffness can be increased or the mass of the cutter can be decreased. In this case, due to practical constraints, it is easier to decrease the mass of the cutter than to order new springs, the delivery of which takes a long time.

Criticism of the cutter design

It is clear from the above analysis that the mass of the cutter is more than it should be in order to be able to run smoothly at frequencies close to the resonance frequency of the system. Other than this, a careful observation of the system in Fig. 6.5 reveals a major drawback of this design. None of the forces pass through the centre of gravity of the cutter. The forces acting on the cutter are the resonance spring force, the pressure spring force the force exerted by the motor, the friction force between the cutter & the guard, and the friction force in the linear bearings. All of these forces create unnecessary moments around the centre of gravity of the cutter. Ideally, all these forces should pass through the centre of gravity. This is not practically possible in this case but an effort is made to minimize the moments arising due to these forces by redesigning the cutter such that all of these forces except for the pressure spring force act in the same plane as the plane made by the centre line of the two resonance springs and the centre line of the shaft. Furthermore, the spring force and the force exerted by the motor act in the same line and this line passes through the centre of gravity of the cutter. The CAD model of the newly designed cutter is shown in Appendix C.

6.1.3. Second design of the experimental setup

With changes required to be done to the design of the cutter, changes have to be made to the design of some of the other parts. The above analysis of the cutter design resulted into some additional requirements for the setup to fulfill. The original requirements still hold true.

Additional requirements

1. The resonance frequency of the system should be around $25\,\mathrm{Hz}$
2. As far as possible, all external forces acting on the cutter mass should be balanced about the centre of gravity such that there is no moment created around it because of the forces.
3. If that is not practically possible, all the forces should be brought in one plane such that if any moments are created around the centre of gravity, they will be in the same plane.
4. If that is also not practically possible, the forces should act as close to the centre of gravity as possible to minimize the moments.

A new setup is designed keeping these requirements in sight. The mass of the new cutter is $12\,\mathrm{g}$ and the stiffness of the resonance springs is still the same, that is $320\,\mathrm{N\,m^{-1}}$. Thus, the the resonance frequency of the new system is about $26\,\mathrm{Hz}$. Important aspects of the new setup are shown in Fig. 6.5. It can be seen from Fig. 6.9 that in the new setup the friction force between the cutter & the guard, the resonance spring forces, the centre line of the shaft around which the linear bearing friction acts and the driving force exerted by the motor are all in one and the same plane.

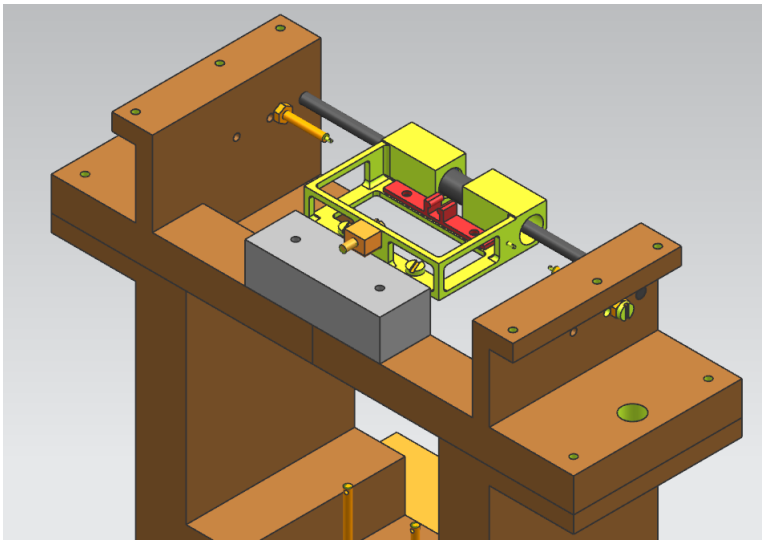

Figure 6.8: New experimental setup in NX

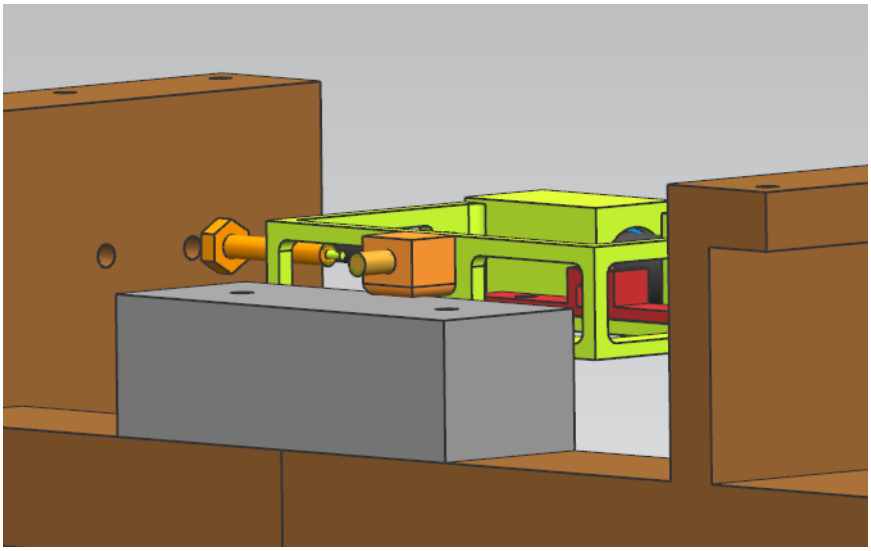

Figure 6.9: New experimental setup in NX

6.1.4. Experiments on the second experimental setup

Having manufactured the second experimental setup, the next step is to carry out experiments on the setup using the following steps:

1. A variable voltage source is connected across the motor terminals. The motor used is Faulhaber 2224 006SR, which has an encoder inside it. The encoder output is read by a digital frequency sensor. A digital ammeter is connected in series with the motor to measure the current through the motor at different speeds.
2. Python is used to write a computer program that controls the voltage supplied to the motor and reads the values sensed by the ammeter and the frequency sensor. It is to be noted that the motor speed is not controlled by any controller. It is determined by the voltage supplied, the friction losses in the motor and the load torque that it experiences as it reciprocates the cutter mass.
3. The setup is made ready to start the experiment. The springs are attached to the cutter so that the system becomes a mass-spring-damper system and all screws are tightened.

4. The program commands the motor to run at various voltages ranging from 0.5 V to 3 V in 35 equidistant steps. This results in the motor running at frequencies between 10 Hz and 65 Hz.
5. The values of current drawn by the motor to reciprocate the system at different speeds are noted. Using the motor equations mentioned in section 4.1.2, corresponding values of torque required by the motor are calculated.
6. Using the values of current drawn and voltage supplied, values of power consumed by the motor at different speeds are calculated.
7. The springs are removed from the system. Now the reciprocating system is a mass-damper system which represents the current hair clippers.
8. Steps 4,5 and 6 are repeated.

The values of torque required by the motor to reciprocate the system at different speeds in both conditions, that is when the springs are attached to and detached from the system, are plotted on a chart for comparison. The same is done for the values of power drawn by the motor. The same experiment is repeated again and again to check repeatablility.

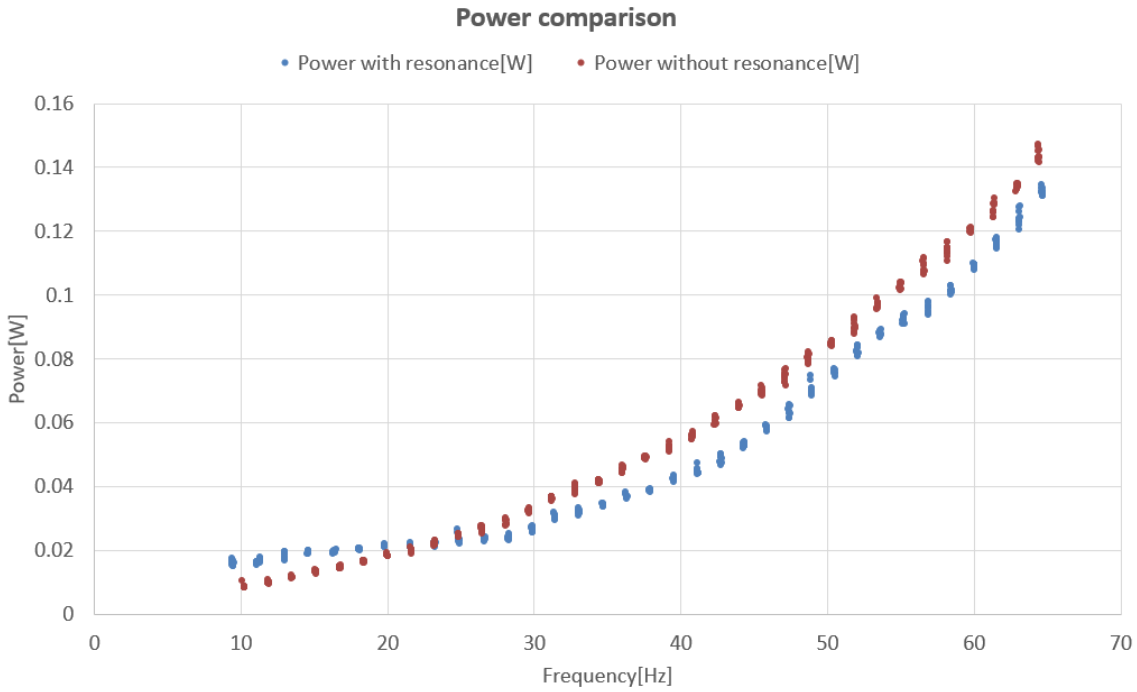

Figure 6.10: Comparison of power consumed with and without springs in the second experimental setup

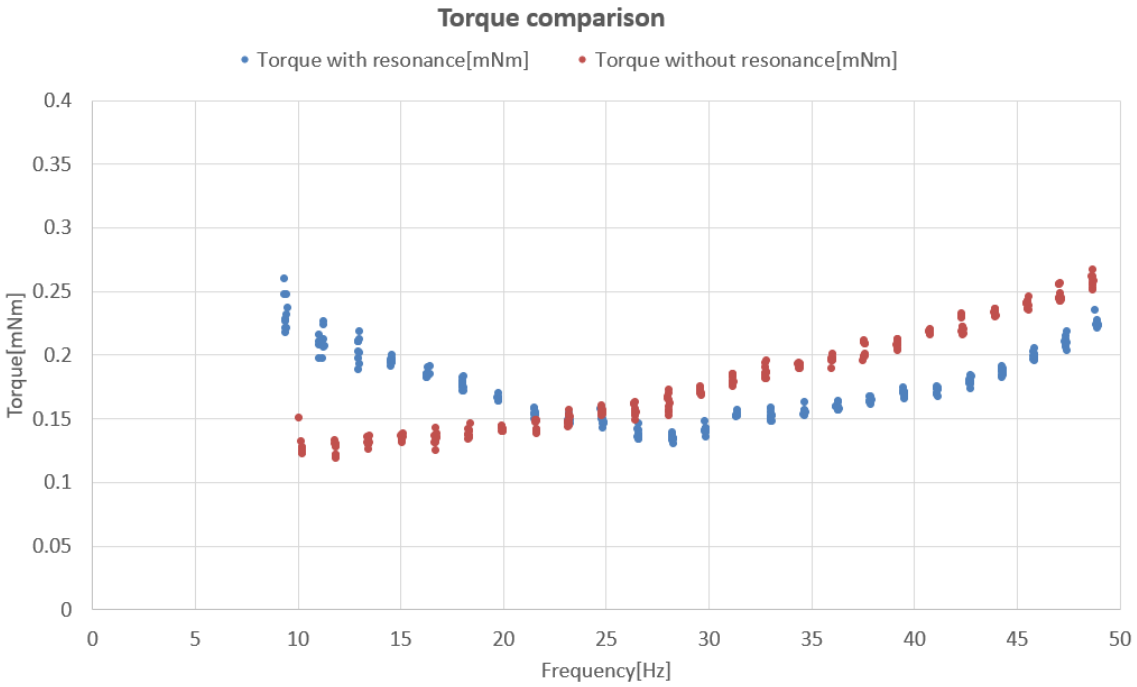

Figure 6.11: Comparison of torque required to run the motor with and without springs in the second experimental setup

It can be seen from Fig. 6.11 that the least amount of torque required to run the system corresponds to the motor speed of 26 Hz, which is the resonance frequency of the system. It can be seen from Fig. 6.10 that the power required to run the system at 26 Hz reduces when the springs are introduced in the system. It can be inferred from Fig 6.10 and 6.11 that the change in the design of the cutter has helped in reducing the variations in the recorded data around the resonance frequency.

The data obtained from the experiments is processed in MATLAB to filter out the variations and find the average power consumed at each frequency step. The plot thus obtained is shown in Fig. 6.12. It can be seen that the power consumed around 26 Hz is about 27 mW when springs are not used in the system and it reduces to about 24 mW when springs are used. This accounts to a reduction of about 12% in power consumed. Hence, the experiments conclude that running the system at its resonance frequency is indeed beneficial in terms of power consumed and this principle can be readily used in Philips hair clippers.

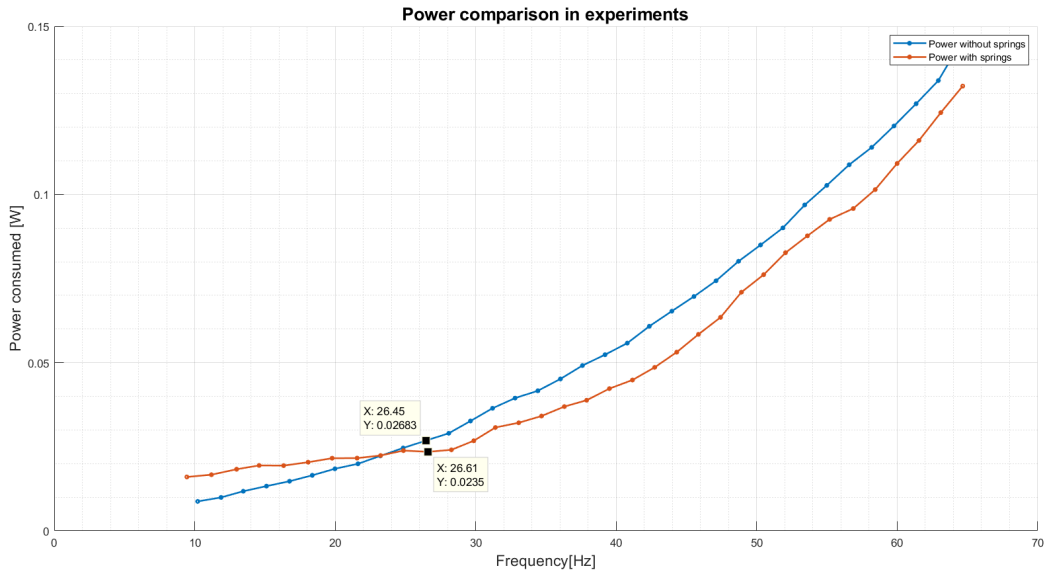

Figure 6.12: Comparison of average power consumed with and without springs in the second experimental setup

6.2. Investigation of parameters in the experimental setup

Having done the experiments using the experimental setup, the next step is to run the simulation and compare the simulation results with the experimental results. For this step to be accurate, it is necessary for the mathematical model to represent the experimental setup accurately. There are many parameters in the experimental setup that can affect the results. The values of some of these parameters can be known from their design or the available product data sheets while for some other parameters experiments need to be carried out. The parameters investigated and the experiments carried out to obtain their values are mentioned in the sections below.

6.2.1. Spring constant

As mentioned earlier while investigating the sensitivity of the model with respect to resonance frequency, to get the maximum power saving possible with the use of resonance phenomenon, it is important to precisely know the resonance frequency of the system. This frequency can vary if there is a variation in spring stiffness and not always are the springs manufactured of the same stiffness as desired. Hence, to know the stiffness of the springs used in the experimental setup accurately, they are tested using a computer-controlled tensile & compression tester system from Mecmesin. It has a load cell which is a transducer that converts a load or force acting on it into an electronic signal. Based on this electronic signal and the calibration of the sensor, the load cell gauges the load acting on it [16].

Figure 6.13: Mecmesin load tester used in the experiment

Courtesy: [15]

One of the springs used in the experimental setup is attached to the steady end of the load cell and is pulled from the other end by the load cell as it moves

up slowly. As the spring stretches, this creates a force on the load cell which is gauged and plotted against the displacement of the spring, as shown in Fig. 6.14. For the first few millimeters of the stretch the spring is very compliant and hence there is negligible force on the load cell. As it is stretched more, it starts resisting the load cell movement progressively as seen in the plot. A trend line is plotted on the graph and its governing equation is shown. If F_s is the spring force in Newtons and x is the deflection of the spring in millimetres, the governing equation is of the trend line is $F_s = 0.16x + 0.26$. The spring constant which is the slope of the trend line is equal to $0.16\,\mathrm{N/mm}$, which is $160\,\mathrm{N/m}$. This is the desired spring constant to have resonance at the target resonance frequency. The test is carried out for the other spring as well and the results are the same. Both the springs have the desired spring constants.

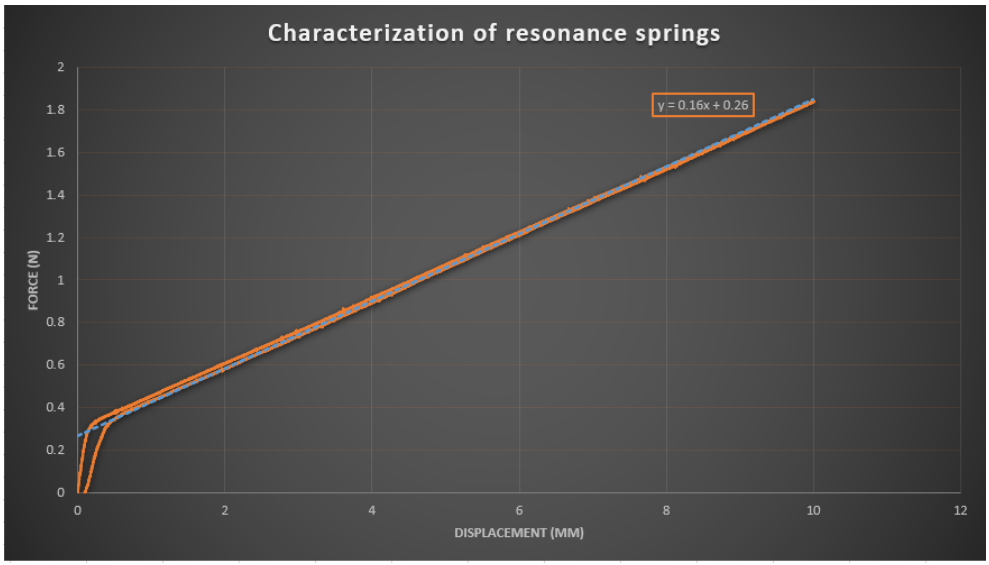

Figure 6.14: Characterization of resonance springs

6.2.2. Friction in the motor

Another parameter that may be different from the one expected in design is the motor friction. All motors have inherent friction in them and this friction may vary with time and also according to working conditions. Although it was seen in section 5.3 that the percentage power saved in the simulated system was not very sensitive to motor friction losses, it should be noted that the parameters of the experimental setup are different than the parameters of the system simulated earlier. In the system that was simulated in 5.3, the friction co-efficient between cutter and guard was 0.4 and that between eccentric head and drive bridge was 0.25. The normal force at the cutter-guard contact surface was $3.5\,\mathrm{N}$. In the experimental setup, all these values are lesser than this. So, the amount of losses due to motor friction in the experiment setup will constitute a larger percentage of the total friction losses in the system as compared to that in the system simulated in section 5.3. Hence, it becomes important to know the friction losses in the motor precisely to make the model more accurate. The experiment carried out to know these values is called characterization of the motor. With this experiment, a plot like that shown in Fig. 6.15 is sought to be obtained. The angular speed of the motor is represented on the x-axis and the friction torque lost in the motor is represented on the y-axis. The part of friction that is independent of motor speed is the Coulomb friction and that linearly varying with the motor speed is called viscous friction.

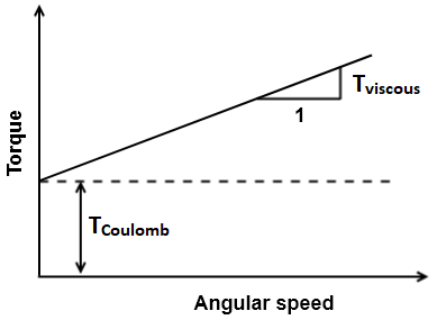

Figure 6.15: Generic representation of friction torque characteristics in a motor

Characterization of the motor is done by using another motor and a mechanism to couple the shafts of the two motors. The motor that needs to be characterized is called the test motor and one that is used as assistance is called the reference motor. A computer program is written in Python to carry out this experiment in multiple steps.

Step 1: The output shafts of the reference motor and the test motor are coupled to each other manually. A speed controller controls the speed of the reference motor. The computer program commands the controller to run the reference motor at different speeds. Let the speed of the reference motor be ω_1 and that of the test motor be ω_2. As the two motors are mechanically coupled to each other, $\omega_1 = \omega_2$.

As the reference motor causes the test motor to rotate, an electromotive force (EMF) is generated across the test motor terminals. This EMF is called the back EMF (e_{b2}). It is sensed by a voltmeter and the values of this EMF for different running speeds of the test motor are recorded. From the motor equations stated section 4.1.2 $e_{b2} = K_2\omega_2$, where K_2 is the motor constant of the test motor. By plotting the back EMF sensed (e_{b2}) against the rotational speeds of the test motor (ω_2) and calculating the slope of the line, the motor constant K_2 is calculated. This plot is shown in Fig. 6.16 and the value of K_2 is $0.0072\,\mathrm{V}\cdot\mathrm{sec}/\mathrm{rad}$

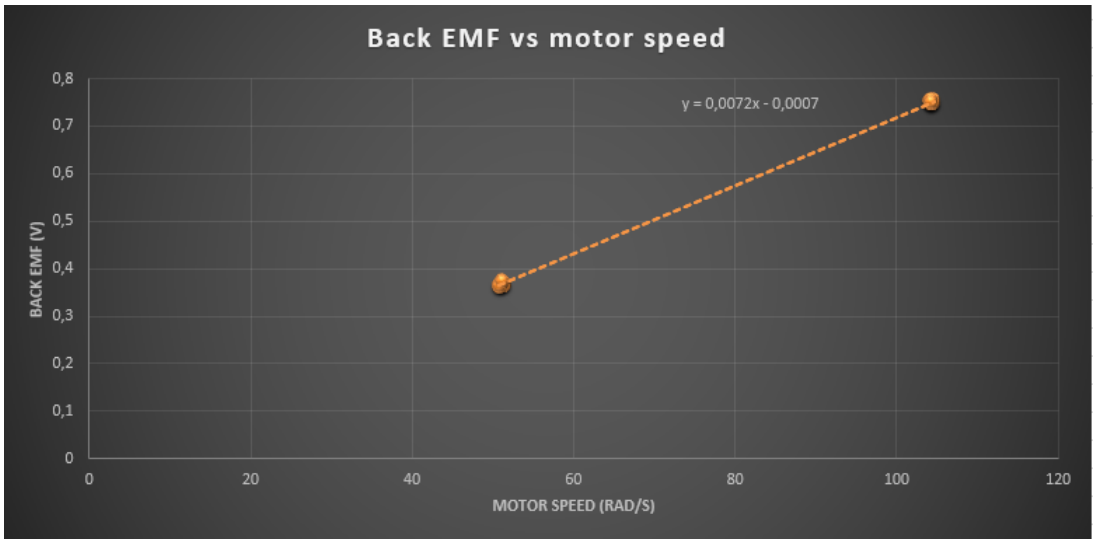

Figure 6.16: Plot of back emf generated in the test motor against its running speeds. the slope of this graph is the motor constant

There are two types of friction in motors, namely, Coulomb friction and viscous friction. Coulomb

friction does not depend on motor speed but viscous friction does. As the motor speed increases, viscous friction in it goes on increasing. It is directly proportional to the motor's angular frequency. If T_{vm2} is the torque loss due to viscous friction in the test motor and B_2 is the co-efficient of viscous friction in the test motor,

$$T_{vm2} = B_2 \cdot \omega_2$$

If T_{cm2} is the torque loss due to Coulomb friction in the test motor, the total friction loss in the test motor is

$$T_{fm2} = T_{cm2} + T_{vm2} \tag{6.1}$$
$$= T_{cm2} + B_2 \cdot \omega_2 \tag{6.2}$$

Figure of a plot of Friction torque loss vs motor frequency.

The plot of total friction loss in motor versus motor frequency is a straight line intersecting the torque loss axis at the value of Coulomb friction loss T_{cm2} as shown in Fig. **??**. Further steps are carried out to obtain this plot to know the values of friction in the test motor.

Step 2: The current drawn by the reference motor (i_1) while doing the first step is also recorded. Using the motor equation between the current drawn and the torque experienced, $T_1 = K_1 i_1$, the values of torque are calculated. Here T_1 is the torque experienced by the reference motor while driving the test motor at speed w_1 and K_1 is the motor constant of the reference motor, which is already known from calibration. A graph of the torque required against the motor frequencies is plotted and the equation of the trend is noted. This equation is of the form

$$T_{fmc} = T_{cmc} + B_{mc} \cdot \omega_1 \tag{6.3}$$

Here T_{cmc} is the torque loss due to Coulomb friction in both motors combined, B_{mc} is the co-efficient of viscous friction in both motors combined, T_{vmc} is the torque loss due to viscous friction in both motors combined and T_{fmc} is the total torque loss due to friction in both motors combined.

Step 3: Both the motors are decoupled and the reference motor alone is run at different speeds. The current drawn by the motor at all the speeds is recorded and the torque required to run the reference motor alone at various speeds is calculated in the same way as mentioned before. A graph of the torque required against the motor frequencies is plotted and the equation of the trend is noted. This equation is of the form

$$T_{fm1} = T_{cm1} + T_{vm1} \tag{6.4}$$
$$= T_{cm1} + B_1 \cdot \omega_1 \tag{6.5}$$

Here T_{cm1} is the torque loss due to Coulomb friction in the reference motor alone, T_{vm1} is the torque loss due to viscous friction in the reference motor alone, B_1 is the co-efficient of viscous friction in the motors combined and T_{fm1} is the total torque loss due to friction in the reference motor alone. The plots obtained in steps 2 and 3 are shown in Fig. 6.17

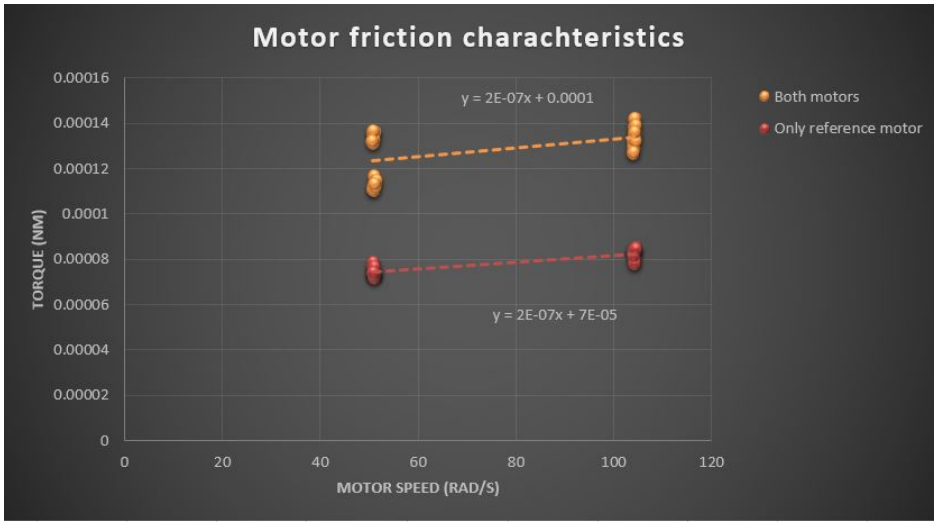

Figure 6.17: Plot showing the difference between motor friction torque when both motors are coupled and are run by the reference motor and when only reference motor is running.

Step 4: Friction losses in the test motor (T_{fm2}) are equal to the difference between the torque required to run the combined system (T_{fmc}) and the torque required to run the reference motor alone (T_{fm1}) . Hence, by subtracting the equation of the trend line obtained in step 3 from the trend line obtained in step 2, the equation for friction losses in the test motor is obtained.

$$T_{fm2} = T_{fmc} - T_{fm1} \tag{6.6}$$

Parameters obtained: After following these steps, important parameters of the test motor are found and are mentioned in Tab. 6.2 along with other important motor parameters. The values of motor inductance and motor inertia are taken from the data sheet as they tend to not change over time.

Parameter	Symbol	Value	Unit	Reason
Resistance	R	2	ohm	Motor characterization
Inductance	L	45×10^{-6}	H	Data sheet
Motor inertia	J	2.7×10^{-7}	$kg \cdot m^2$	Data sheet
Motor constant	K	0.0072	$V \cdot s/rad$	Motor characterization
Motor Coulomb friction	T_{cm}	5×10^{-5}	$N \cdot m$	Motor characterization
Motor viscous friction	B_2	3.92×10^{-8}	$N \cdot m \cdot s/rad$	Motor characterization

Table 6.2: Values of motor parameters obtained from motor characterization experiment

6.2.3. Friction between the cutter and the guard

One more parameter that is not known accurately at the point of design is the friction between the cutter and the guard, that is the x-direction friction. Again in this case, the friction is expected to be of two types, namely, Coulomb friction and viscous friction. Knowing the friction in a reciprocating system is basically knowing the damping characteristics of the system. If the cutter with springs attached is given a certain displacement and then let go, it will start reciprocating. The amplitude of oscillation will reduce progressively in successive cycles of oscillation because of the damping present in the system and after some time the cutter will come to rest. By observing the trend of successive amplitudes and noting

the pattern in which they reduce successively, the type of friction present in the system can be known and also calculated. This concept is used to get the values of friction between the cutter and the guard.

A laser vibrometer for Polytec as shown in Fig. 6.18 is used to carry out this experiment. The vibrometer has 2 lasers pointed at 2 different surfaces; one is pointed at a steady surface and the other is pointed at the moving surface of the cutter. The laser ray from the laser pointed at the cutter is oriented exactly parallel to the x-direction so that the ray reflected back towards the pointer is also parallel to the x-direction and goes straight back to the pointer. The pointer also collects the reflected rays. The same happens at the other pointer that is pointed at an immovable object. These two reflected rays are compared and the relative velocity between them is calculated using the Doppler effect. Hence this process is called laser Doppler vibrometry. Depending on the velocity and displacement of the cutter, the reflected laser ray is changed in frequency and phase. These shifts are detected by a high precision interferometer inside the Polytec laser vibrometer and it produces voltages corresponding to the velocity of the cutter. These voltages can be easily converted to velocities using a simple mapping.

Figure 6.18: Polytec laser vibrometer OFV-552

Note: The Philips prototyping department at Drachten, where the experimental setups were manufactured, is an extremely busy department. The first experimental setup took about a month and a half to be manufactured. After the experiments were carried out on the first setup, it was concluded that a new cutter needed to be made. This would take another month as the design of the new cutter is intricate. This would mean a huge loss of time in a project that is planned for 9 months. Hence, it is decided to go ahead with the parameter investigation using the old cutter. In addition to that, the laser vibrometer is not readily available to check the amplitude decay in natural vibration. Valuable time is also lost in waiting for its availability. This makes the use of the vibrometer after the manufacturing of the second experimental setup unfeasible. Due to this, the parameter investigation is carried out using the first setup while the experiments will be carried out using the second setup. This may cause some inaccuracies in the model.

The cutter is given an initial displacement and it is let go. The laser vibrometer records the varying velocity of the cutter at a sample rate of 100 kHz. The velocity data is then integrated to get the displacements. Eight measurements are taken with different initial displacements. One of them is shown in Fig. 6.19.

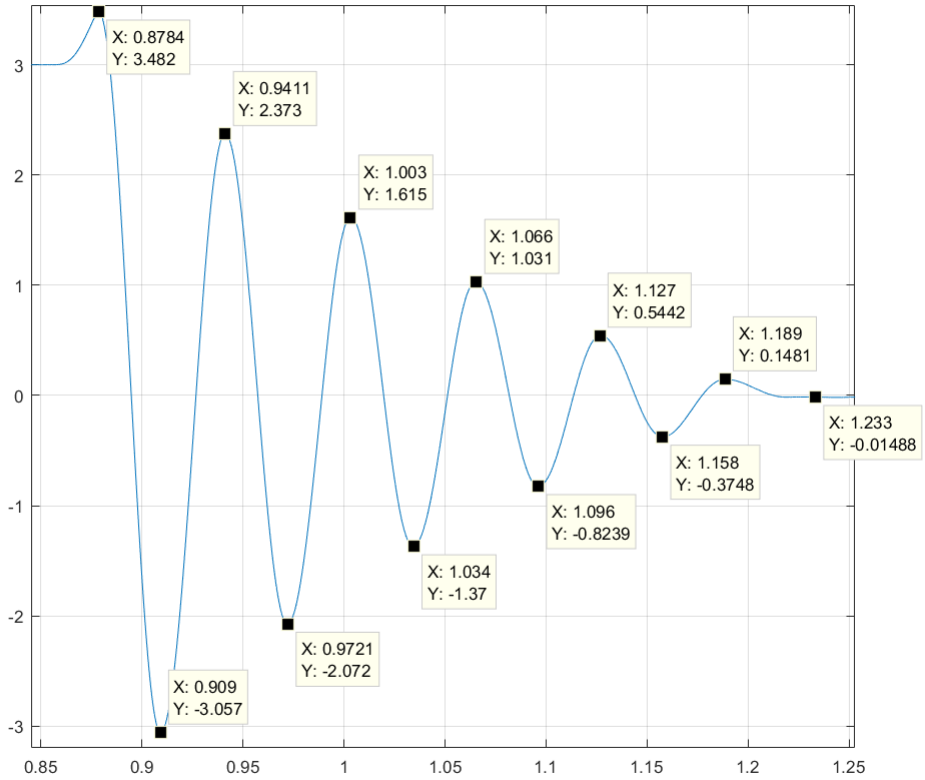

Figure 6.19: Measurement of free vibration taken with a laser vibrometer

If the friction in the system was purely of Coulomb type, the amplitude would decay linearly with time[2]. A close look at the maximum displacement points reveals that the points do not lie on a straight line. In spite of that, it is good to know how much error is caused if the points are assumed to be on a straight line. To do this, the negative displacements are multiplied by -1 and made positive. Then a program for curve fitting is written in MATLAB that uses the least squares method to fit a straight line. The sum of squared errors comes out to be 0.55. The equation of the line fitted is given by the following:

$$x = mt + x_0 \tag{6.7}$$

where m is the slope of the line and x_0 is the initial displacement of the mass. The line fitted through the points is shown in Fig. 6.20. It does not come close to all the points.

If the friction in the system was purely of viscous type, the amplitude would decrease exponentially with time[2]. To check whether that is the case, a fit of a purely exponential curve is tried on these extreme displacement points using. This is also done by writing a code in MATLAB. The fit is of the following form:

$$x = e^{-t/\tau} \tag{6.8}$$

The curve fit is shown in Fig. 6.21. Such a curve also does not come close to all the points, which means that the friction is not purely viscous. The sum of squared errors in this case is 0.13 in this case.

Thus, it is evident that the friction is not purely of Coulomb or viscous type. There is a possibility that

it is a combination of both. Hence, an exercise of fitting a curve with the following equation is done:

$$x = at + be^{-t/\tau} \tag{6.9}$$

This is also done by writing a code in MATLAB. The sum of the squares of the errors with such a fit was 0.022 which is extremely less than the sum of squared errors noted in previous two curve fitting exercises. The extreme displacement points fitted with a combination of a straight curve and an exponential curve are shown in Fig. 6.22. The curve comes really close to all the points.

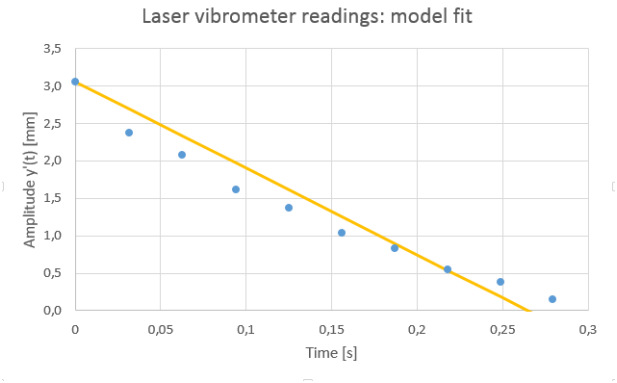

Figure 6.20: The extreme displacement points fitted with a straight curve

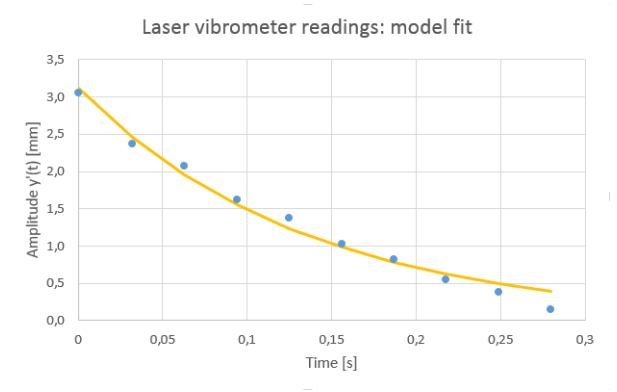

Figure 6.21: The extreme displacement points fitted with an exponential curve

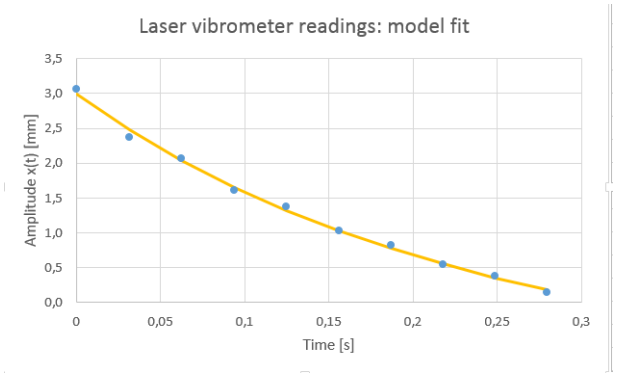

Figure 6.22: The extreme displacement points fitted with a combination of a straight curve and an exponential curve

It is concluded that the friction in the system is a combination of Coulomb and viscous friction. The same curve fitting exercise is repeated for all eight measurements. Values of the parameters a and τ obtained from the curves resulting from these exercises are very close to each other. This shows that the experiment is repeatable and the results are precise. To calculate the values of parameters a and τ, averages of all the values obtained from different curves are taken. Parameter values thus obtained are as follows:

$$\begin{aligned} a &= -2.84\,\text{mm/s} \\ \tau &= 0.187 \end{aligned} \tag{6.10}$$

From these values of a and τ the values of Coulomb friction and viscous friction present in the system can be calculated. For a system with Coulomb friction, the amplitude of oscillation reduces linearly with every cycle of oscillation.

After every period of oscillation, the amplitude reduces by a value Δx

$$\Delta x = \left(\frac{4\mu_x N}{k}\right) [2] \tag{6.11}$$

where,
k = Stiffness in the system,
N = Normal force on the cutter,
μ_x = Co-efficient of friction in x-direction.

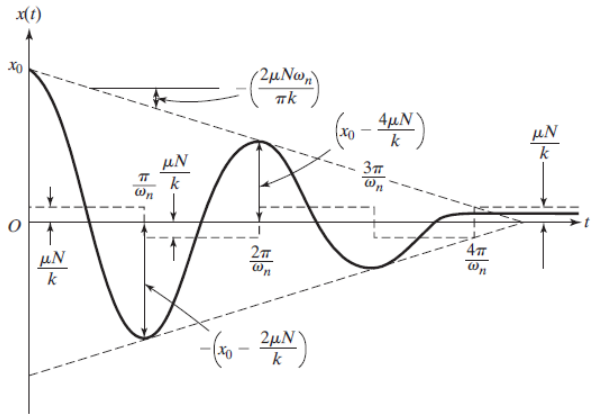

Figure 6.23: Linear decay of amplitude in presence of pure Coulomb friction

Courtesy: [2]

Hence, in one second, the amplitude decays by the following value:

$$\Delta x = \left(\frac{4\mu_x N}{kT}\right) \tag{6.12}$$

where,
T = Time period = $2\pi/\omega_n$,
ω_n = natural frequency of the system.

This is nothing but the parameter a obtained from the curve fitting exercise. Hence, from equations 6.10 and 6.12 the following is obtained:

$$\therefore \quad \frac{4\mu_x N}{kT} = \frac{2.84}{1000}$$

The time period of oscillation observed in the experiment is 0.06 seconds. The normal force on the oscillating mass during the experiment is only its weight, which is 0.028×9.81N, as the mass of the oscillating cutter is $28\,\mathrm{g}$. The total stiffness in the system is $320\,\mathrm{N/m}$. Substituting these values in the above equation, the following is obtained:

$$\mu_x = \frac{2.84 \times 320 \times 0.06}{4 \times 1000 \times 0.028 \times 9.81}$$

$$\therefore \quad \mu_x = 0.05 \tag{6.13}$$

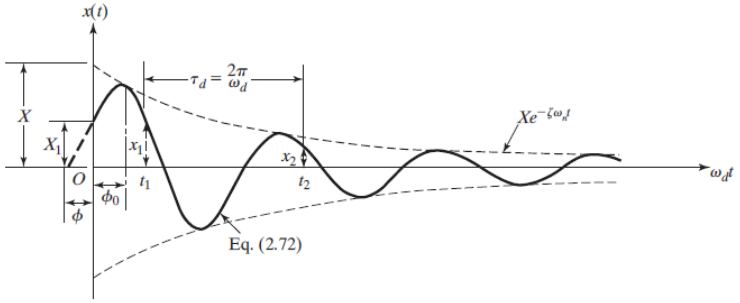

Figure 6.24: Exponential decay of amplitude in presence of pure viscous friction[2]

When there is pure viscous friction in the system, the amplitude of the oscillation decays exponentially following the curve $e^{-\zeta\omega_n t}$ [2], where ζ is the damping ratio, ω_n is the natural frequency of oscillation and t is the time elapsed since the start of the free vibration. The curve fitting done with the decay of amplitude in the experiments, had an exponential component which followed the curve $e^{-t/\tau}$. Comparing these two curves and using the value of τ obtained through curve fitting, it can be deduced that

$$\begin{aligned} \zeta\omega_n &= 1/\tau \\ &= 1/0.187 \\ &= 5.32 \\ \zeta &= \frac{5.32}{\omega_n} \\ \therefore \quad \zeta &= 5.32 \times \sqrt{\frac{m}{k}} \\ \zeta &= 5.32 \times \sqrt{\frac{0.028}{320}} \\ \zeta &= 0.05 \end{aligned}$$

The damping ratio ζ can be expressed as the ratio of the damping co-efficient in x-direction, which is c_x and the critical damping in x-direction(c_{cx}) [2].

$$\begin{aligned} \zeta &= \frac{c_x}{c_{cx}} \\ &= \frac{c_x}{2\sqrt{km}} \\ \therefore \quad c_x &= 2\zeta\sqrt{km} \end{aligned} \tag{6.14}$$

Substituting the values of k, m and ζ,

$$c_x = 0.3\,\mathrm{Ns/m} \tag{6.15}$$

6.2.4. Friction between the eccentric head and the drive bridge

The last parameter to be found out by experimentation is the friction between the steel eccentric head and the plastic drive bridge as they make contact in the scotch-yoke type driving mechanism. To find this friction amount is relatively simple as compared to finding out the friction amount in the x-direction.

Step 1: The motor is run at various speeds without any load and values of current drawn by the motor at those speeds are noted. The torque needed by the motor to run at different speeds is calculated using the motor equations. Using these values, an equation for torque consumed by the motor for different motor speeds is derived. The equation is of the following form:

$$\begin{aligned} T_{fm} &= T_{cm} + T_{vm} \\ &= T_{cm} + B_m \cdot \omega \\ &= T_{cm} + B_m \cdot 2 \cdot \pi \cdot f \end{aligned} \tag{6.16}$$

Here ω is the angular speed of the motor in $\mathrm{rad/sec}$, f is the motor frequency in Hz, T_{cm} is the torque consumed to overcome Coulomb friction in the motor, T_{vm} is the torque consumed to overcome viscous friction in the motor, B_m is the co-efficient of viscous friction in the motor and T_{fm} is the total torque consumed by friction in the motor. All torques are in $\mathrm{N\,m}$. This is just like the exercise done in the experiment for characterization of motor.

Step 2: An extension to the motor shaft which is non-eccentric, as shown in Fig.C.5 in appendix C, is mounted on the motor shaft. This serves as a mere extension of the motor shaft. The tension in each of the two springs is adjusted such that the cutter is pulled on one side more than the other side. This is done by adjusting the deflection in the springs by rotating the adjusting screws. In this situation, even when the system is steady, the drive bridge is pushed against the extended motor shaft. The difference in the lengths of the springs (x_d) is kept $7.5\,\mathrm{mm}$ and the difference in the force exerted by them is calculated. This is the normal force that the drive bridge puts on the extended motor shaft.

Step 3: The motor is given a gradually increasing voltage input which makes the motor rotate at gradually increasing speeds. In this case as well, just like in step 1, the current values are noted, the torque values are calculated and and equation for the torque consumed for different speeds of the motor is derived. The equation is of the following form:

$$\begin{aligned} T_{fms} &= T_{cms} + T_{vms} \\ &= T_{cms} + B_{ms} \cdot \omega \\ &= T_{cms} + B_{ms} \cdot 2 \cdot \pi \cdot f \end{aligned} \tag{6.17}$$

Here ω is the angular speed of the motor in $\mathrm{rad/sec}$, f is the motor frequency in Hz, T_{cms} is the torque consumed by Coulomb friction in the motor and in the contact between the drive bridge and the extended motor shaft, T_{vms} is the torque consumed by viscous friction in these two entities, B_{ms} is the co-efficient of viscous friction in the combined system and T_{fms} is the total torque consumed by them. All torques are in $\mathrm{N\,m}$. Plots of all the readings taken in steps 1 and 3 are shown in Fig. 6.25. An important point to note here is that in these plots, the total friction torque is plotted against the motor frequency in Hz and not in $\mathrm{rad/sec}$. Hence, the slopes of the trend lines plotted for the two experiments, as shown in Fig. 6.25, are the values of the products of the corresponding co-efficient of viscous friction and the factor 2π.

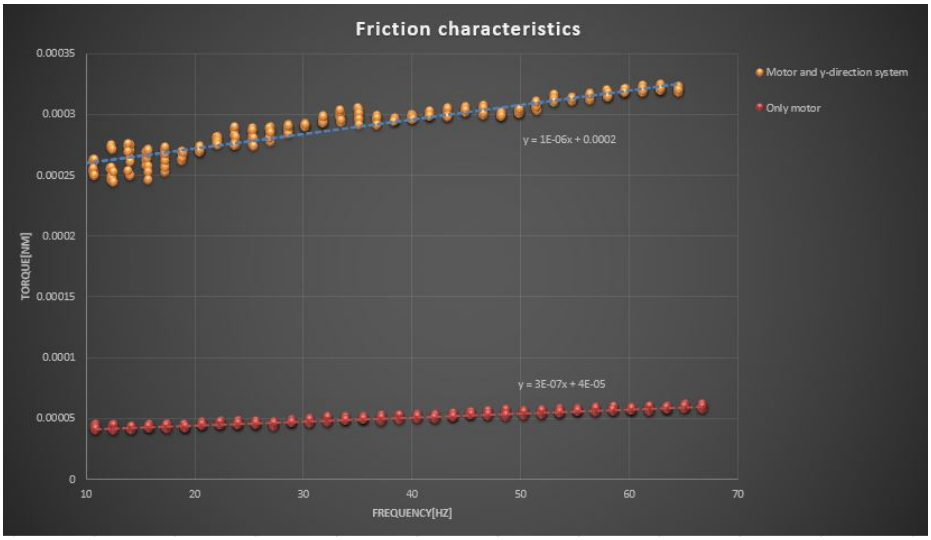

Figure 6.25: Friction characteristics in y-direction

Step 4: Friction losses in y-direction (T_{fy}) in the driven system are equal to the difference between the torque required to run the combined system mentioned in step 3 (T_{fms}) and the torque required to run the motor alone (T_{fm}) . Hence, by subtracting the equation of the trend line obtained in step 3 from the trend line obtained in step 2, the equation for friction losses in the test motor is obtained.

$$\begin{aligned} T_{fy} &= T_{cy} + T_{vy} \\ &= T_{fms} - T_{fm} \\ &= (T_{cms} - T_{cm}) + (B_{ms} - B_m) \cdot \omega \\ &= (T_{cms} - T_{cm}) + (B_{ms} \cdot 2 \cdot \pi - B_m \cdot 2 \cdot \pi) \cdot f \end{aligned} \tag{6.18}$$

Here T_{cy} is the Coulomb friction loss in y-direction and T_{vy} is the viscous friction loss in y-direction, both in N m.

Parameter	Symbol	Value	Unit
Y-direction viscous friction coefficient	B_y	1.12×10^{-7}	Nm · s/rad
Y-direction Coulomb friction	T_{cy}	2×10^{-3}	N m

Table 6.3: Values of system parameters obtained from the y-direction friction characterization experiment

Table 6.3 makes it clear that the dominant part of y-direction friction is Coulomb friction. It should be noted that the y-direction Coulomb friction value obtained here is the value of torque required by the motor to overcome friction in y-direction. This values cannot be put directly as the y-direction friction value in the mathematical model. In the model, a y-direction Coulomb friction co-efficient and not the friction torque, is modeled. To derive this parameter, the kinematics of motion as explained in section 4.2.1 are again referred to. As shown in Fig. 4.15, the y-direction friction force creates a load torque on the motor which is a multiple of the friction force in y-direction and the radius of the moment arm which is the same as the amplitude of oscillation of the cutter (r_1).

$$\begin{aligned} \therefore \quad & T_{fy} = F_{fy} \cdot r_1 \\ \text{and} \quad & T_{cy} = F_{cy} \cdot r_1 \\ \text{and} \quad & T_{vy} = F_{vy} \cdot r_1 \end{aligned} \tag{6.19}$$

As the viscous friction is negligible, $T_{fy} = T_{cy}$. The value of y-direction Coulomb friction force (F_{cy}) is given by the product of the normal force between the drive bridge and the eccentric head (N_y) and the co-efficient of Coulomb friction between them (μ_{cy}).

$$F_{cy} = \mu_{cy} \cdot N_y \tag{6.20}$$

$$\therefore \quad T_{cy} = \mu_{cy} \cdot N_y \cdot r_1 \tag{6.21}$$

The normal force between the eccentric head and the drive bridge is given by the formula:

$$N_y = k \cdot x_d \tag{6.22}$$

where, k is the stiffness of one spring and x_d is the difference in deflections in the two springs.

$$\therefore \quad T_{cy} = \mu_{cy} \cdot k \cdot x_d \cdot r_1 \tag{6.23}$$

Using the value of T_{cy} obtained from the experiment and the values of system parameters, equation 6.23 produces the value of the co-efficient of Coulomb friction in y-direction.

$$\begin{aligned} \therefore \quad & 2 \times 10^{-3} = \mu_{cy} \times 160 \times 7.5 \times 10^{-3} \times 0.0015 \\ & \mu_{cy} = \frac{160 \times 7.5 \times 10^{-3} \times 0.0015}{2 \times 10^{-3}} \\ \therefore \quad & \mu_{cy} = 0.11 \end{aligned} \tag{6.24}$$

Results of parameter investigation

All the values of various parameters that determine the performance of the experimental that were obtained from the experiments described above are mentioned below in Tab. 6.4.

Parameter	Symbol	Value	Unit
Circuit electrical resistance	R	2	ohm
Motor constant	K	0.0072	V · s/rad
Motor Coulomb friction	T_{cm}	0.00005	N · m
Motor viscous friction co-eff.	B_m	negligible	N · m/rad
Spring constant of each spring	k	160	N/m
X-direction viscous friction co-eff.	c_x	0.3	N · sec /m
X-direction Coulomb friction co-eff.	μ_{cx}	0.05	
Y-direction viscous friction co-eff.	c_y	negligible	N · sec /m
Y-direction Coulomb friction co-eff.	μ_{cy}	0.11	

Table 6.4: Values of parameters of the experimental setup which are obtained from experiments

6.3. Simulations using the obtained parameters

After having carried out various experiments to find the values of important parameters used in the mathematical model, the model is simulated to observe the power required to run the system at various speeds when there are no springs used and when springs are attached to the system. The power consumed in both the scenarios is shown in Fig. 6.26. It can be seen that the power consumed

around 26 Hz is about 25 mW when springs are not used in the system and it reduces to about 20 mW when springs are used. This accounts to a reduction of about 22% in power consumed.

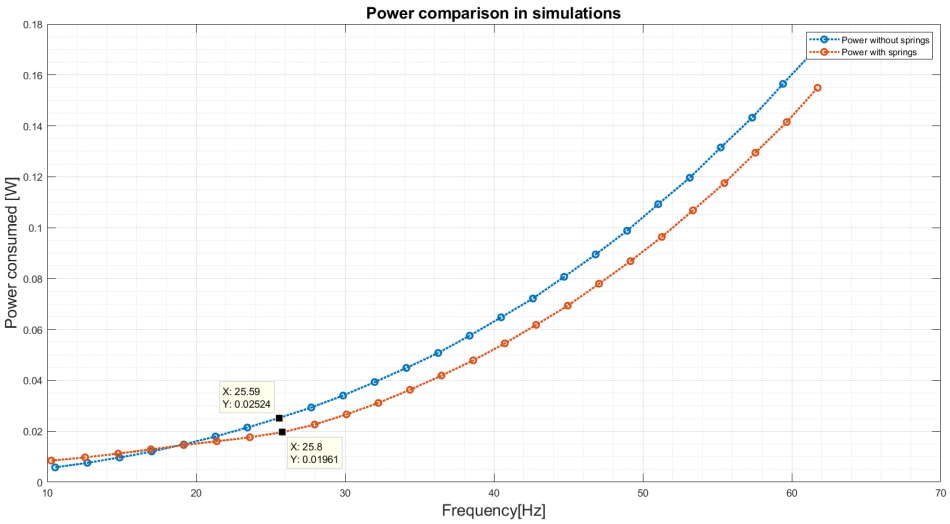

Figure 6.26: Comparison of power consumed with and without springs in simulations

7. Results and discussion

7.1. Comparison between simulations and experiments

To check the accuracy of the model it is necessary to compare the results obtained through the simulations with those obtained through experiments. The reduction in power consumed at the resonance frequency of 26 Hz observed through simulations and experiments are compared in Tab. 7.1

	Simulations	**Experiments**
Power consumed without springs [mW]	25	27
Power consumed with springs [mW]	20	24
Power reduction achieved [%]	22	12

Table 7.1: Comparison between simulations and experiments

It is clear that there is a difference between the simulated results and the experimental results. To view this difference graphically, the plots of power consumed at different motor speeds with and without springs observed through simulations and experiments are plotted on top of each other. This is shown in Fig. 7.1.

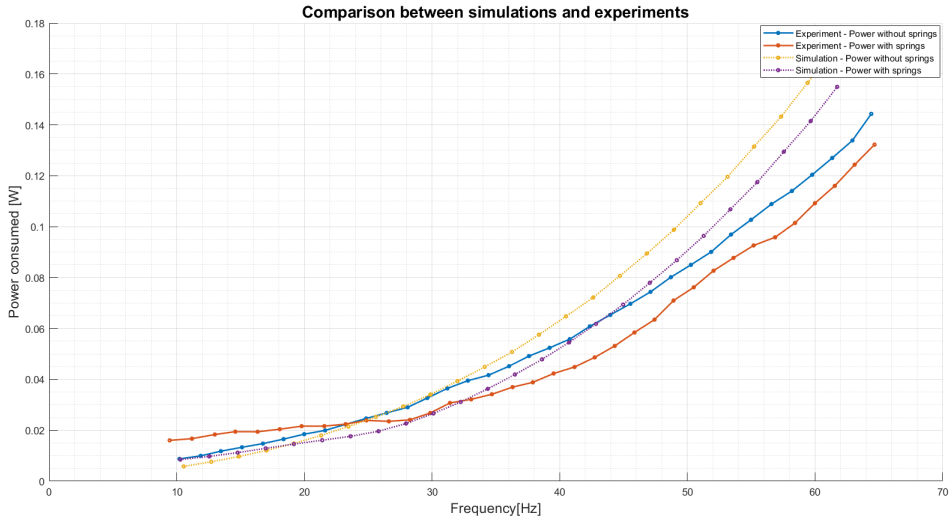

Figure 7.1: Comparison of power consumed in the experiments with that predicted by simulations

7.2. Analysis of the comparison between simulations and experiments

There are some differences in the plots of power consumed at different motor speeds obtained through simulations and those obtained through experiments. Some peculiar observations can be made from Fig. 6.12, 6.26 and 7.1

Fig. 7.1 shows that the rising pattern of the simulation curves is different than that of the experimental curves. The simulations predict a steeper rise in power consumed as the motor speed increases. At low frequencies, the simulations predict the power consumed to be lower than than that observed through experiments. It also shows that at high frequencies, the simulations predict the power consumed to be higher than than that observed through experiments. This could mean that the effect of viscous friction is more pronounced in the simulations than in the experiments.

As mentioned earlier, the Philips prototyping department at Drachten, where the experimental setups were manufactured, is an extremely busy department. The first experimental setup took about a month and a half to be manufactured. After the experiments were carried out on the first setup, it was concluded that a new cutter with a modified design needed to be made. This would take another month as the design of the new cutter is intricate. This would have resulted in a huge loss of time in a project that was planned for 9 months. Hence, it was decided to go ahead with the parameter investigation using the unmodified cutter.

In addition to that, the laser vibrometer was not readily available to check the amplitude decay in natural vibrations. Valuable time was also lost in waiting for its availability. This made the use of the vibrometer after the manufacturing of the second experimental setup unfeasible. Due to this, the parameter investigation was carried out using the first setup while the experiments were carried out using the second setup.

This also meant that there was a gap of about a month between the parameter investigation experiments and the final experiments carried out on the new setup. The values of friction might have changed in this period. A little bit of moisture or the lack there of is enough to change the value of viscous friction. Formation of minute rust particles on the guard might also change the value of friction.

If the model is conceptually correct but the values of parameters are modeled incorrectly, the results obtained from simulations and experiments will not match. In such a case, logical modification of the model parameters should lead to reasonable matching of the simulation and experimental results.

7.2.1. Modification of parameters in the model

To check whether there is a difference between the actual friction parameters and the modeled parameters, all the parameters in the model except the viscous friction in x-direction are kept the same and the simulations are run again. The viscous friction is made zero and the results are compared with the experiments again. This can be seen in Fig. 7.2

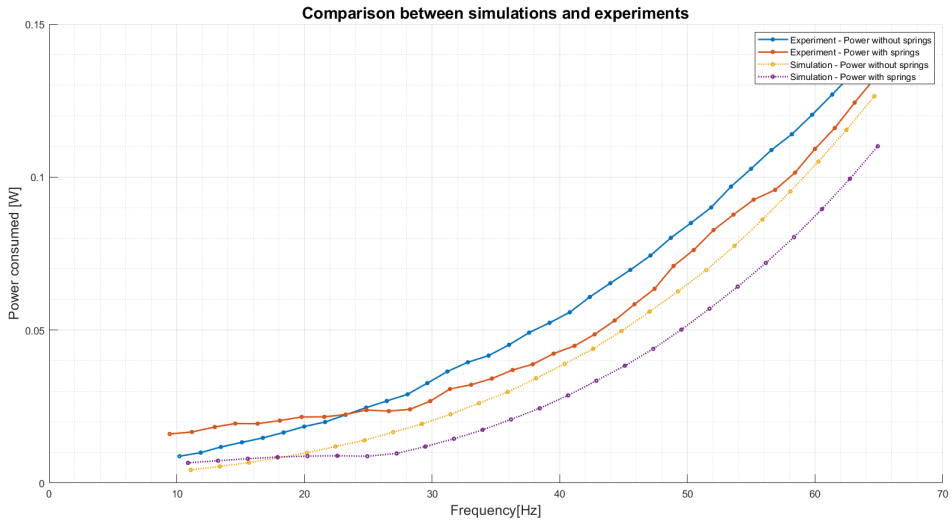

Figure 7.2: Comparison of power consumed in the experiments with that predicted by simulations without viscous friction in x-direction

Clearly, the removal of viscous friction from the model results in the power curves having similar rising pattern as that shown by the power curves obtained from the experiments. It can also be seen that the simulation curves seem to be the down-shifted versions of the experimental curves. This suggests that the Coulomb friction in the experimental setup is more than that in the simulated model. The general value of Coulomb friction co-efficient between dry steel and steel obtained from the internet is 0.6. This value is put in the model and the power curves are compared again. This is shown in Fig. 7.3. Careful observation reveals that the power curve obtained without springs in simulations matches well with its counterpart obtained through experiments at all frequencies. The power curve obtained for the case with springs in the system, however, matches its counterpart well only at frequencies above 30 Hz but not so much at frequencies below 30 Hz. This seems to be because of the presence of resonance at 26 Hz.

Tab. 7.2 shows a comparison between the reduction in power consumed at the resonance frequency of 26 Hz observed through simulations and experiments.

	Simulations	**Experiments**
Power consumed without springs [mW]	27	27
Power consumed with springs [mW]	21	24
Power reduction achieved [%]	22	12

Table 7.2: Comparison between simulations and experiments after modification of parameters

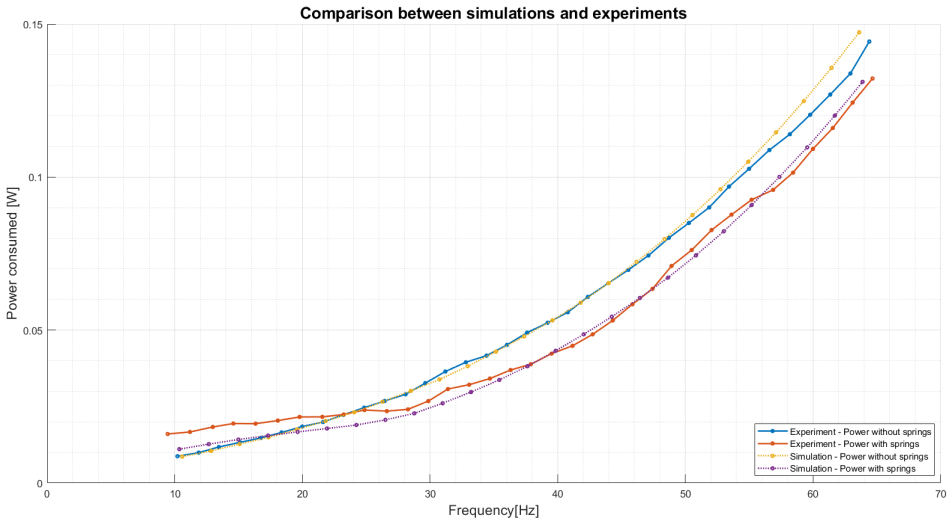

Figure 7.3: Comparison of power consumed in the experiments with that predicted by simulations with zero viscous friction and elevated Coulomb friction in x-direction

Looking back at the parameter estimation

As mentioned earlier, the parameters of friction in x-direction were estimated using the first experimental setup while the experiments were carried out using the second experimental setup. As a result, the initial simulations did not match the experimental results. Following are the possible reasons for the difference in friction parameters between the first and the second experimental setup.

1. The linear bearings installed in the setup were new at the time of investigation of friction parameters. Linear bearings are oiled by the manufacturer for better performance and this could be the source of viscous friction in the setup. Due to the time lost in the manufacturing of the second setup, the period between the experiments for parameter investigation and the experiments to observe the power curves was about a month. It is possible that the oil in the bearings got depleted over time and caused the absence of viscous friction during the experiments done using the second setup.
2. The difference in viscous friction could be caused by a drop of water or oil falling on the first experimental setup before the parameters were investigated.
3. When the design of the cutter was changed, the type of contact between the cutter and the guard was also changed. In the first design, the contact between the cutter and the guard was a line. This is because the guard surface is flat and the surface of the first cutter that touched the guard was cylindrical. A detailed drawing of the first cutter is included in appendix C. When the second cutter was designed, it was designed to be light in weight. Hence, it was manufactured using aluminium. In order to replicate the real hair clipper, where a steel cutter rubs on a steel guard, the cutter was designed in such a way that a small steel block could be attached to it with a nut & bolt joint. The bottom surface of this steel block makes contact and rubs on the top surface of the steel guard in the second setup. This change in contact type seems to be the most likely reason for the increase in Coulomb friction in x-direction because the power curve obtained without springs in simulations matches well with its counterpart obtained through experiments at all frequencies when the model is modified to include the general co-efficient of friction between two steel surfaces.

7.3. Power saved in a Philips hair clipper

Dennis William van der Meulen, a thesis project student at Philips, carried out some experiments on one of the models of Philips hair clippers that are currently available in the market. He investigated

parameters like the mass of the cutter, the stiffness in the direction of motion of the cutter provided by the torsion springs used to keep the cutter and the guard in contact at all times, and the force with which these springs press the cutter on the guard. He found that the mass of the cutter was $2.19\,\mathrm{g}$, the stiffness in the direction of motion of the cutter was $800\,\mathrm{N\,m^{-1}}$ and the normal force between the cutter and the guard was $2.9\,\mathrm{N}$. This shows that the Philips hair clipping system has a resonance frequency around $96\,\mathrm{Hz}$.

In his report, he mentioned that the friction co-efficient between the eccentric head and the drive bridge is known to design engineers at Philips and it varies between 0.14 and 0.25. During his project, he and his supervisor at Philips settled on a value of 0.12 for the case when lubrication is applied, which is the case in Philips hair clippers. The parameter that was left to be investigated was the friction between the cutter and the guard. Again, in this case, they settled for a value of 0.2, in presence of lubrication. In both the cases, it was assumed that there is only one layer of lubrication, which results into pure Coulomb friction while the viscous friction is zero.

Using the above mentioned values, he simulated the mathematical model made in this project and observed the torque required to run the system at a particular frequency. He then ran the hair clipper at the same frequency and noted the torque required to run it. The torque required was 10% higher than that predicted by the model. This error could be because of the assumptions about the friction coefficients as mentioned earlier.

As he noted the torque required to run the hair clipper at different speeds, he observed that there was a drop in the torque around $105\,\mathrm{Hz}$, which is close to the resonance frequency of the system. This error could be because of the error in measurement of the stiffness of the torsion springs. In reality, when that particular hair clipper is sold in the market, it runs at a frequency of $100\,\mathrm{Hz}$, which is pretty close to the resonance frequency. This shows that the concept of resonance is already being used in Philips hair clippers to save power.

Through mathematical modeling, simulations and experiments, in this project, it was proved that resonance can be used in Philips hair clippers to reduce the energy consumption. Experiments carried out by Dennis William van der Meulen proved that this is concept is already in use. The knowledge that resonance is used in Philips hair clippers to save energy was not available to the design engineers at Philips before or even during this project. The reason for this seems to be that knowledge was lost over the years of development of hair clippers.

It is interesting to know the amount of power that is being saved in a Philips hair clipper. For this, it is important to know the exact values of the parameters in the hair clipper. For the purpose of this report, the values found by Dennis are used in the model and the simulated results are shown in Fig. 7.4. Resonance helps to save about 8% of power in an actual Philips hair clipper.

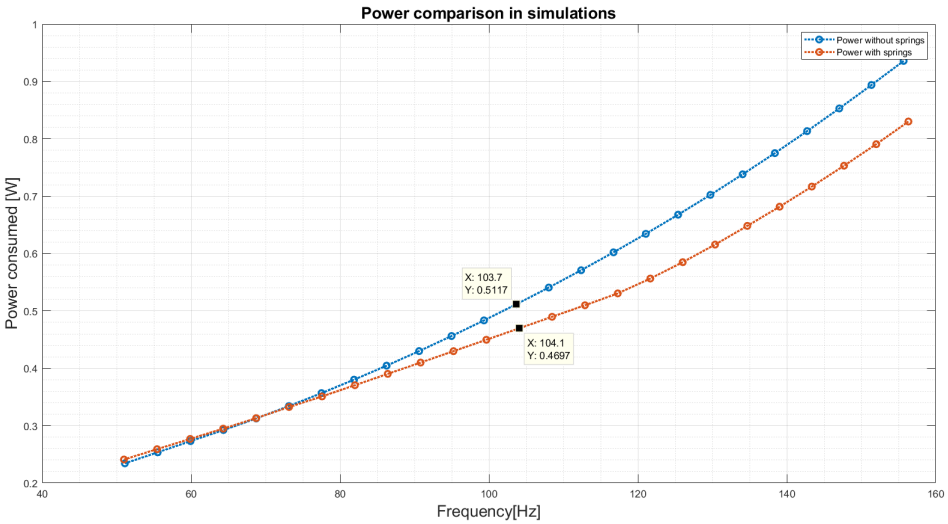

Figure 7.4: Comparison of power consumed in a Philips hair clipper with and without springs

As concluded in the sensitivity analysis carried out in chapter 5, the friction between the cutter and the guard is the most important factor to get a reduction in the power consumed in a hair clipper. If that can be reduced to a lower value, the the percentage of power reduction will be larger.

8. Conclusion and recommendations

At this point, it is good to recall the problem statement of this thesis project:

1. The aim of this project was to answer the question of whether the concept of resonance can be used in Philips hair clippers to reduce the overall power consumption without having to modify the currently available driving mechanism for the reciprocating cutter, which is a combination of a permanent magnet direct current (PMDC) rotary motor and a Scotch-yoke type mechanism.
2. It was also a goal of this project to mathematically model the hair clipper so that the model can be used for predicting the power consumption in a Philips hair clipper.

8.1. Conclusion

1. The experiments clearly show that the concept of resonance can be used in Philips hair clippers to reduce the overall power consumption without having to modify the currently available driving mechanism for the reciprocating cutter, which is a combination of a permanent magnet direct current (PMDC) rotary motor and a Scotch-yoke type mechanism.
2. A mathematical model of the hair clipper is made and modeled in SIMULINK. The results from the simulations of the model are compared with the results from the experiments in Tab. 8.1. The results are graphically compared in Fig. 8.1.

   The values in these results correspond to the analysis done for the parameters in the experimental setup. It should be noted that these values depend on various parameters related to this specific system and should not be mistaken to represent the power consumed in actual Philips hair clippers.

	Simulations	**Experiments**
Power consumed without springs [mW]	27	27
Power consumed with springs [mW]	21	24
Power reduction achieved [%]	22	12

Table 8.1: Comparison between simulations and experiments after modification of parameters

3. The mathematical model made in SIMULINK can be used to predict the power consumed by a Philips hair clipper at different running speeds. This could be a useful technique to avoid over-designing of electrical elements in hair clippers, if it happens, and subsequently save a lot of money for the company. To do this, parameter investigation needs to be carried out to know all the independent parameters that affect the power consumption related to the specific hair clipper.
4. The model can also be used to make predictions about the amount of power that can be saved by

designing a hair clipper with a stiffness element in it and then running the clipper at the resonance frequency of the system.

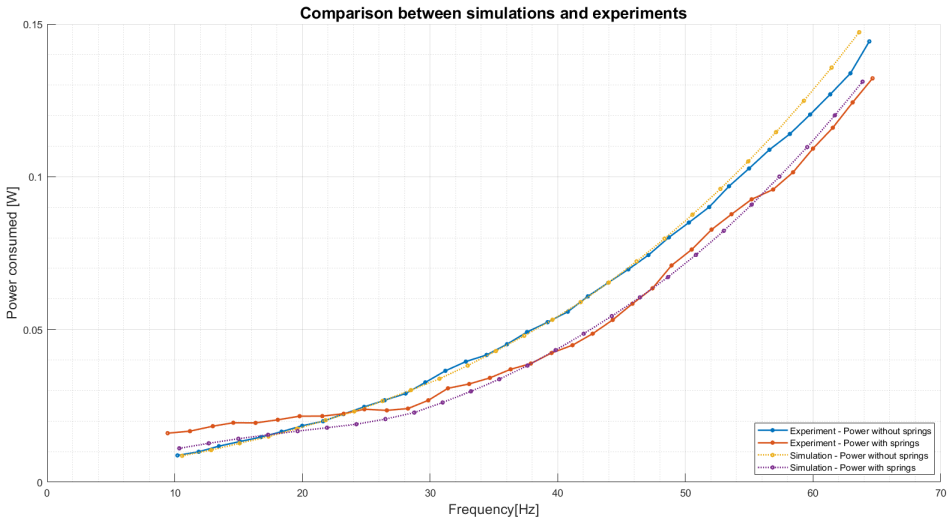

Figure 8.1: Comparison of power consumed in the experiments with that predicted by simulations

8.2. Recommendations

1. Ideally, the slot of the drive bridge needs to be of the exact width as the diameter of the eccentric head. This is not practically possible; the two dimensions will always differ a bit. Generally, the drive bridge is designed to have a narrower slot than the diameter of the eccentric head. This is done because the drive bridge is made of plastic which is extremely compliant as compared to the eccentric head and it has been observed that the width of the slot increases over time as the clipper gets operated by the consumer.

   When the drive bridge is designed to have a slot that is narrower than the diameter of the eccentric head, the drive bridge clamps the eccentric head throughout the operation of the hair clipper. This kind of a drive bridge was manufactured and experiments were carried out on the setup. It was observed that because the clamping increases the friction forces between eccentric head and the drive bridge, there could be no power reduction observed at the resonance frequency. The mathematical model could be upgraded to include this effect and study it. This will help in deciding on how narrow the slot can be in order to still be able to benefit from the resonance phenomenon.

2. If the width of the slot in the drive bridge increases to an extent such that there is play between the eccentric head and the drive bridge slot, there could be loss of contact between the drive bridge and the eccentric head. When the two come in contact again, it might cause unnecessary forces to arise. The mathematical model could be upgraded to view this effect. This will help to predict the power consumed in the hair clipper when the slot widens a lot over a period of time.

3. Experiments could be carried out using the same experimental setup by increasing the mass of the cutter. This can be easily done by attaching metal plates at the bottom of the cutter. The plates can be fastened to the cutter using the same nuts and bolts that used to fasten the drive bridge to the cutter. This will help to validate the model at various resonance frequencies.

4. Similarly, other parameters in the experimental setup like the friction in the motor, the friction between the cutter and the guard, and the friction between the eccentric head and the drive bridge can be varied to check the sensitivity of the power reduction with respect to these parameters.

It can be then compared to the results obtained from simulations by varying these parameters in the model. This could be another way of validating the model.

5. If a model of the shearing of a human hair is known, the mathematical model of the hair clipper made in this project could be used to see the effect of cutting hair on the speed of the trimmer and power consumption. It can also be used to study how the power reduction due to resonance gets affected by the hair cutting operation.

A. Electrical - mechanical analogies

It is difficult to depict the dynamics of the electrical and the mechanical sides of an electro-mechanical system in a single picture if these sides are to be shown in their own domains. It is a lot simpler to depict them both in the electrical domain in the form of an electrical circuit. Voltage, translation velocity and angular velocity are the across variables that correspond to each other. Current, force and torque are the through variables that correspond to each other. If the input is electrical and the output is mechanical, the conversion from electrical to mechanical is achieved by an electrical actuator, for example, a motor. If the input is mechanical and the output is electrical, the conversion is achieved by an electrical generator. In this project, the input is a battery voltage and the output is the velocity of the knife blade. The conversion is achieved with the use of a DC motor with a motor constant $K = 3.7\,\text{mNm/A}$

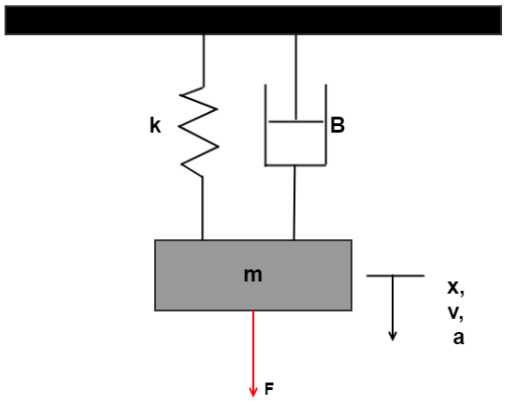

Figure A.1: A simple spring-mass-damper system

Let us consider a simple mass, spring and damper system as shown in figure A.1. The mass is driven by a force F and has a displacement x. Subsequently, it has a velocity $v = \dot{x}$ and acceleration $a = \ddot{x}$.

At equilibrium, the force through the system can be written as follows:

$$\begin{aligned} F &= F_m + F_d + F_k \\ &= m\ddot{x} + c\dot{x} + kx \end{aligned}$$

Here,
F_m = Force due to the inertia of the mass
F_d = Force due to the damper
F_s = Force due to the spring

Note that the velocities of the ends of the spring and the damper are the same as that of the mass but the forces through these elements are different.

To find the corresponding elements in the electrical domain, it is worthy of noting that a speed source in the mechanical domain would translate to a DC voltage source, that is a battery, and a force acting on a system would translate to a current source.

Inertia in electrical domain

Inertia is related to force in the following way:

$$F = ma = m\dot{v} \tag{A.1}$$

This means the corresponding electrical element to the mass has to have a constant property P that satisfies the equation:

$$I = P\dot{V}$$

Such an element is the capacitor. The current flowing through a capacitor with a capacitance C is given by the following equation:

$$I = C\dot{V} \tag{A.2}$$

Thus, a capacitor corresponds to mass with a capacitance value of $C = m$. In the rotational domain, the value of capacitance would be $C = J$ where J is the rotational inertia of the system.

Viscous friction in electrical domain

Viscous friction is related to force in the following way:

$$F = B\dot{x} = Bv \tag{A.3}$$

This means the corresponding electrical element to the viscous friction has to have a constant property P that satisfies the equation:

$$I = PV$$

Such an element is the resistor. The current flowing through a resistor with resistance R is given by the following equation:

$$I = \frac{V}{R} \tag{A.4}$$

Thus, a resistor of the value $R = \frac{1}{B}$ corresponds to viscous friction.

Stiffness in electrical domain

Stiffness is related to force in the following way:

$$F = kx$$

Differentiating on both sides, it can be seen that

$$\therefore v = \frac{\dot{F}}{k} \tag{A.5}$$

This means the corresponding electrical element to the viscous friction has to have a constant property P that satisfies the equation:

$$V = \frac{\dot{I}}{P}$$

Such an element is the inductor. The voltage over an inductor with inductance L is given by the following equation:

$$V = L\dot{I} \tag{A.6}$$

Thus, a inductor of the value $L = \frac{1}{k}$ corresponds to stiffness.

This system can be represented by an electrical circuit diagram as shown in figure A.2

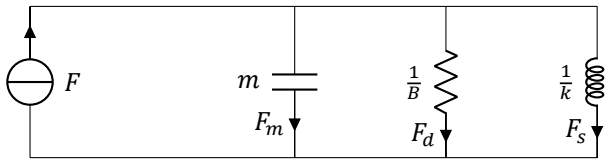

Figure A.2: Electrical analogy of the mass-spring-damper system

Note that the voltage across all the elements is the same but the currents through them are different. Here it is evident that voltage corresponds to velocity and current corresponds to force. In a rotational system, force would get replaced by torque, translation velocity would get replaced by angular velocity and mass would get replaced by rotational inertia. An electrical representation of a rotational-inertia-torsion-spring-torsion-damper system driven by a torque is shown in figure A.3

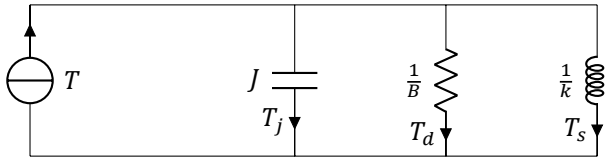

Figure A.3: Electrical analogy of a rotational-inertia-torsion-spring-torsion-damper system

B. SIMULINK models

B.1. Ideal model in 1D

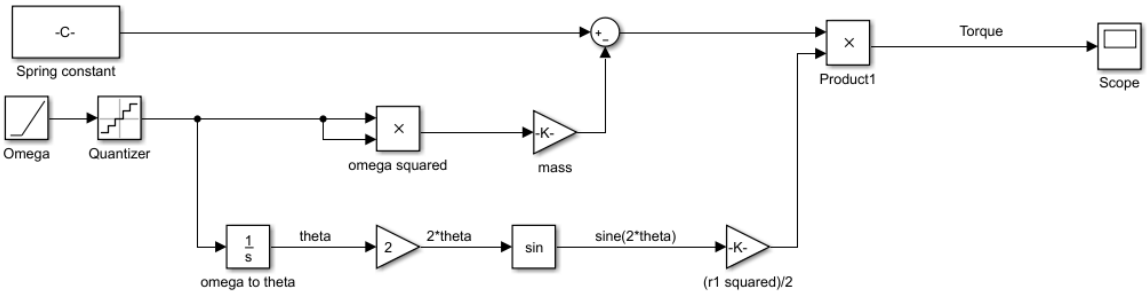

Figure B.1: SIMULINK model of the system with angular speed of the motor as input

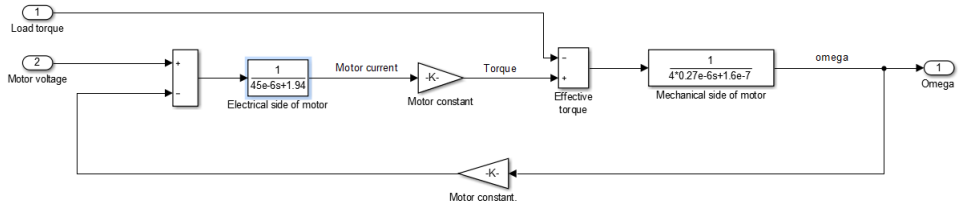

Figure B.2: SIMULINK model of the motor

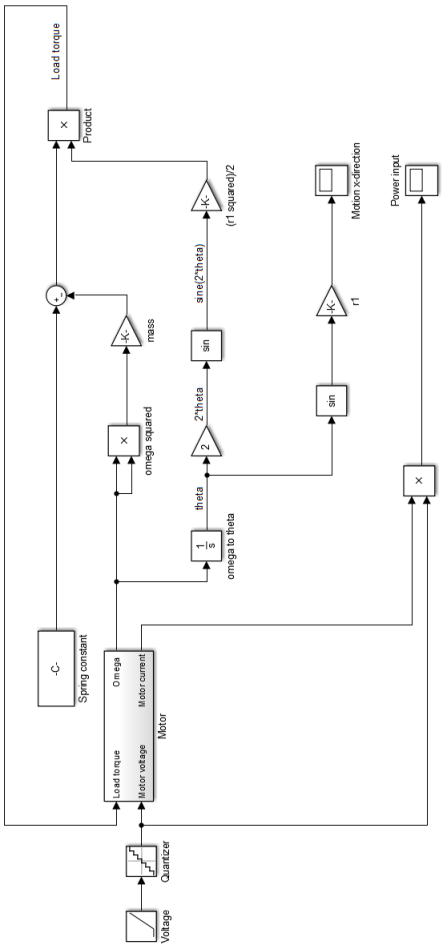

Figure B.3: SIMULINK model of the whole system with voltage as input to the motor

The supply voltage shown in figure B.3 is in the form of a ramp. This is done when the intention is to excite the system on a range of frequencies. As the supply voltage increases slowly according to the slope of the ramp, the angular velocity of the motor increases and so does the exciting frequency. A quantizer block is used so that the supply voltage and thus, the exciting frequency, increases in steps.The supply voltage shown here is in the form of a ramp. This is done when the intention is to excite the system on a range of frequencies. As the supply voltage increases slowly according to the slope of the ramp, the angular velocity of the motor increases and so does the exciting frequency. A quantizer block is used so that the supply voltage and thus, the exciting frequency, increases in steps.

B.2. Real model in 2D

Instead of taking an analytic approach of modeling the system, as done in the case of a 1D groomer, Simscape environment was used to make a model of the 2D resonant groomer system.

Different components of the model are as follows:

1. Supply voltage
2. DC motor
3. Conversion of rotary motion of the motor to translation motion of the cutter/knife.

4. Dynamics of motion of the cutter in the x-direction
5. Dynamics of motion of the cutter in the y-direction

These components were explained in the chapter of mathematical modeling of the system. The complete SIMULINK model is shown in the figure B.4.

The model of the DC motor is shown in figure B.5. The parameters used in it are as follows:
J = Rotational inertia of the motor in kgm^2
R_{fr} = Viscous friction in the system in rad/(Nms)
$T_{coulomb}$ = Coulomb friction torque in the motor in N m
L_m = Inductance of the motor winding in H
R_m = Resistance of the motor winding in
K_m = Motor constant in rad/s/V

The calculation of load torque T_{load} is done in the block of conversion of rotary motion to translation motion and is added to the total torque as shown in figure B.6. To calculate the Coulomb friction torque the direction of the mass velocity is sensed and a constant friction torque is added in the direction opposite to the direction of the motor velocity. The load torque is calculated in SIMULINK according to equation 3.15 that shows that

$$[T_{load}] = \begin{bmatrix} r_1 \cos\theta & r_1 \sin\theta \end{bmatrix} \begin{bmatrix} F_x \\ F_y \end{bmatrix}$$

Here, F_x and F_y are the forces exerted by the motor on the cutter mass in x- and y-directions respectively.

Also done in this block are the calculations for the velocity of the cutter/eccentric head in the x-direction (V_x) and the velocity of the eccentric head in the y-direction (V_y). These calculations are done according to the equations of kinematics of motion, as explained earlier.

$$V_x = \dot{x} = \omega r_1 \cos(\theta)$$
$$V_y = \dot{y} = \omega r_1 \sin(\theta)$$

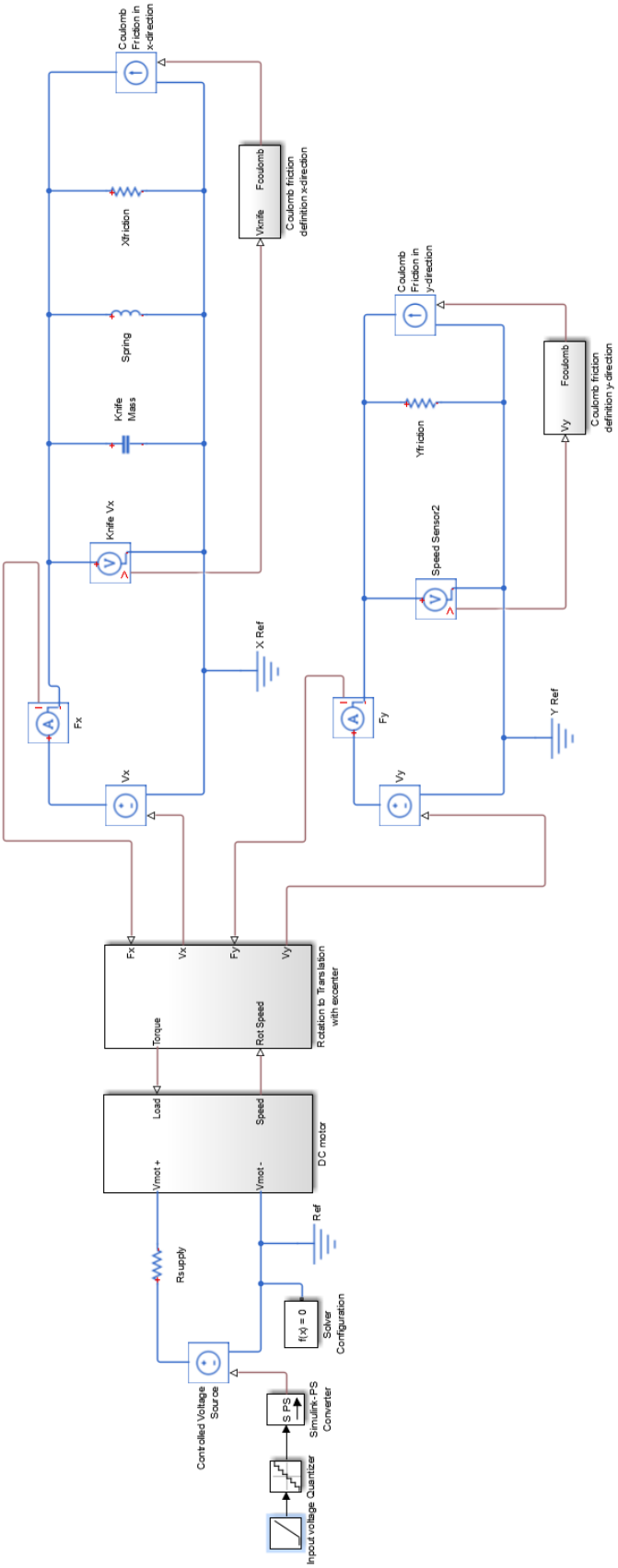

Figure B.4: SIMULINK model of the whole system

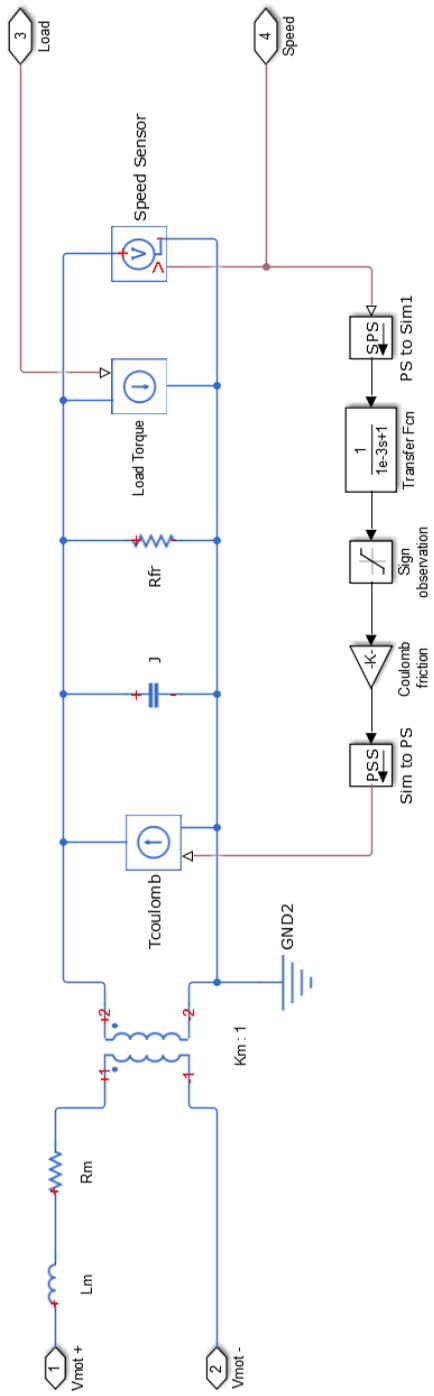

Figure B.5: SIMULINK model of the DC motor

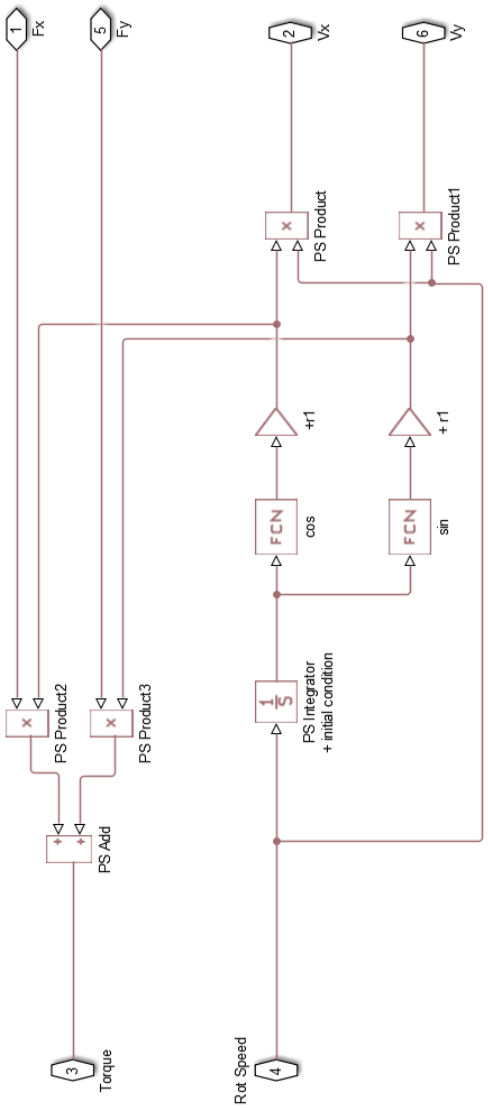

Figure B.6: SIMULINK model of the motion conversion from rotary to translation

C. CAD drawings and pictures

The CAD models and the drawings for some important parts of the experimental setup are shown in this chapter. The parts shown are the first design of the cutter, the second design of the cutter, the drive bridge, the shaft on which the linear bearings are mounted and along which the cutter moves, and the non-eccentric motor shaft extension used for the investigation of friction between the eccentric head and the drive bridge. Pictures of the experimental setup and some individual parts are shown in the later part of the chapter.

PART NAME : CUTTER
MATERIAL : STEEL

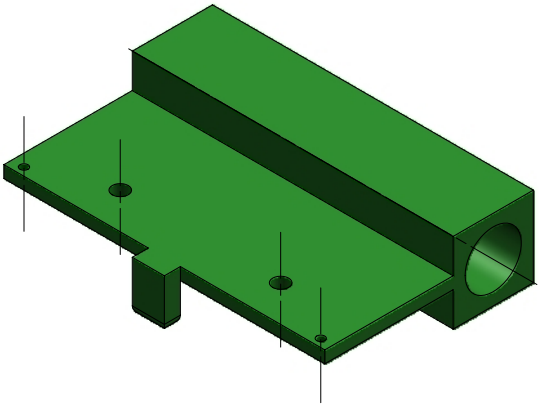

Isometric view

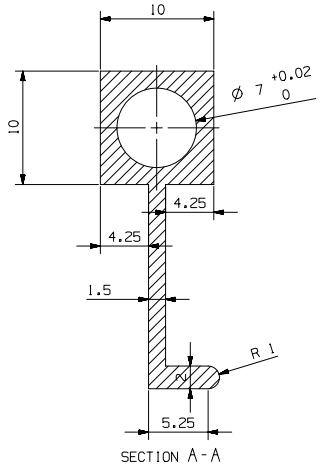

SECTION A-A

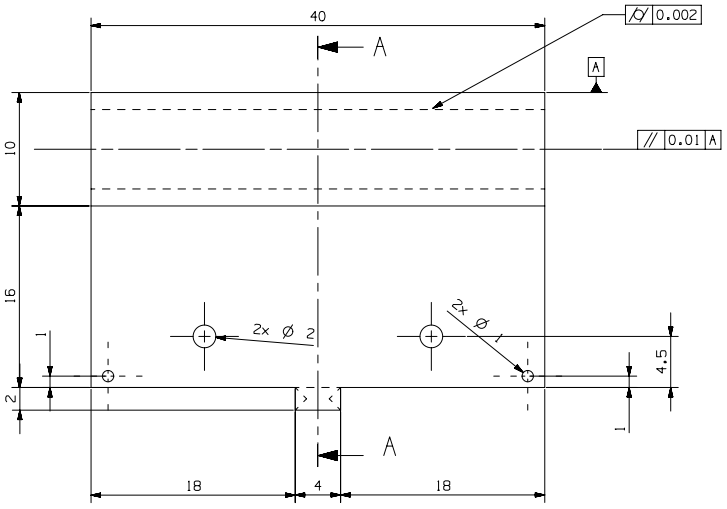

Top view

PART NAME : CUTTER
MATERIAL : ALUMINIUM

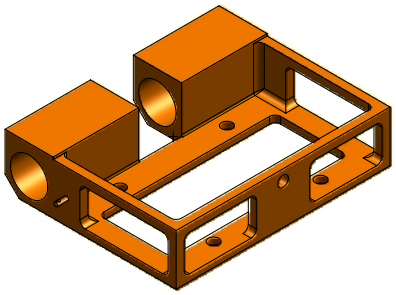

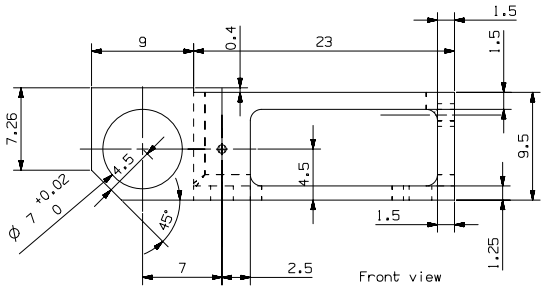

The two dia. 7mm bores should be concentric in tolerance of 10 micometers

Fillets at all edges are of radii 1mm unless specified otherwise.

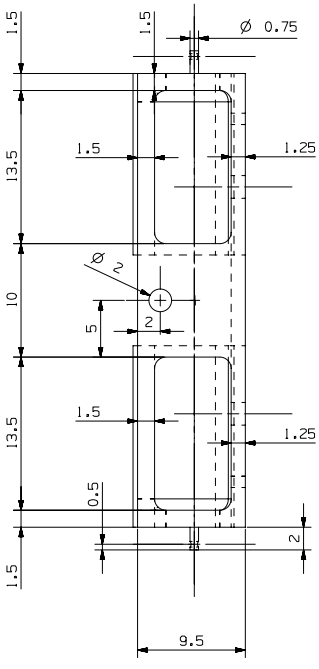

Right hand side view

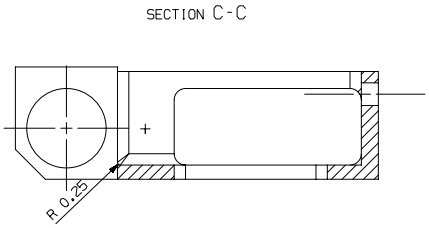

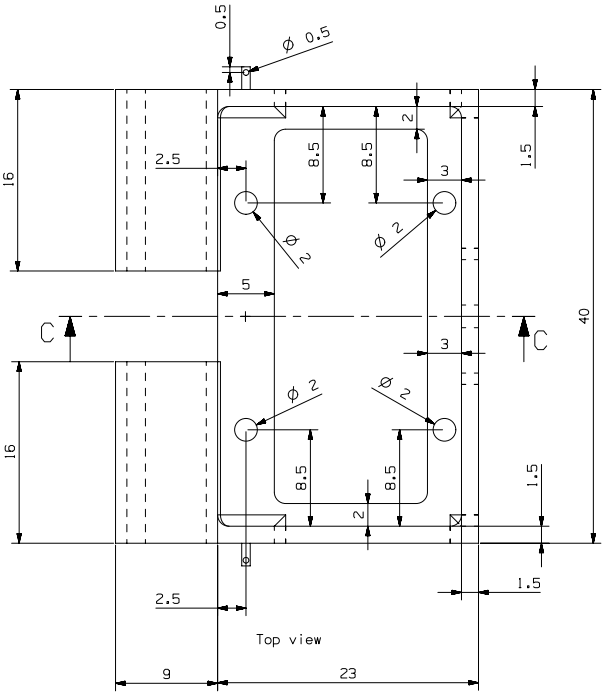

PART NAME : DRIVE BRIDGE

MATERIAL : POM

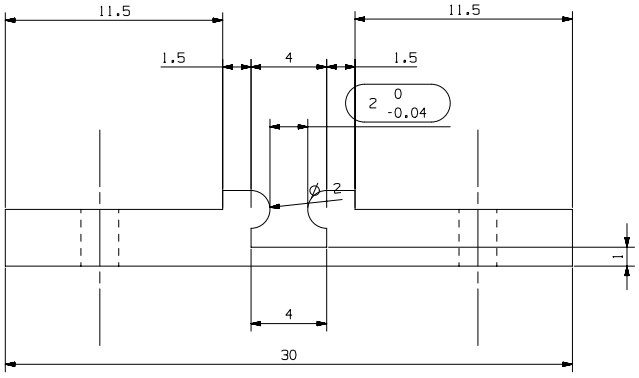

Front view

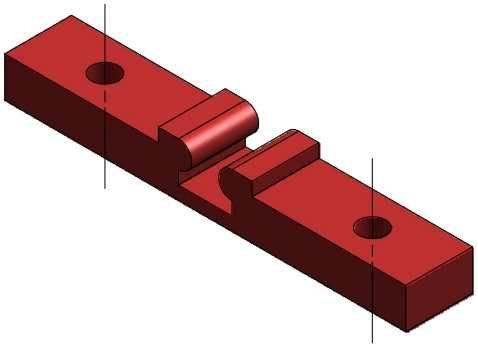

Isometric view

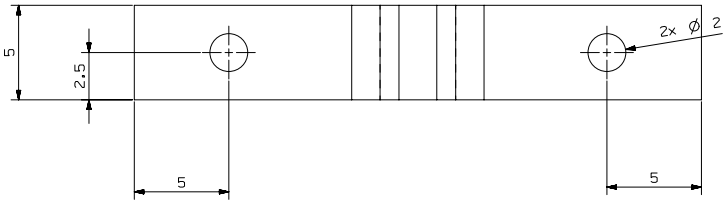

Top view

PART NAME : SHAFT

MATERIAL : STEEL

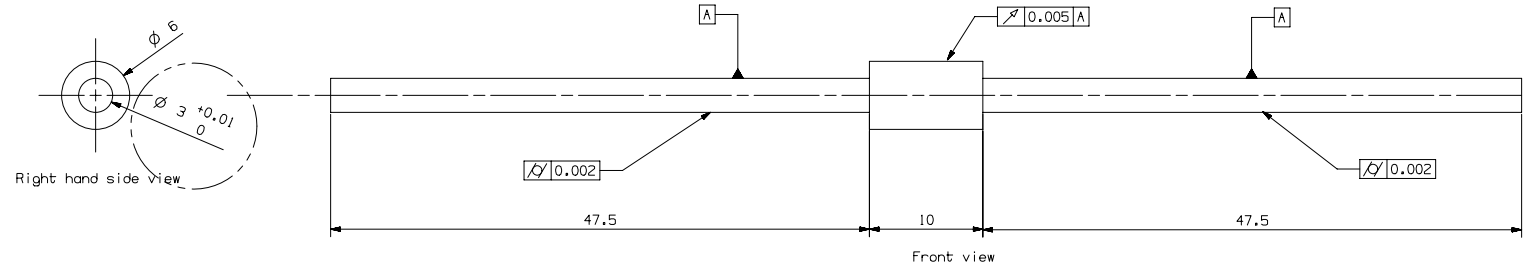

Isometric view

PART NAME: MOTOR SHAFT
MATERIAL : STEEL

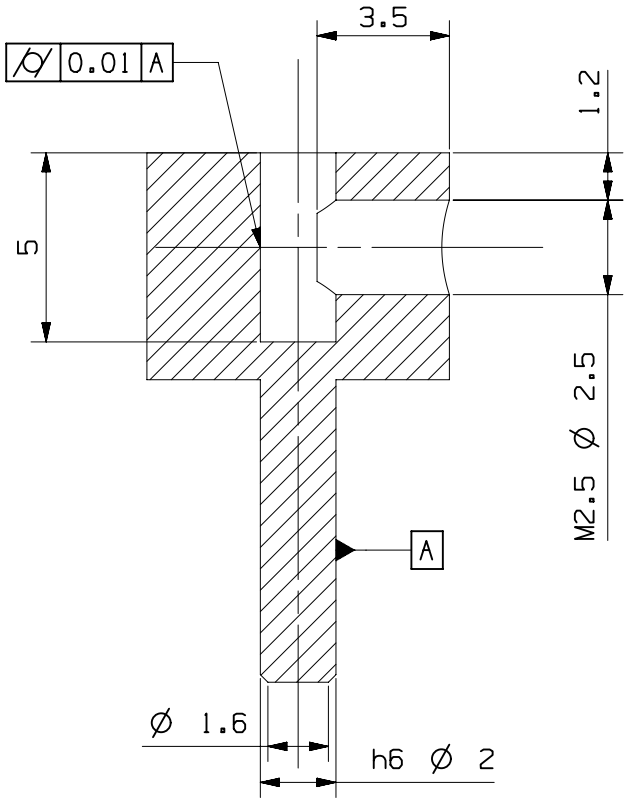

SECTION A-A

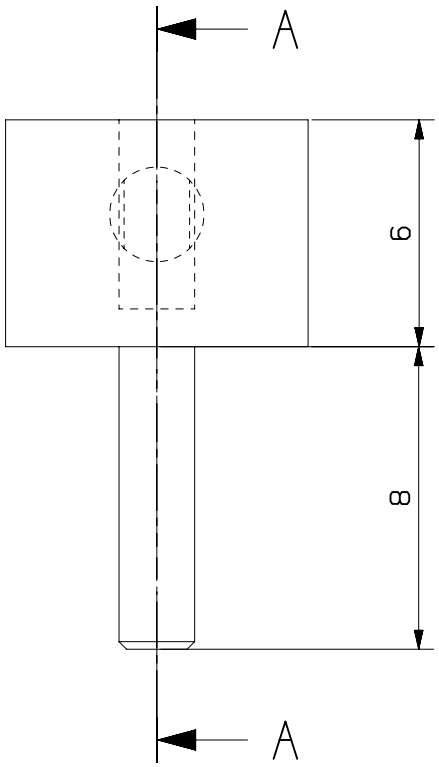

A grub screw is to be inserted in the M2.5 hole during assembly

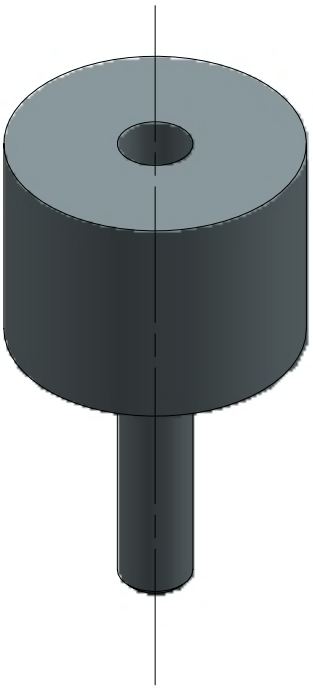

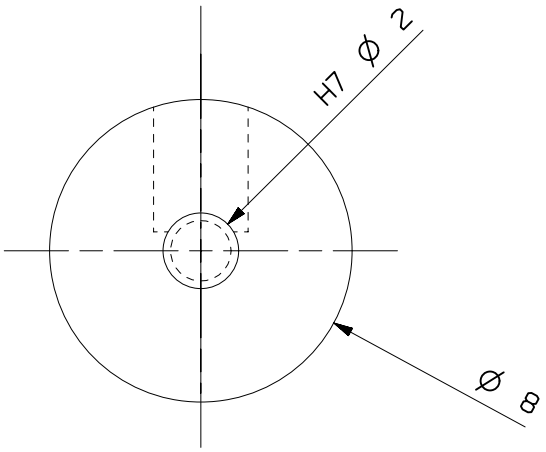

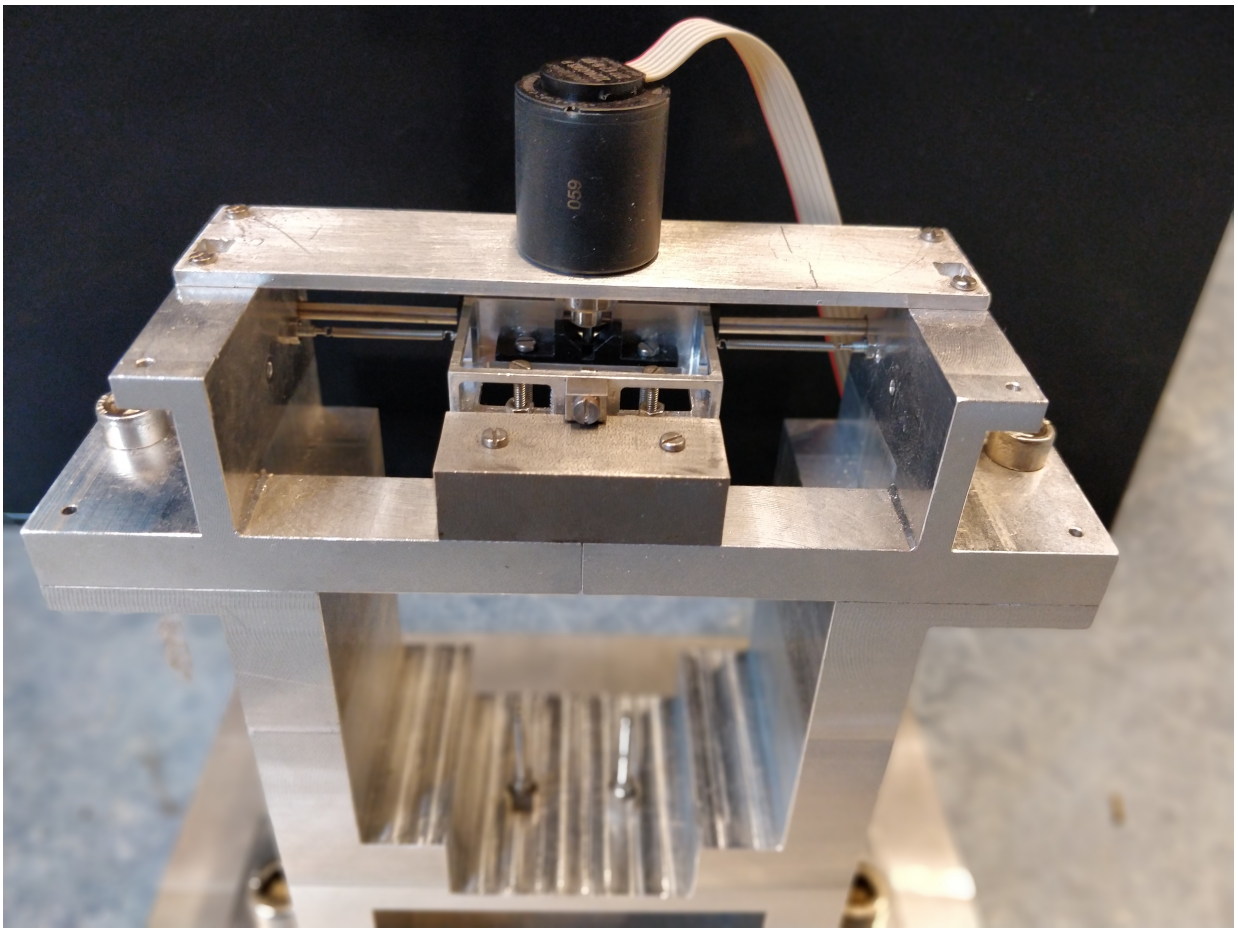

Figure C.1: A picture of the experimental setup

Figure C.2: A picture of the motor and the eccentric head

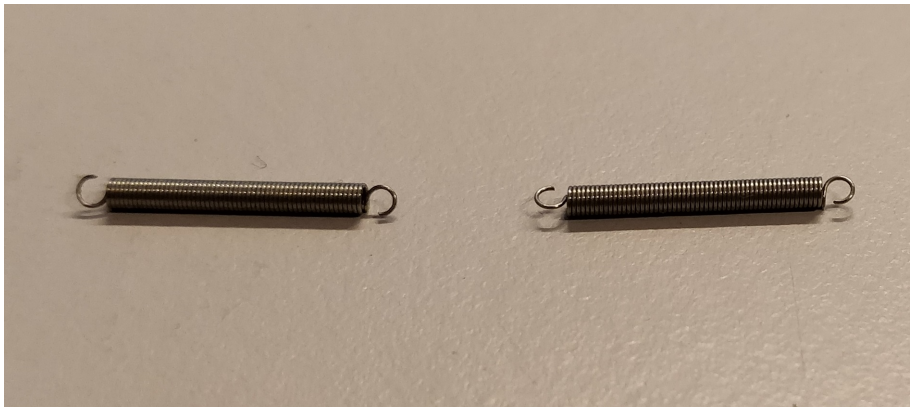

Figure C.3: A picture of the springs used in the setup

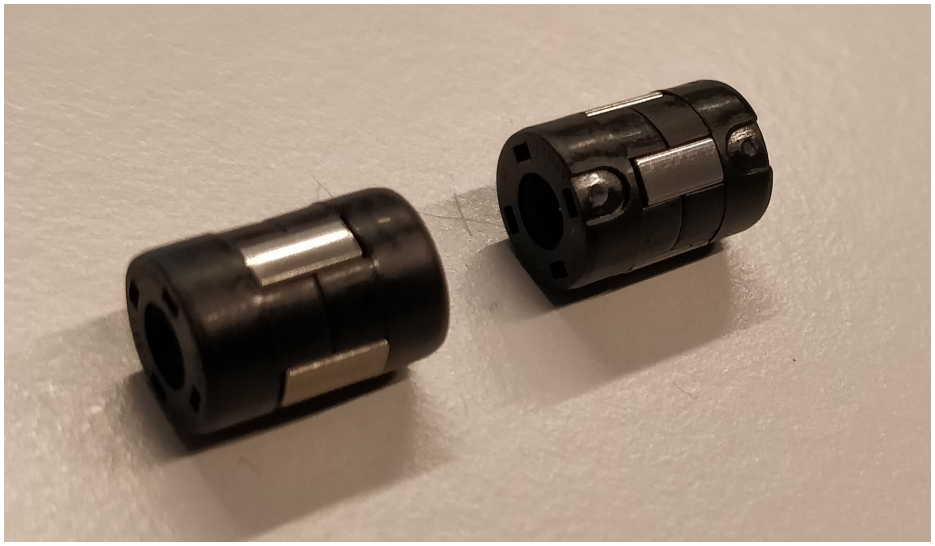

Figure C.4: A picture of the linear bearings used in the setup - SKF LBBR3

Figure C.5: A picture of the extension of the motor shaft used to find out the friction between the eccentric head and the drive bridge

Bibliography

[1] Eric, *Quantifying the current drawn by a motor at half speed,* Physics Stack Exchange, uRL:https://physics.stackexchange.com/q/107776 (version: 2014-04-10), https://physics.stackexchange.com/q/107776 .

[2] S. S. Rao, *Mechanical Vibrations* (Pearson, 2011).

[3] Philips, *Philips - the most reputable company in the netherlands,* (2018).

[4] M. Ringel and H. Zablit, *Innovation in 2018,* (2018).

[5] Philips, *Philips named among top 50 global innovators,* (2018).

[6] W. Fiebig and J. Wrobel, *Use of Mechanical Resonance in Machines Drive Systems,* (2017) pp. 1–8.

[7] A. J. Pagani, *Razor with reciprocating guard - United States Patent,* (1975).

[8] H. V. Green, *Alternating-current oscillating motor - United States Patent,* (1924).

[9] G. Heyek, *Vibratory motors - United States Patent,* (1966).

[10] M. Marinescu, *Electric motor with alternating linear motion - United States Patent,* (1969).

[11] Y. Ibuki and T. Ohba, *Epilator and method for driving epilator - United States Patent,* (2017).

[12] S. S. Rao, *Recherche*, Vol. 67 (2010) p. 1104.

[13] V. C. Kumar and I. M. Ã. Hutchings, *Reduction of the sliding friction of metals by the application of longitudinal or transverse ultrasonic vibration,* **37**, 833 (2004).

[14] W. Littmann, H. Storck, and J. Wallaschek, *Reduction of friction using piezoelectrically excited ultrasonic vibrations,* .

[15] Mecmesin, *Mecmesin's premium range computer-controlled tensile compression tester system,* (2018).

[16] Loadstarsensors, *What is a load cell,* (2018).